NASA TECHNICAL NOTE

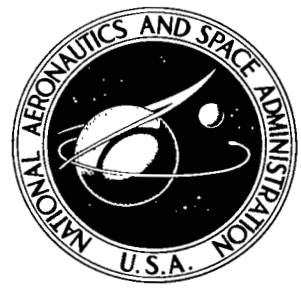

NASA TN D-8070

DESCRIPTION AND CALIBRATION OF THE LANGLEY 6- BY 28-INCH TRANSONIC TUNNEL

Charles L. Ladson

Langley Research Center
Hampton, Va. 23665

NATIONAL AERONAUTICS AND SPACE ADMINISTRATION • WASHINGTON, D. C. • DECEMBER 1975

1. Report No. NASA TN D-8070	2. Government Accession No.	3. Recipient's Catalog No.
4. Title and Subtitle DESCRIPTION AND CALIBRATION OF THE LANGLEY 6- BY 28-INCH TRANSONIC TUNNEL		5. Report Date December 1975 6. Performing Organization Code
7. Author(s) Charles L. Ladson		8. Performing Organization Report No. L-10386
9. Performing Organization Name and Address NASA Langley Research Center Hampton, Va. 23665		10. Work Unit No. 505-06-31-02 11. Contract or Grant No.
12. Sponsoring Agency Name and Address National Aeronautics and Space Administration Washington, D.C. 20546		13. Type of Report and Period Covered Technical Note 14. Sponsoring Agency Code
15. Supplementary Notes		

16. Abstract

This report presents a description and calibration of the Langley 6- by 28-inch transonic tunnel, a two-dimensional facility with slotted top and bottom walls, used for testing two-dimensional airfoil sections. Basic tunnel-empty Mach number distributions, noise surveys, and test-section total-pressure surveys are presented. The Mach number capability of the facility is from about 0.3 to 1.2. The stagnation pressure can be varied from 207 kN/m^2 (30 lb/in^2) absolute to 620 kN/m^2 (90 lb/in^2) absolute. This range of pressure can provide a Reynolds number of about 10×10^6, based on a 15.2 cm (6.0 in.) model chord at Mach numbers from 0.5 to 1.0. The maximum Reynolds number capability at a Mach number of 1.0 is about 15×10^6, based on the same model chord.

17. Key Words (Suggested by Author(s)) Transonic tunnels Two-dimensional tunnels Wind-tunnel noise	18. Distribution Statement Unclassified – Unlimited Subject Category 09

19. Security Classif. (of this report)	20. Security Classif. (of this page)	21. No. of Pages	22. Price*
Unclassified	Unclassified	65	$4.25

*For sale by the National Technical Information Service, Springfield, Virginia 22161

DESCRIPTION AND CALIBRATION OF THE LANGLEY 6- BY 28-INCH TRANSONIC TUNNEL

Charles L. Ladson
Langley Research Center

SUMMARY

The Langley 6- by 28-inch transonic tunnel is a two-dimensional facility with slotted top and bottom walls, which is used for testing two-dimensional airfoil sections. The tunnel is capable of operation from a Mach number of about 0.3 to 1.2 with variable stagnation pressure. For a 15.2 cm (6.0 in.) model chord, the Reynolds number can be held constant at about 10×10^6 for Mach numbers from 0.5 to 1.0, and the maximum Reynolds number at a Mach number of 1.0 is about 15×10^6. Tunnel-empty calibrations show that for Mach numbers below about 1.0 the local Mach number distribution obtained from wall static-pressure orifices varies less than ± 0.002 from the average value in the test region occupied by the model. Power-spectra noise distributions in the test section show a large peak at a frequency of about 150 Hz, but no appreciable spikes are noted at higher frequencies. The broadband noise data, normalized to 1 atmosphere stagnation pressure, show the noise level in this facility to be about the same, when compared at the same test conditions, as that in two large continuous transonic facilities. Data obtained from a total-pressure probe in the test section show that oscillations in total pressure at a Mach number of 0.7 have a magnitude of approximately 1 percent of dynamic pressure at a frequency of about 100 Hz. Electrical filters in the transducer output are provided to damp this oscillation so that the data-acquisition system can track the pressure adequately.

INTRODUCTION

The only testing of two-dimensional airfoils conducted at the Langley Research Center from the late 1950's to 1970 was the work on supercritical wing sections in the Langley 8-foot transonic pressure tunnel (ref. 1). In order to provide the capability for testing small two-dimensional airfoil sections from subsonic through sonic speeds, designs were initiated in 1968 to convert two existing facilities for this purpose. The first of these designs, in which the Langley 22-inch transonic tunnel was modified to the Langley 6- by 19-inch transonic tunnel, was placed in operation in 1971 and is described in reference 1. The operational mode of this facility does not permit independent control of Mach number and Reynolds number. The Reynolds number range (based on model chord) varies from

about 1.5×10^6 at subsonic speeds to 3.0×10^6 at sonic speeds, which is too low for many of the present airfoil research and development needs.

The second design was for the modification of the Langley 20-inch variable supersonic tunnel (described in ref. 2) to obtain a research facility with a higher Reynolds number capability and the ability to vary Mach number and Reynolds number independently by utilizing as much of the existing hardware as possible. This modification was completed in mid-1974 and routine testing in the facility began in late 1974. This facility, redesignated as the Langley 6- by 28-inch transonic tunnel, is a horizontal, two-dimensional wind tunnel with slotted top and bottom walls and operates on direct blowdown from a supply of dry compressed air. In its present configuration, this wind tunnel is capable of operation at Mach numbers from about 0.3 to 1.2 at stagnation pressures of 207 kN/m^2 (30 lb/in^2) absolute to about 620 kN/m^2 (90 lb/in^2) absolute. Mach number and stagnation pressure are independently controllable so that tests may be conducted at Mach numbers from 0.5 to 1.0 at a constant Reynolds number (based on a model chord of 15.2 cm (6.0 in.)) of up to about 10×10^6. The maximum Reynolds number capability at a Mach number of 1.0 for this same model chord is about 15×10^6. The facility was designed to operate at stagnation pressures up to 1034 kN/m^2 (150 lb/in^2), the pressure of the air storage tank. Thus, the potential exists to operate at higher pressures for very short duration runs and to increase the Reynolds number capability by about 20 percent.

The purpose of this paper is to present a description and calibration of the Langley 6- by 28-inch transonic tunnel. Included are descriptions of the facility, instrumentation, typical models, the data-acquisition system, and test procedures. Tunnel-empty longitudinal and vertical Mach number surveys, test-section stagnation-pressure surveys, and sound pressure-level measurements are presented. The sound pressure levels of this blowdown-type tunnel are also compared with similar test results from larger continuous-operation transonic tunnels. All sound pressure measurements for facilities at the Langley Research Center were obtained by Joseph D. Brooks of the Transonic Aerodynamics Branch.

SYMBOLS

Values are given in both SI and U.S. Customary Units. The measurements and calculations were made in U.S. Customary Units.

c model chord

f_c low-pass filter cutoff frequency

M average stream Mach number

M_{TC} test-chamber Mach number

ΔM_{AV} average deviation of local Mach number from average stream Mach number

$p_{t,p}$ total pressure measured on the survey probe

$p_{t,\infty}$ stream stagnation pressure

Δp_t incremental total pressure, $p_{t,\infty} - p_{t,p}$

q stream dynamic pressure

R Reynolds number

T_t stagnation temperature

X,Y,Z distances along longitudinal, lateral, and vertical axes, respectively, on computer-generated plots

x,y,z distances along longitudinal, lateral, and vertical axes, respectively

APPARATUS

History of Facility

The Langley 6- by 28-inch transonic tunnel is a modification of the Langley 20-inch variable supersonic tunnel which was designed in 1957 and was operational until 1965. As shown in reference 2, the 20-inch variable supersonic tunnel was a horizontal facility mounted above the Langley 26-inch transonic blowdown tunnel. The settling chambers of these two facilities were interconnected through an isolation valve and piping manifold so that both could make use of a common hydraulically operated air-regulation system to control tunnel stagnation pressure. When a decision was made to provide a facility for two-dimensional airfoil testing at moderate Reynolds numbers, the 20-inch variable supersonic tunnel was chosen for modification because it had not been operational for several years and much of the existing hardware could be utilized for the modified facility, thus providing a large cost savings.

General Description

The Langley 6- by 28-inch transonic tunnel, which is a two-dimensional facility with solid sidewalls and slotted top and bottom walls, operates on direct blowdown from a supply

of dry compressed air. The test section is 15.24 cm (6.00 in.) wide and measures 72.39 cm (28.50 in.) between the slotted top and bottom walls. A photograph of the facility, taken during the assembly of the tunnel, is shown in figure 1, and a drawing is shown in figure 2. The physical relationship and interconnecting piping between this facility and the 26-inch transonic blowdown tunnel (TBT) are evident in both of these figures. Also indicated in figure 2 is the portion of the facility which was replaced to provide for the two-dimensional test section.

Air enters the settling chamber of the 26-inch transonic blowdown tunnel through three servo-controlled hydraulically operated plug valves, each with a diameter of 61.0 cm (24.0 in.). With the gate valve closed for the 26-inch TBT and the isolation valve open to the 6- by 28-inch transonic tunnel, the air then passes through the interconnecting piping into the settling chamber of the two-dimensional tunnel. The settling chamber, as seen in figures 1 and 2, consists of a conical diffuser and a constant-diameter section. Inside the conical diffuser is a conical baffle plate with a porosity of about 55 percent. Three 30-mesh screens, each with a porosity of about 65 percent, are located downstream of the baffle plate. The contraction ratio between the 2.13-m- (7-ft-) diameter settling chamber and the 15.24-cm (6.00-in.) by 72.39-cm (28.50-in.) rectangular test section is about 32:1.

A photograph and cross-section drawing of the entrance section, test section, downstream transition section, and enclosing pressure shell are presented in figures 3 and 4, respectively. The pressure shell, which forms the test-section plenum chamber, is cylindrical with a length of 380 cm (149.8 in.) and an inside diameter of 193 cm (76.0 in.). The rectangular test section begins at station -96.5 cm (-38.0 in.) and ends at station 112.4 cm (44.25 in.). Circular windows with a diameter of 24.1 cm (9.5 in.) are located in the sidewalls and provide for the model support. The center line of the windows is located at station 0.0. Four longitudinal slots are located in both of the 15.24-cm-wide (6.00-in.) walls and consist of three full slots and a half slot on either outer edge. The slots begin at station -89 cm (-35.0 in.), have an included divergence angle of 0.6° to station -40.7 cm (-16.0 in.), and have a constant width to station 14.0 cm (5.5 in.). From this point, the slots diverge linearly to a fully open condition at station 57.2 cm (22.5 in.). The slotted walls are removable so that changes in slot design can be made if desired. The present slot design has been used in previous tunnel designs and provides an open area ratio of 0.125. The slotted walls are also adjustable so that their slope with respect to the tunnel axis may be changed. For these tests they were set parallel to the tunnel axis, as were the fixed solid sidewalls. The slotted walls are formed by mounting 0.32-cm-(0.125-in.-) thick steel plates on a rectangular cross-section support structure forming a set of T-shaped bars. The upper surface of the "T" is the airstream surface. The

upstream end of the bars is connected in a flex-joint arrangement, and the bars are tied together near the downstream end to provide for the wall divergence capability. (See fig. 4.)

Air which has passed through the slotted walls into the test chamber is returned to the airstream over reentrant flow fairings which begin at tunnel station 27.3 cm (10.75 in.). The minimum cross-section area in this mixing region is located at station 112.4 cm (44.25 in.) and is 20 percent larger than the test-section area to provide space for the low-energy reentrant flow to return to the airstream. At tunnel station 112.4 cm (44.25 in.) two sliding choker doors are located and are used to control Mach number. The two doors extend the full height of the tunnel and may be inserted into the airstream by means of a hydraulic control system. When inserted, these doors decrease the local cross-section area, thus decreasing the tunnel mass flow. Because sonic velocity is maintained at the choker-door location, the test-section Mach number can be set to any value, depending upon the amount of area reduction by the doors.

A transition section is located downstream of the choker door which provides a linear increase in cross-section area from the test section of the 6- by 28-inch tunnel to the existing 20-inch-square cross section second minimum and conical diffuser of the previous supersonic tunnel installation. The air is exhausted to atmosphere through a vertical stack which has sound-attenuation baffles installed.

The facility has three independent primary control systems: a valve control system for maintaining stagnation pressure while the tank supply pressure decreases, a choker-door system for Mach number control, and a test-section window system for rotation of the window to provide model angle of attack. All three of these systems use closed-loop operation of servo valves connected to hydraulic cylinders. The controls are located on a console in the control room which is shown in figure 5. Real-time visual displays of all tunnel parameters are provided on this panel. The analog setpoints for the control systems can be input either manually from the control console or automatically from the computer used in the data-acquisition system. By use of the computer-controlled input, setpoints can be reached more rapidly so that more efficient use of the stored air supply is possible in this mode of operation.

A plot of the tunnel Reynolds number capability as a function of Mach number for several stagnation pressures is shown in figure 6. The Reynolds number shown is for a 15.2 cm (6.0 in.) model chord which is the nominal model size for this facility. Although this curve is for a constant stagnation temperature, there is no control over this parameter and it will vary during a tunnel run. With automatic tunnel control, the stagnation pressure can be adjusted to compensate for stagnation-temperature changes, thus providing a constant Reynolds number for the duration of the run.

INSTRUMENTATION

Pressure Instrumentation

At present, the facility is designed to obtain static-pressure measurements on the airfoil surface and in the wake downstream of the model. A total of 64 channels of commercially available high-precision capacitive potentiometer-type pressure transducers are available for this program. A more complete description of this type of pressure instrumentation is presented in reference 3. The model pressure leads are brought out through the tunnel pressure shell and are connected to the transducers which are mounted in instrument racks located adjacent to the test section as shown in figure 7. The transducers are mounted on thermostatically controlled heat bases to maintain a constant temperature and are also shock mounted to reduce possible vibration effects. The electrical outputs from the transducers are connected to individual signal conditioners (fig. 8) located in the control room. These signal conditioners are autoranging and have seven ranges available. By means of the autoranging capability, the electrical output to the data-acquisition system is kept at a high level even though the transducer may be operating at the low end of its range. Transducers with ranges of 690 kN/m^2 (100 lb/in^2) and 345 kN/m^2 (50 lb/in^2) are available for model surface pressures and tunnel parameters, and a maximum range of 69 kN/m^2 (10 lb/in^2) is available for pressures in the model wake. These tranducers have an accuracy of ± 0.25 percent of reading from -25 percent of full scale to 100 percent of full scale.

Traversing Survey Probe

A vertical traversing probe system is located at tunnel station 38.1 cm (15.0 in.) and has a traversing range of ± 25.4 cm (± 10.0 in.) from the tunnel center line. The probe is driven by a closed-loop-control electric drive system and is capable of drive speeds from about 2.54 cm/sec (1 in/sec) to about 25.4 cm/sec (10 in/sec). The stroke and speed of the system can be remotely controlled from the operator's panel in the control room. Although the primary purpose of the system is to survey the impact pressure in airfoil wakes by use of a pitot-tube survey rake, the system can be equipped with other types of rakes such as thermocouples, hot wires, or static-pressure probes if desired. The ball screw and guide rods which are part of the survey system are visible to the left of the model-support window in figure 9. The position of the system is recorded by use of a digital shaft encoder which is also visible in this figure. Details of the multitube pitot probe which was used for these tests are shown in figure 10. The transducer used with the probe was a low-volume type and was located inside the tunnel pressure shell adjacent to the survey system so that the pressure response time could be kept low.

Schlieren System

The facility is also equipped with a schlieren-flow visualization system, and still pictures as well as motion-picture records are available. For still pictures, a 70-mm camera is used with a short-duration flash of a xenon lamp for the light source. Motion-picture records are provided on 35-mm film using synchronized flash from the xenon lamp. Film speeds up to about 40 frames per second are available with this system. For special purposes, 16-mm film can be used at speeds of several hundred frames per second. Real-time displays are also provided by a closed-circuit television system in place of the cameras. All schlieren-system and camera controls can be remotely selected and operated from the operator's panel in the control room.

Real-Time Displays

Figure 11 shows the real-time display console in the control room. A 50-channel bargraph display is located in the right-hand side and is used to display the model surface pressures in bargraph form, similar to a manometer board. In this manner, the model pressure distribution is continuously displayed during the run and conditions such as unsteady flow or rapid separation can be noted at once. Also provided are the closed-circuit television monitor in the center panel and a video tape recorder at the bottom of the left-hand panel. Selector switches are provided to monitor either a camera in the schlieren system or a camera in the tunnel test-section pressure shell. This camera can be used for oil-flow studies or other model surface observations. Also located on the left panel is a two-channel strip chart recorder which provides a trace of survey probe position and a trace of pressure for one of the rake pitot tubes.

Noise Measurements

For the noise survey tests conducted during the facility calibration, special instrumentation which is not part of the standard tunnel instrumentation was used. For the stream noise measurements, 3.2-mm- (0.125-in.-) diameter microphones mounted flush with the tunnel wall were used. These microphones have a frequency response of from 30 Hz to about 140 kHz. The output was displayed on root-mean-square meters to give sound pressure levels and was also recorded on tape driven at a speed of 152 cm/sec (60 in/sec) for later analysis to give the frequency spectrum of the data.

DATA-ACQUISITION SYSTEM

The data-acquisition system used for the 6- by 28-inch transonic tunnel is shared with other facilities located in the same complex. The system consists of the following: a computer, teletype input, and associated electronics (fig. 12); a high-speed tape transport (fig. 13); a card reader, line printer, and two-axis plotter (fig. 14); and a cathode-ray-tube

display panel located on the operator's control console (fig. 5). For the 6- by 28-inch transonic tunnel, this system provides three functions: data acquisition, tunnel control, and preliminary postrun data reduction.

For data-acquisition purposes, the system at present is programed to record 110 channels per scan. These include 64 analog channels, four special shaft-encoder channels, as well as digital input channels and information channels input from the teletype. Digital channels are used to record the gain code from each of the autoranging signal conditioners for the pressure instrumentation as well as other digital signals. The system can record from 1 to 9 scans of data with a variable time between scans of from 5 ms to 1.0 sec in a single-point mode or can take continuous data at a scan rate of 200 Hz. The control system for the traversing probe system can be computer controlled so that continuous data are taken while the probe is traveling between two setpoints. Because the system is computer controlled, the software may be changed to provide other desirable functions, but the time and cost involved are such that frequent changes are not made.

As was stated in the "Apparatus" section of the paper, stagnation pressure, choker-door position, and angle of attack are controlled by closed-loop systems which can be computer controlled. Thus, the desired combinations of stagnation pressure, Mach number, and angle of attack can be input in card form before the run and the computer can operate the facility for the entire run. Any control function may be operated manually while the others are under computer control. Values of free-stream Mach number, Reynolds number, and angle of attack are computed and displayed on the cathode-ray-tube unit at the operator's panel. These values are updated about every 0.5 sec.

Because of the limited-memory capability of the data system and short-duration run time, no real-time data reduction is possible. However, between runs, while the air supply tanks are being recharged, the computer is available for some data-reduction purposes. Software programs are being prepared which will provide preliminary plots of airfoil pressure distribution, wake pressure distribution, and some integrated forces and moments. This capability will suffice for a "quick-look" analysis of the data as the test progresses so that alterations to the research program can be made when necessary.

MODELS

A photograph of two typical models to be tested in the facility is shown in figure 15. Both models are constructed of stainless steel, are of 15.2 cm (6.0 in.) span, and are instrumented for pressure-distribution tests. The 10.16 cm (4.0 in.) model chord is typical of models used in the 6- by 19-inch transonic tunnel (ref. 1) in which the tubes are laid in the surface and covered with an epoxy-type resin. However, at the high stagnation pressures at high lift coefficients in the 6- by 28-inch tunnel, this type of construction may not

provide sufficient model strength unless a stainless steel of very high strength is used. These models are also held in place by dowel pins and these pins carry a high stress. A preferred type of model construction is shown on the 15.2 cm (6.0 in.) model chord. In this case, rectangular tangs, machined on the model, transfer the model aerodynamic loads to the model support system. The tubes have been placed inside the model, a cover plate has been placed over the tubes, and the plate has been welded in place. Both types of model construction have yielded accuracies of better than 2×10^{-4} model chord. Typically, orifices have a diameter of 0.0343 cm (0.0135 in.) (No. 80 drill) and are located in chordwise rows on both surfaces near the model midspan.

PRESENTATION OF RESULTS

The results of the sidewall static-pressure measurements are presented as plots of local Mach number distribution in figures 16 to 31. Power-spectra distributions and broadband measurements of the fluctuating pressure are presented in figures 32 to 37, and results from a pitot tube on the tunnel center line are shown in figures 38 and 39. An index to the Mach number distribution figures is presented in the following table:

Results	$p_{t,\infty}$		Probe, z		Figure
	kN/m^2	lb/in^2	cm	in.	
Longitudinal sidewall Mach number distribution	207	30	-29.2	-11.5	16
	414	60	-29.2	-11.5	17
	207	30	7.6	3.0	18
	414	60	7.6	3.0	19
Mach number distribution in region of model	207	30	-29.2	-11.5	20
	310	45	↓	↓	21
	414	60	↓	↓	22
	517	75	↓	↓	23
	620	90	↓	↓	24
	207	30	7.6	3.0	25
	310	45	↓	↓	26
	414	60	↓	↓	27
Ratio of stream-to-chamber Mach number	Vary	Vary	Vary	Vary	28
Comparison of left and right sidewall distributions	207	30	-29.2	-11.5	29
	414	60	↓	↓	30
	620	90	↓	↓	31

DISCUSSION

Local Mach Number Distribution

Longitudinal sidewall distribution.- Longitudinal Mach number distributions are presented in figures 16 to 19 for two stagnation pressures and two locations of the survey probe. Distributions are shown at 7.6 cm (3.0 in.) above and below the tunnel center line because a structural web is welded along the center line making it impossible to instrument the wall at this location. A sketch of a slot and the location of the survey probe are also shown in the figure for ease in the correlation of results. Tunnel station 0 is at the center of rotation of the model support window as was shown on the tunnel drawing in figure 4. With the survey probe in the stored position (z = -29.2 cm (-11.5 in.)), the longitudinal Mach number distribution is essentially flat from 100 cm (39 in.) upstream to about 50 cm (20 in.) downstream of the center line for Mach numbers up to about 1.0 as shown in figures 16 and 17. At the supersonic speeds, the length of near-constant Mach number region decreases to about one-half that at the subsonic speeds and a disturbance from the survey probe is also noted. The probe and its bow shock wave interact with the tunnel sidewall boundary layer causing a blockage or decrease in Mach number near the probe location followed by a rapid expansion downstream of the probe. This disturbance increases in magnitude as the distance from the probe to the plotted orifice row is decreased, and there is a maximum shown in figures 18(a) and 19(a) because the probe is in line with the orifice row. For this maximum case, some small local effects of the probe are noted at Mach numbers as low as 0.8. These disturbances, however, do not extend upstream beyond about the 10-cm (4-in.) tunnel station for the worst cases and are, thus, well downstream of the airfoil trailing edge for the nominal model chords envisioned. Also, at stream Mach numbers below about 0.95, the effects of the probe are small, and reliable wake survey data could be obtained in the Mach number range of interest.

Test-section distribution.- The actual tunnel calibration was obtained from tests throughout the range of stagnation pressures with three horizontal and three vertical rows of flush surface orifices located in one of the movable model-support windows. In this manner, the Mach number distribution in the area occupied by the model at various angles of attack could be determined. The average stream Mach number M is defined as the numerical average of all the local Mach numbers in the window region (37 separate orifices for most cases). The results of these tests are shown in figures 20 to 24 for the survey probe in the store position (z = -29.2 cm (-11.5 in.)) and in figures 25 to 27 for the probe in line with one of the horizontal orifice rows (z = 7.6 cm (3.0 in.)). Also tabulated in these figures are the test-chamber Mach number M_{TC}, the average stream Mach number M, and the average deviation of the local Mach number from the average stream Mach number ΔM_{AV}. This average deviation is generally less than 0.002 at subsonic Mach

numbers and 0.005 at supersonic Mach numbers. Variations in stagnation pressure and survey-probe location have little effect on the average deviation of local Mach number. The effects of these parameters on the ratio of stream Mach number to test-chamber Mach number (or calibration factor) are shown in figure 28. With the survey probe in the store position (z = -29.2 cm (-11.5 in.)), little effect of increasing stagnation pressure is noted on the calibration factor except for the highest pressure run. For this case, the factor is about 0.005 lower than for the lower pressures. With the survey probe at the z = 7.6-cm (3.0-in.) station the calibration factor is decreased also, but again by about 0.005 or less depending upon Mach number. For most purposes, the calibration can be assumed to be independent of stagnation pressure or probe position in the tunnel.

In order to verify the lateral Mach number distribution in the facility, a vertical and horizontal row of orifices in both the left hand (y = -7.6 cm (-3.0 in.)) and right hand (y = 7.6 cm (3.0 in.)) model-support windows were instrumented for the same runs. The results of this test are presented in figures 29, 30, and 31 for stagnation pressures of 207 kN/m^2 (30 lb/in^2), 414 kN/m^2 (60 lb/in^2), and 620 kN/m^2 (90 lb/in^2), respectively. The agreement in Mach number distribution between the two sides of the tunnel is considered to be very good. Only small differences are noted at the highest test Mach number for the highest stagnation pressure.

Noise Surveys

Results of the noise measurements are presented as both power-spectra distributions and broadband measurements. The power spectra were obtained only up to a frequency of 8 kHz with a bandwidth of 25 Hz. The broadband measurements were obtained from a root-mean-square meter with a cutoff frequency of about 40 kHz. Typical power-spectra results obtained in the settling chamber are presented in figure 32. The data generally show an increase in magnitude with increase in frequency up to about 1 kHz and a gradual decay in magnitude with further increases in frequency. No predominant spikes are noted and the effects of variation of Mach number are very small. Results obtained in the test section at x = 3.8 cm (1.5 in.) are shown in figures 33 to 35 for different stagnation pressures. For the lowest stagnation pressure (fig. 33), the distribution at M = 0.39 shows peaks at about 150 and 700 Hz with a gradual decrease in magnitude as the frequency is increased. At M = 0.82, the peak at 150 Hz is very dominant and a small spike is noted at about 1500 Hz. As the Mach number reaches sonic and supersonic speeds (figs. 33(c) and (d)), the distribution becomes comparatively flat with the exception of the peak at 150 Hz. At the highest frequencies, the magnitude is about the same for the three higher Mach numbers. Thus, the higher levels indicated at lower frequency at the two lower Mach numbers are probably caused by noise at the choker doors feeding upstream. The peak at 150 Hz is attenuated slightly at sonic and supersonic speeds and is possibly the result of flow through the slotted walls. As the stagnation pressure is

increased (figs. 34 and 35), the trends noted are the same but the magnitude of the oscillating pressure is increased as would be expected.

Results of the broadband measurements are presented in figure 36 for three microphone locations (the settling chamber, test section (x = 3.8 cm (1.5 in.)), and probe location (x = 33 cm (13 in.))), and for the three different stagnation pressures. For the settling-chamber location, the root-mean-square decibel level shows little variation with Mach number as was indicated by the power-spectra distributions. The test-section location shows an increase in the noise level with increasing Mach number up to about M = 0.9. A rapid dropoff in level occurs at M = 1.0 and remains about constant up to the maximum test Mach number. The reduced noise level at the supersonic speeds was indicated by the power-spectra data and by results from the noise generated in the choker-door region not feeding back upstream at these velocities. Results from the microphone located in the region of the survey probe show essentially the same trends as those observed for the test section, but the levels were slightly higher. The data for the different stagnation pressures were normalized to atmospheric pressure and are shown in the figure by flagged symbols. The normalized data show excellent agreement.

Figure 37 shows these normalized data compared with results from other Langley facilities and from one Ames Research Center facility. Results in the settling chamber show that, for Mach numbers of 0.6 to the maximum tested, the noise level in the 6- by 28-inch tunnel is within about 5 dB of the other facilities. At M = 0.3, the 8-foot transonic pressure tunnel (TPT) and 16-foot transonic tunnel (TT) both show much lower values. These are both continuous-flow facilities and, at this Mach number, the fans are operating at a relatively low speed. The pilot injector tunnel shows levels more on the order of the 6- by 28-inch transonic tunnel (TT), probably because of the noise associated with the injector nozzle. In the test section, the noise levels for the 6- by 28-inch TT and the 16-foot TT are in close agreement at Mach numbers above about 0.8. The data for the Ames 11-foot transonic tunnel (TT), taken from reference 4, show a slightly higher noise level at the higher Mach numbers.

Test-Section Total-Pressure Survey

In order to make a tunnel-empty total-pressure survey in the region of the traversing probe mechanism, the pitot probe shown in figure 10 was used. A low-volume, low-range, differential pressure transducer was connected to the probe with the minimum tubing possible. The reference side of the transducer was connected to an upstream total-pressure probe so that the output of the transducer should be zero if no total-pressure loss occurs. The response time of the probe and transducer system to a step pressure

input was determined by bench tests, and the results are presented in figure 38. For the probe, interconnecting tubing, and low-volume transducer, the response time to a step pressure input of one-half the maximum transducer capability is about 30 ms. The rise time for the step pressure input is less than 1 ms as indicated by the lower trace on the oscilloscope record. The center photograph in figure 38 shows that the response time can be almost halved by increasing the diameter of the probe by 50 percent. The bottom photograph, for the transducer alone, shows its response time to be on the order of 5 ms. Although the response time could be decreased by increases in probe diameter, a large probe would not be acceptable for the purposes for which the probe was designed. Response time is also decreased on any system when the input pressure is other than a step function. Thus, for the application of the probe in measuring total-pressure changes in the tunnel flow, the system is adequate.

Typical results from the probe for the tunnel-empty condition are presented in figure 39. These oscilloscope records show oscillations in total pressure of about 0.01q with a filter having a cutoff frequency of 200 kHz. The oscillation is at a frequency slightly greater than 100 Hz and is probably caused by the large peak in the power-spectra distributions of noise which were noted at about this frequency in figure 32. When the cutoff frequency of the filter is reduced to 20 Hz, the amplitude of the oscillation is cut almost in half. For this condition, the data system can track any oscillations which occur in the flow.

CONCLUDING REMARKS

The Langley 6- by 28-inch transonic tunnel is a two-dimensional facility with slotted top and bottom walls which is used for testing two-dimensional airfoil sections. The tunnel is capable of operation from a Mach number of about 0.3 to 1.2 with variable stagnation pressure. For a 15.2 cm (6.0 in.) model chord, the Reynolds number can be held constant at about 10×10^6 for Mach numbers from 0.5 to 1.0, and the maximum Reynolds number at a Mach number of 1.0 is about 15×10^6. Tunnel-empty calibrations show that for Mach numbers below about 1.0 the local Mach number distribution obtained from wall static-pressure orifices varies less than ±0.002 from the average value in the test region occupied by the model. Power-spectra noise distributions in the test section show a large peak at a frequency of about 150 Hz, but no appreciable spikes are noted at higher frequencies. The broadband noise data, normalized to 1 atmosphere stagnation pressure, show the noise level in this facility to be about the same, when compared at the same test conditions, as that in two large continuous transonic facilities. Data obtained from a total-pressure probe in the test section show that oscillations in total pressure at a Mach number of 0.7 have a magnitude of approximately 1 percent of dynamic pressure at a frequency

of about 100 Hz. Electrical filters in the transducer output are provided to damp this oscillation so that the data-acquisition system can track the pressure adequately.

Langley Research Center
National Aeronautics and Space Administration
Hampton, Va. 23665
October 16, 1975

REFERENCES

1. Ladson, Charles L.: Description and Calibration of the Langley 6- by 19-Inch Transonic Tunnel. NASA TN D-7182, 1973.

2. Schaefer, William T., Jr.: Characteristics of Major Active Wind Tunnels at the Langley Research Center. NASA TM X-1130, 1965.

3. Bynum, D. S.; Ledford, R. L.; and Smotherman, W. E.: Wind Tunnel Pressure Measuring Techniques. AGARD-AG-145-70, Dec. 1970.

4. Dods, Jules B., Jr.; and Hanly, Richard D.: Evaluation of Transonic and Supersonic Wind-Tunnel Background Noise and Effects of Surface Pressure Fluctuation Measurements. AIAA Paper No. 72-1004, Sept. 1972.

L-75-224

Figure 1.- Photograph of overall view of the Langley 6- by 28-inch transonic tunnel during assembly.

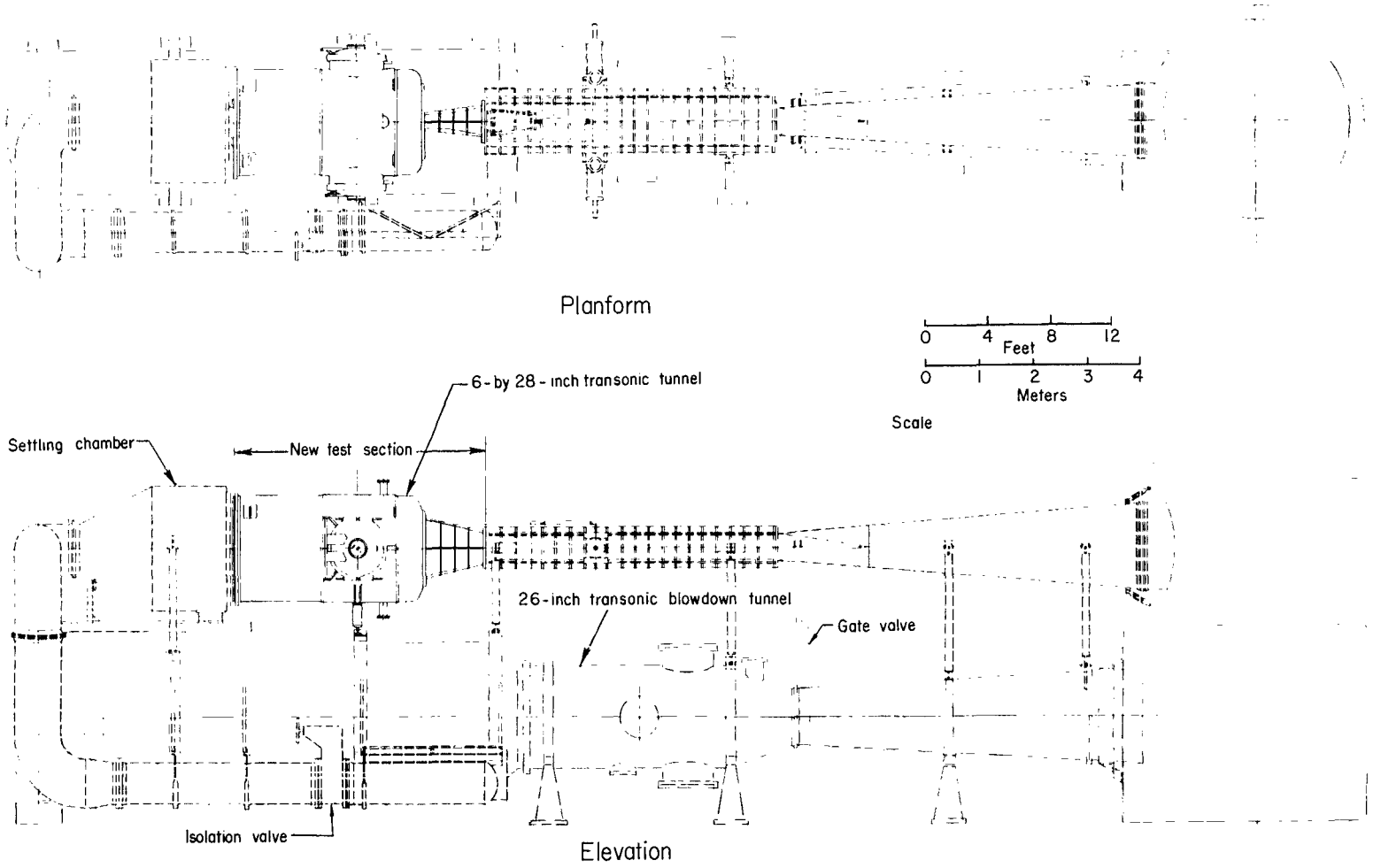

Figure 2.- Assembly drawing of the Langley 6- by 28-inch transonic tunnel.

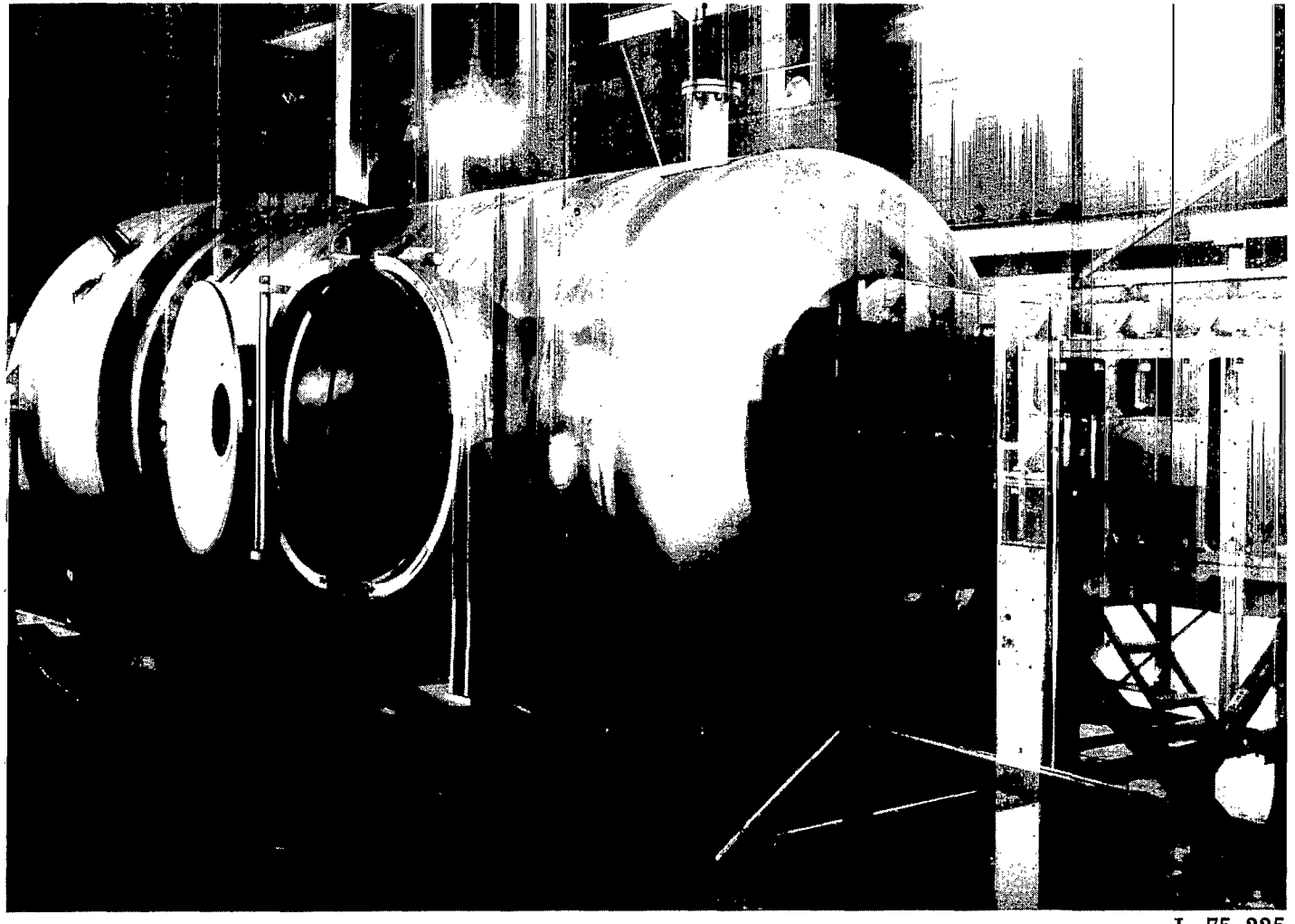

L-75-225

Figure 3.- Photograph of exterior view of pressure shell and access hatch taken during assembly.

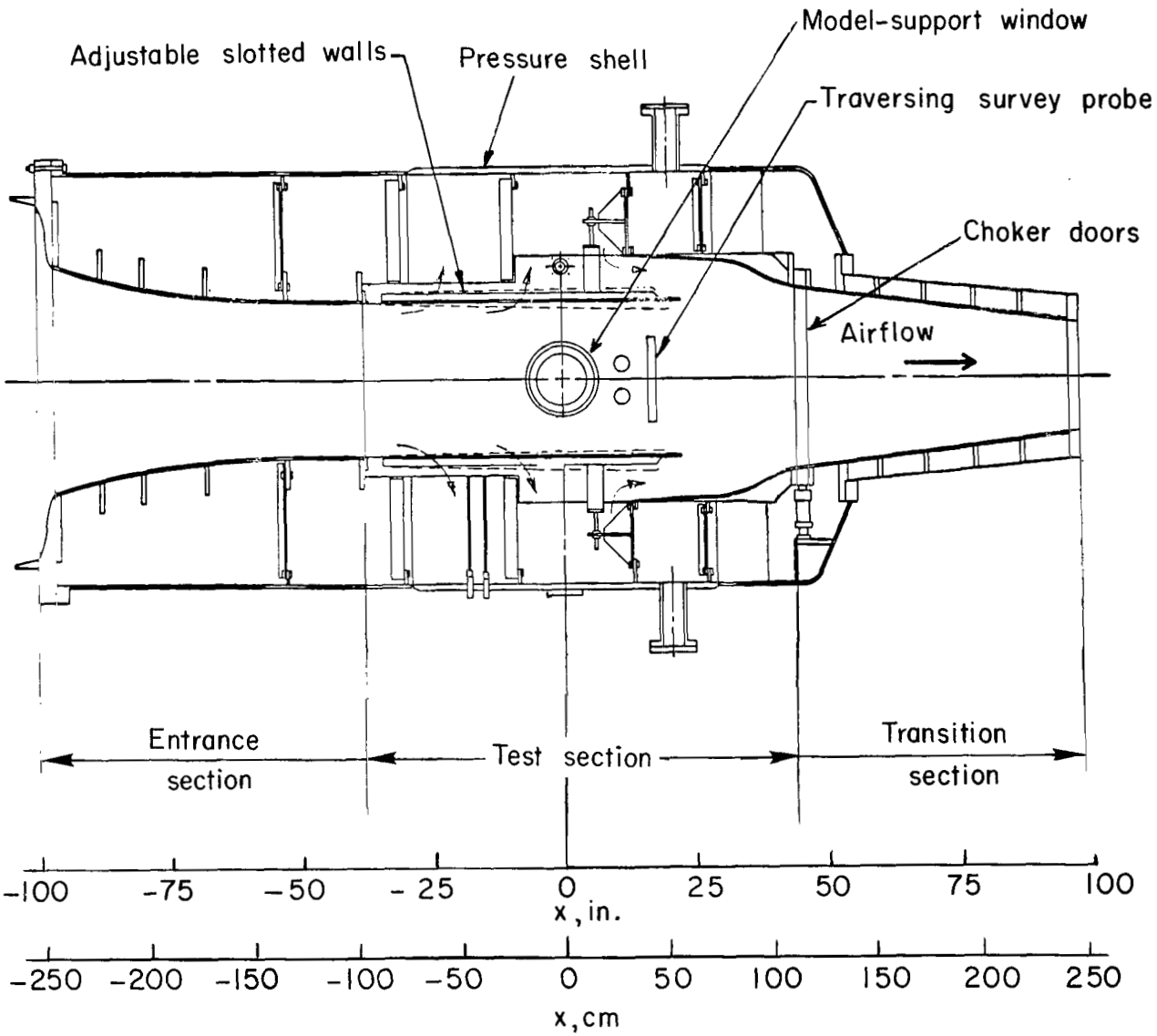

Figure 4.- Cross-section drawing of the test section of the Langley 6- by 28-inch transonic tunnel.

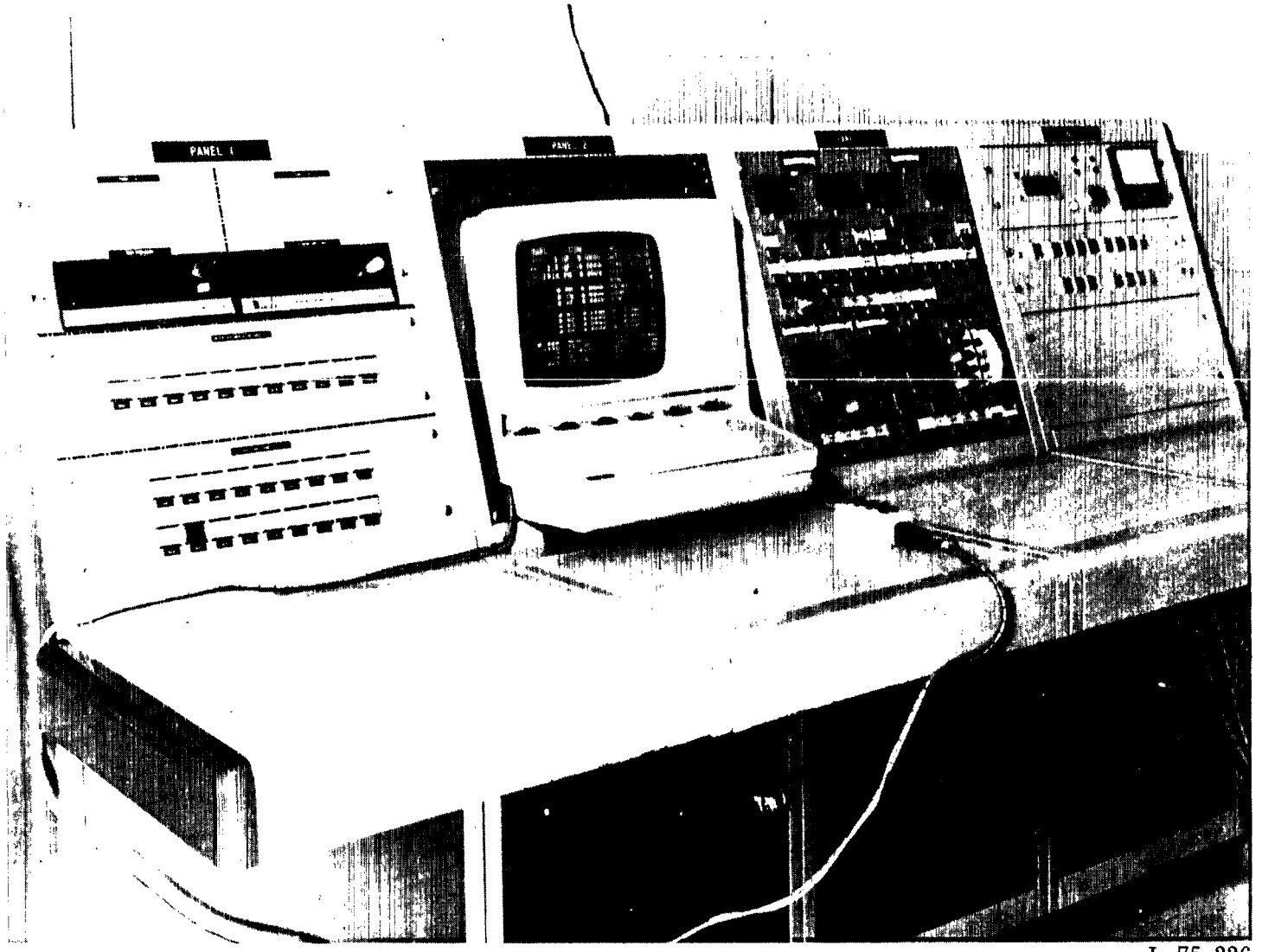

L-75-226

Figure 5.- Photograph of tunnel operator's control console.

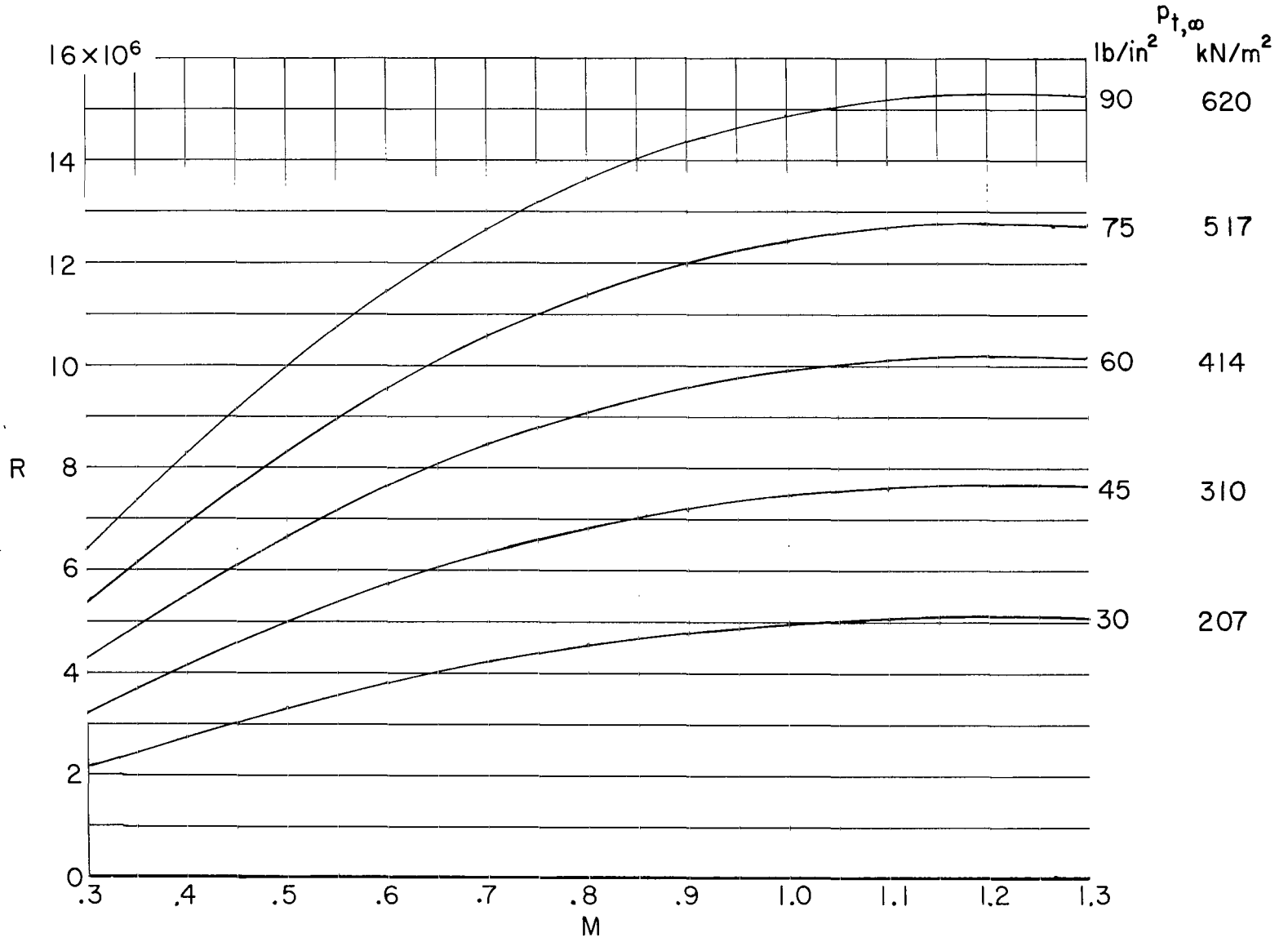

Figure 6.- Reynolds number capability of the Langley 6- by 28-inch transonic tunnel. T_t = 283 K (510° R); c = 15.24 cm (6.00 in.).

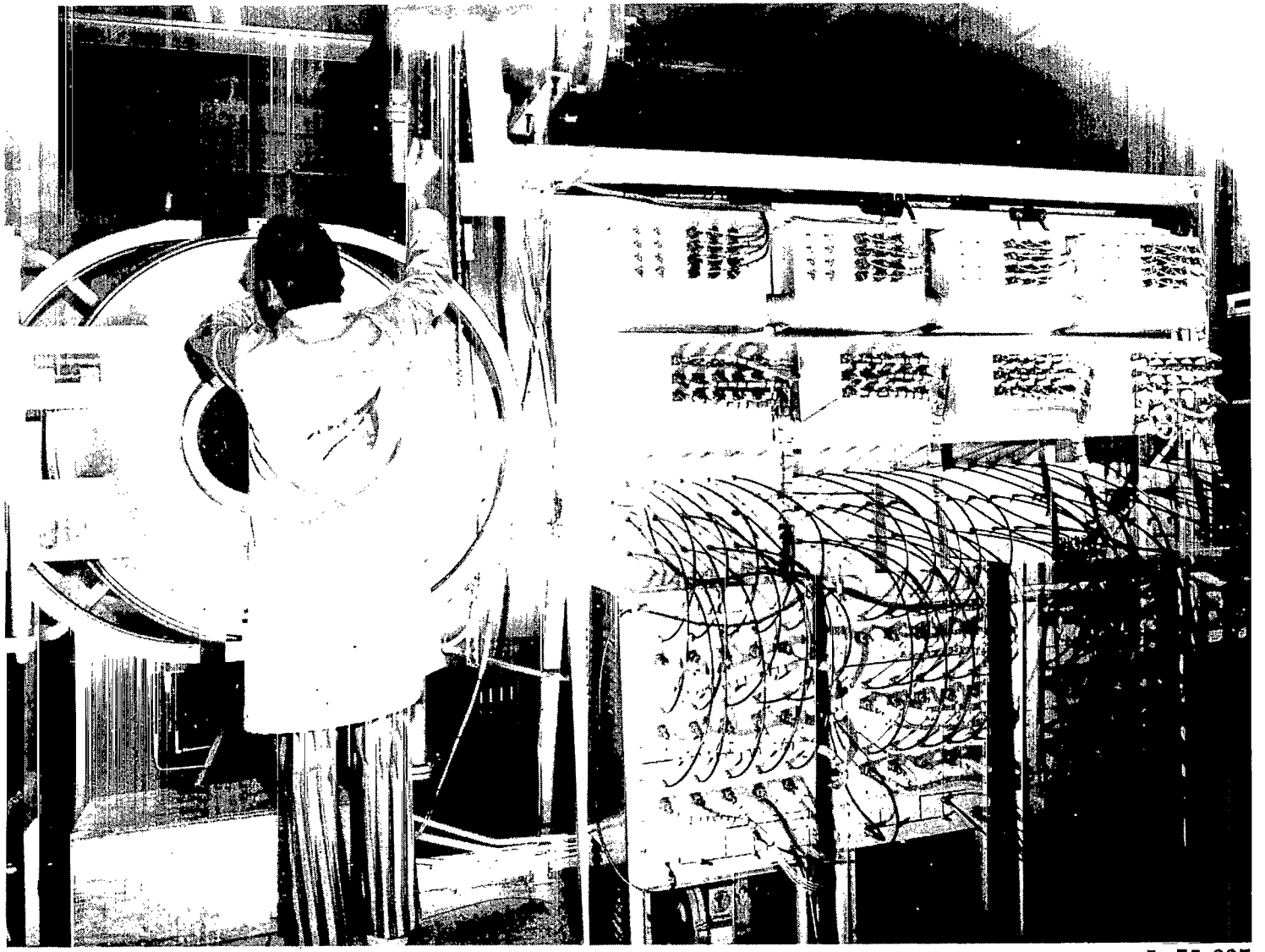

L-75-227

Figure 7.- Photograph of exterior view of tunnel showing access hatch and racks of pressure instrumentaion.

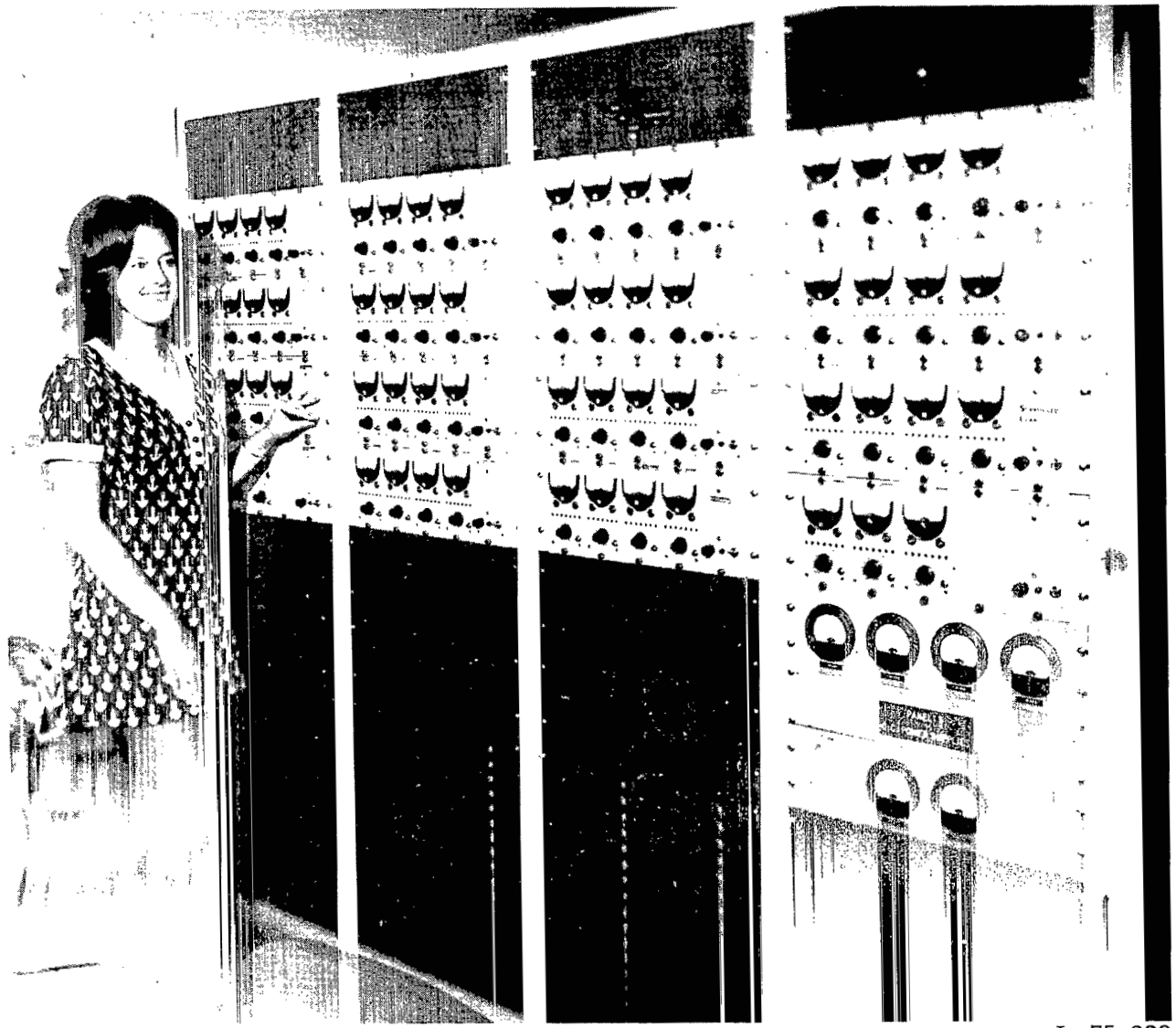

L-75-228

Figure 8.- Photograph of autoranging signal conditioner for pressure instrumentation.

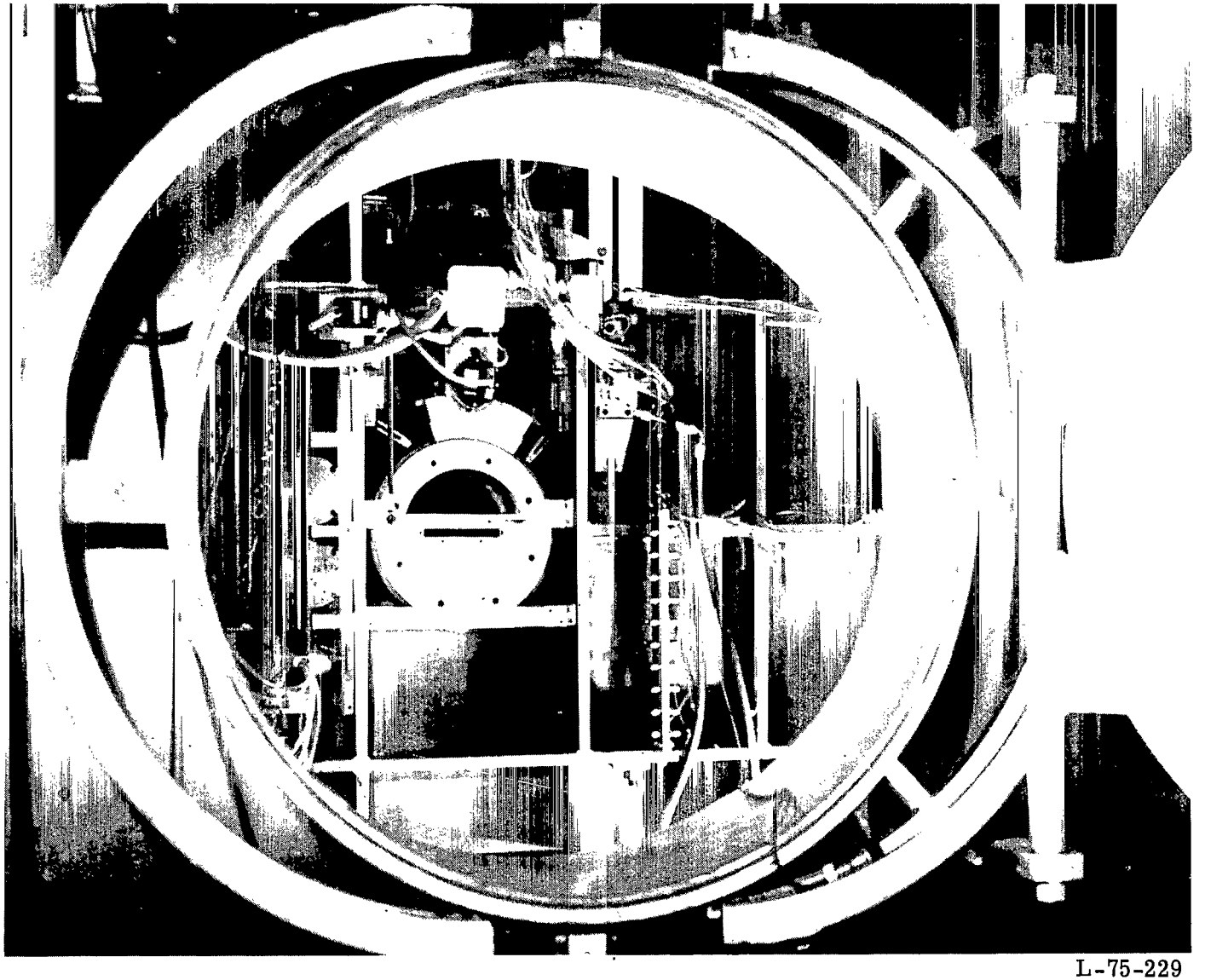

L-75-229

Figure 9.- Photograph of interior view of tunnel showing test-section area, model-support window, and traversing survey-probe mechanism.

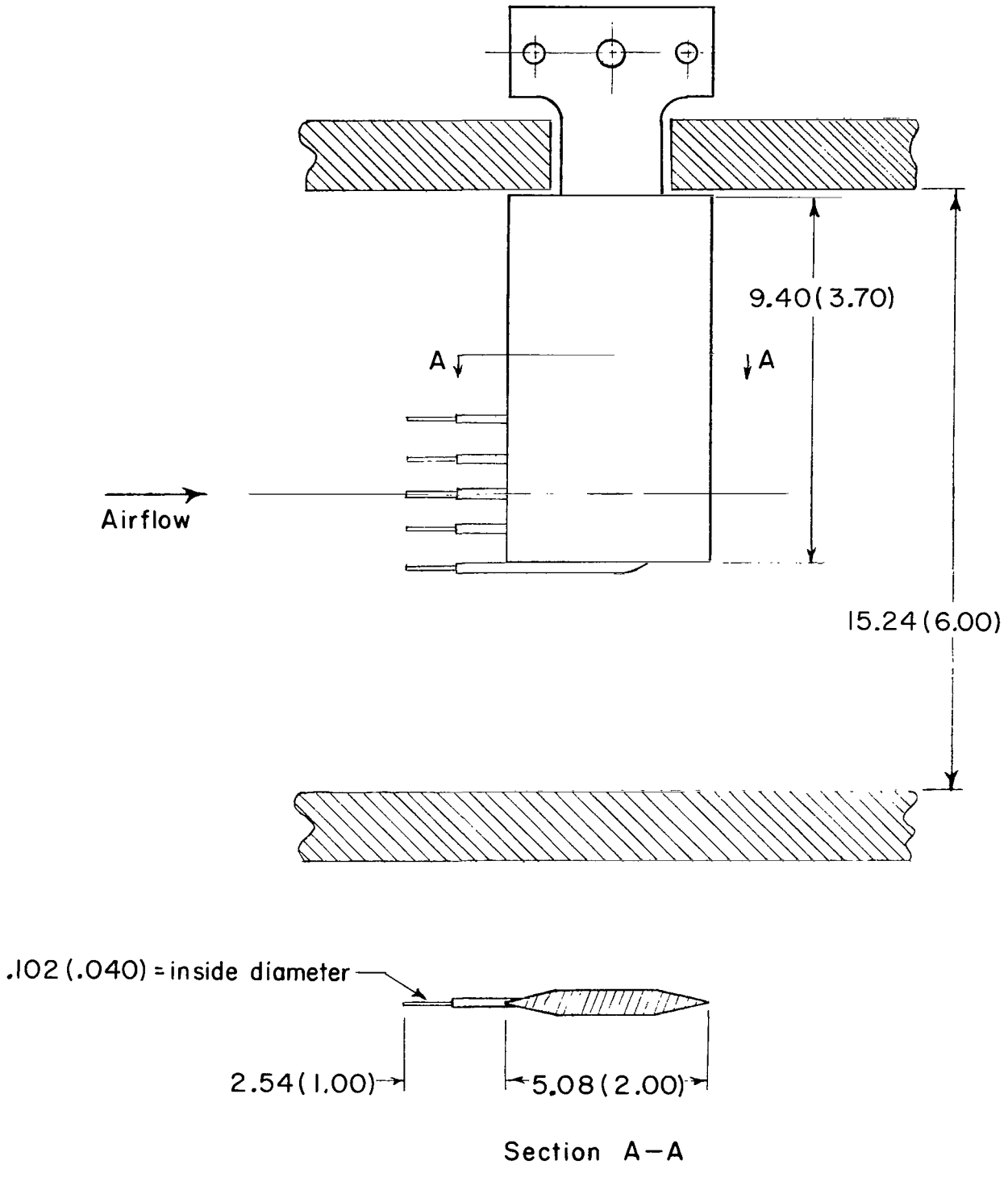

Figure 10.- Details of pitot-tube probe used on traversing survey mechanism. Dimensions are given in cm (in.).

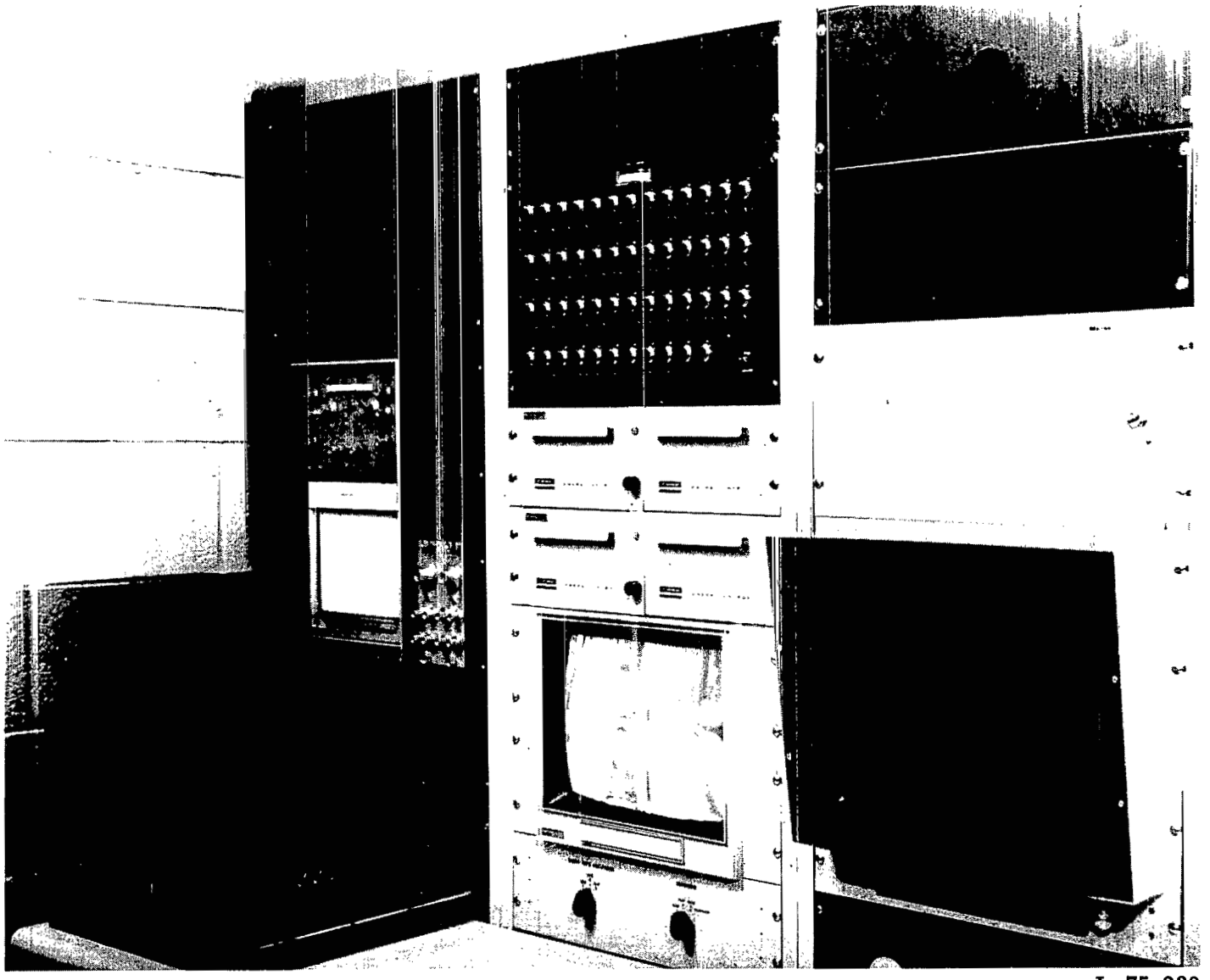

L-75-230

Figure 11.- Photograph of real-time display console.

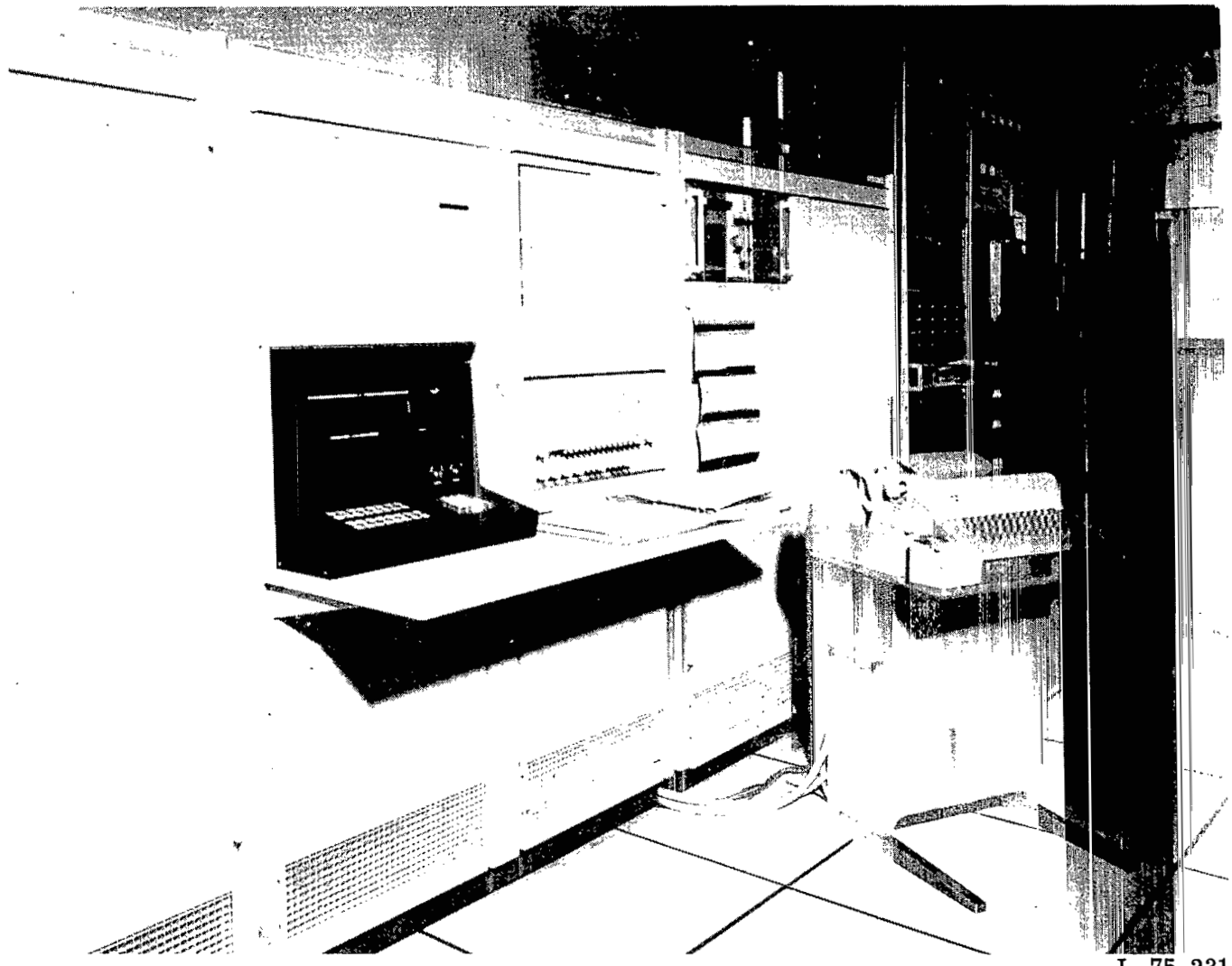

L-75-231

Figure 12.- Photograph of overall view of data-acquisition system showing computer and teletype input.

L-75-232

Figure 13.- Photograph of high-speed tape deck used with data-acquisition system for recording data.

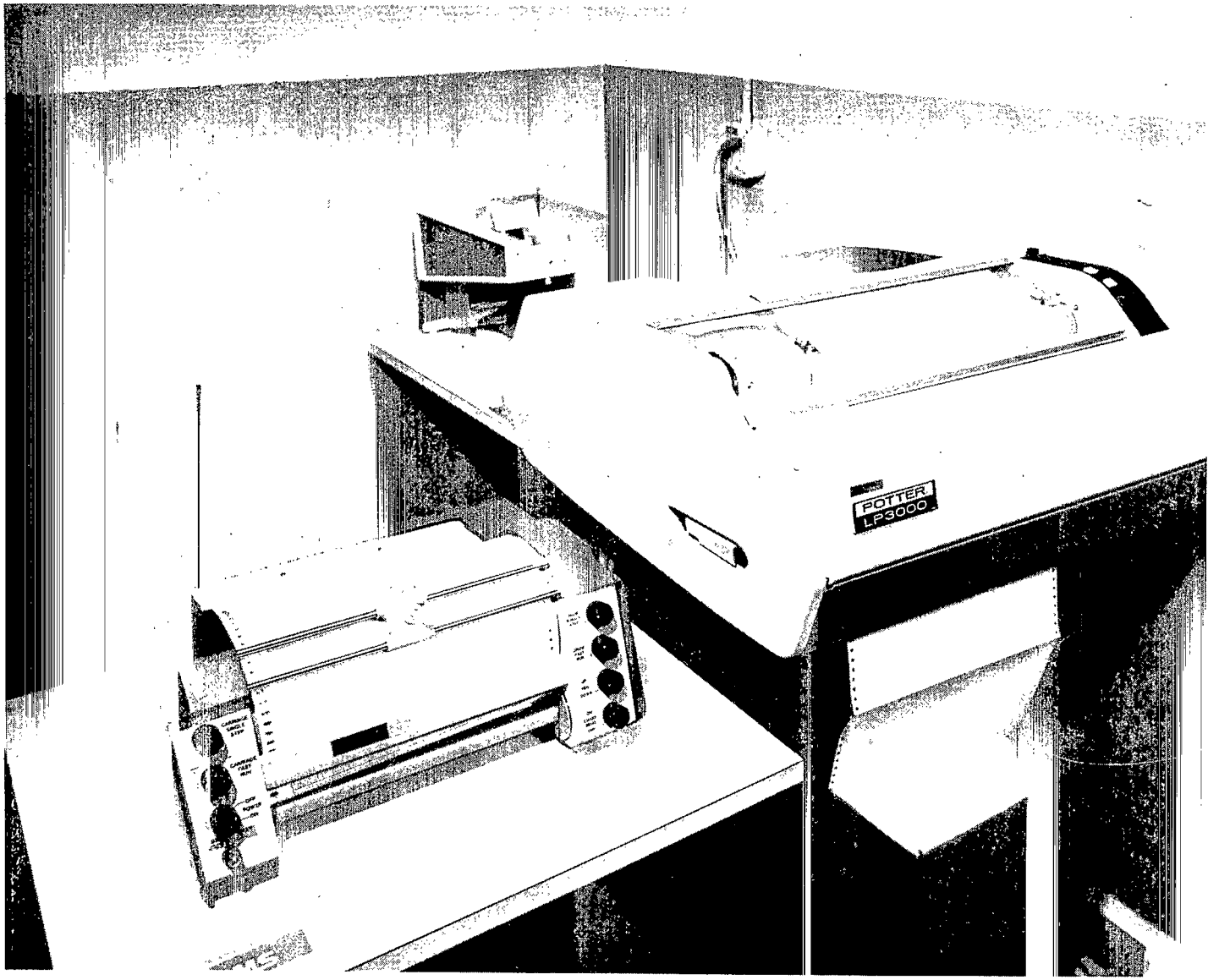

L-75-233

Figure 14.- Photograph of card reader, plotter, and line printer used with data-acquisition system.

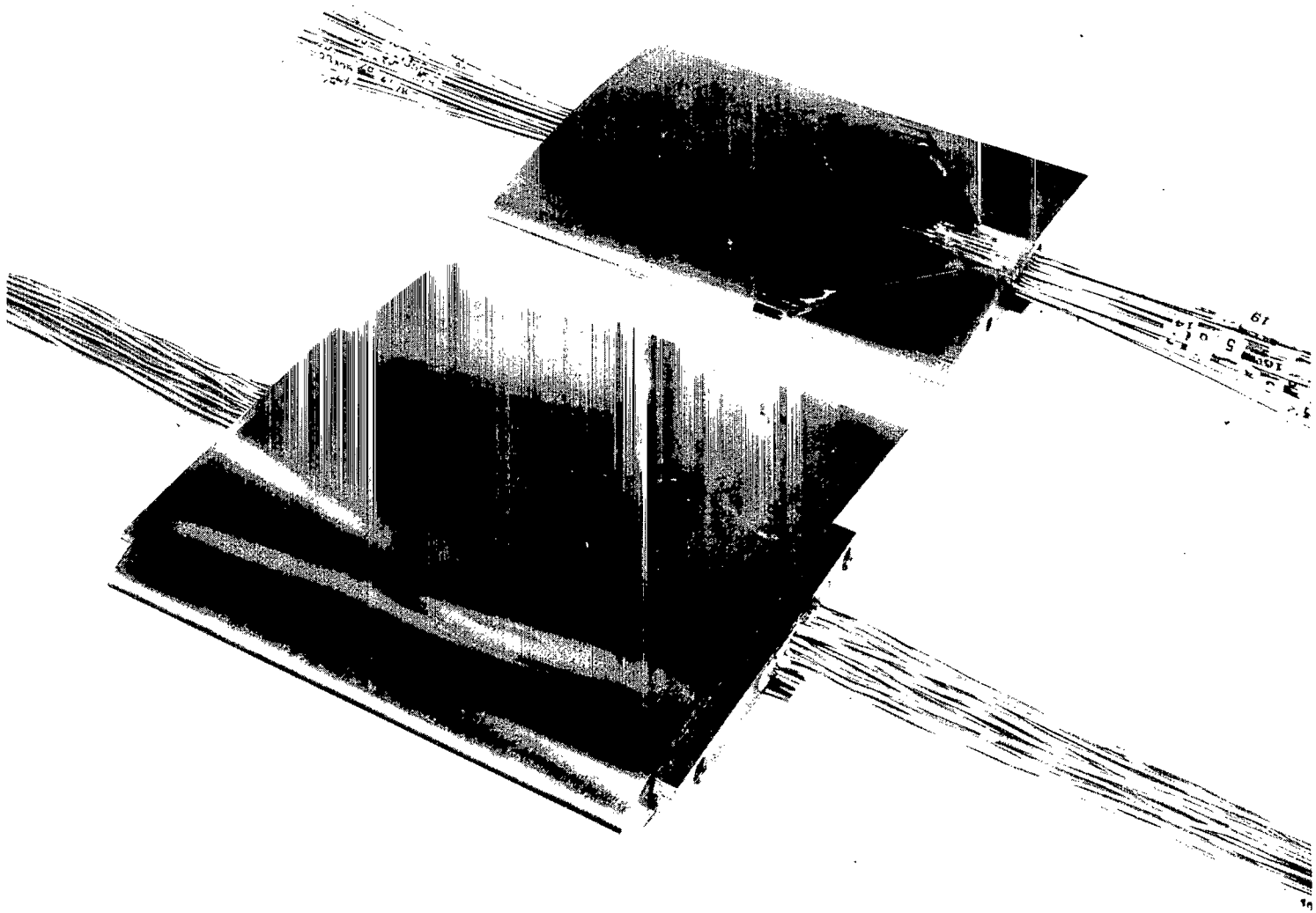

L-75-234

Figure 15.- Photograph of typical airfoil models instrumented for pressure tests. 15.2 cm (6.0 in.) chord in foreground; 10.16 cm (4.0 in.) chord in background.

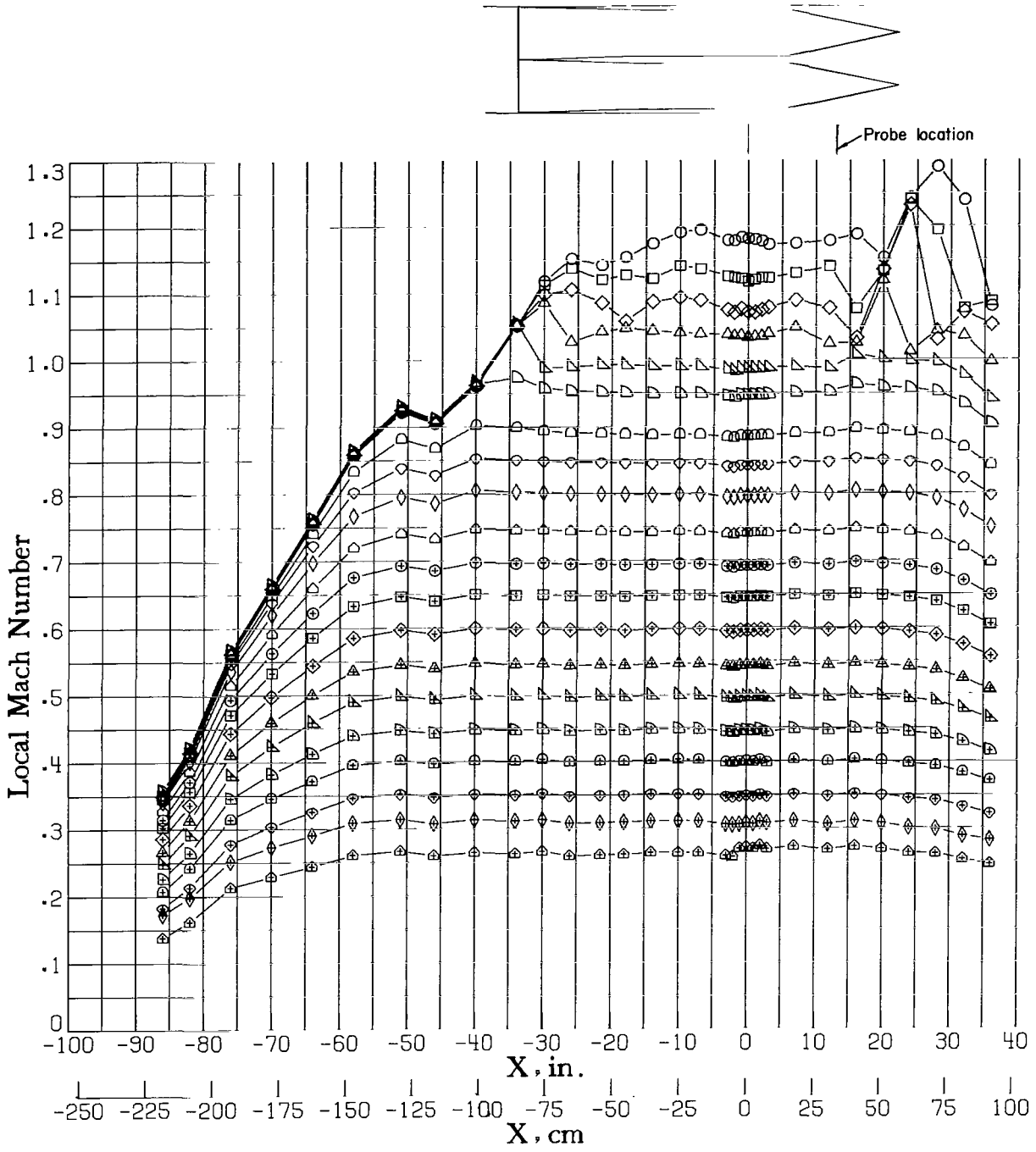

(a) Orifice row at z = 7.6 cm (3.0 in.).

Figure 16.- Longitudinal sidewall Mach number distribution with traversing survey probe at z = -29.2 cm (-11.5 in.). $p_{t,\infty}$ = 207 kN/m^2 (30 lb/in^2).

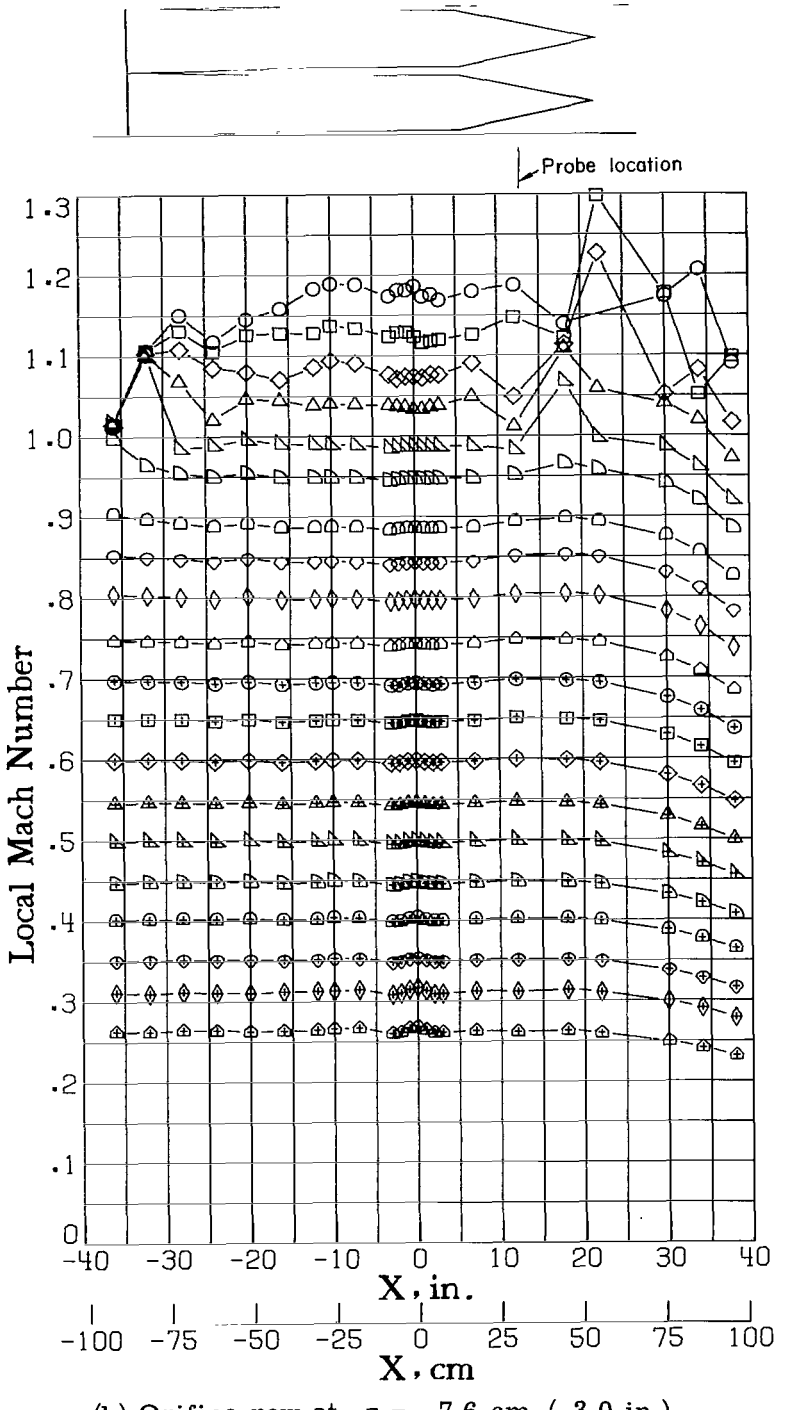

(b) Orifice row at z = -7.6 cm (-3.0 in.).

Figure 16.- Concluded.

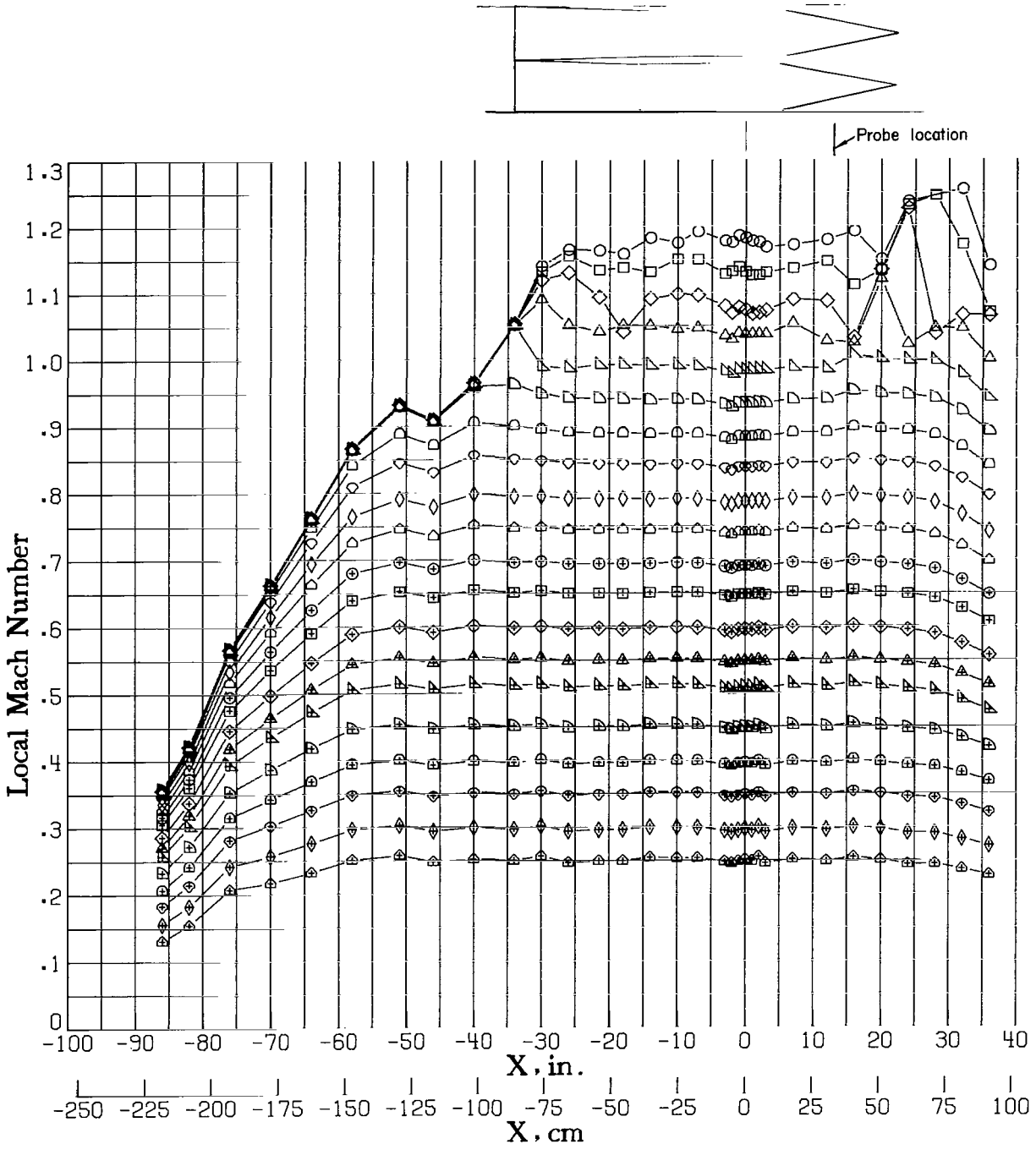

(a) Orifice row at z = 7.6 cm (3.0 in.).

Figure 17.- Longitudinal sidewall Mach number distribution with traversing survey probe at z = -29.2 cm (-11.5 in.). $p_{t,\infty}$ = 414 kN/m^2 (60 lb/in^2).

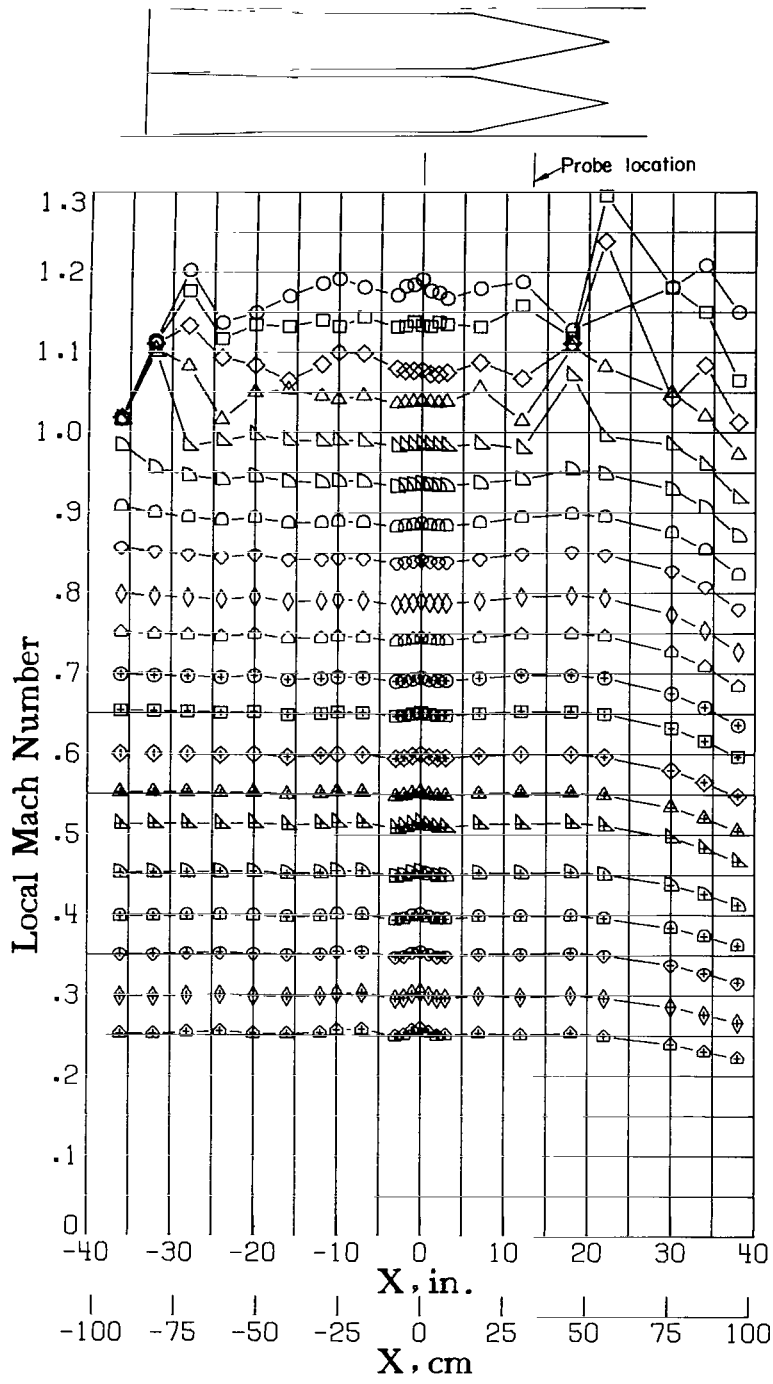

(b) Orifice row at z = -7.6 cm (-3.0 in.).

Figure 17.- Concluded.

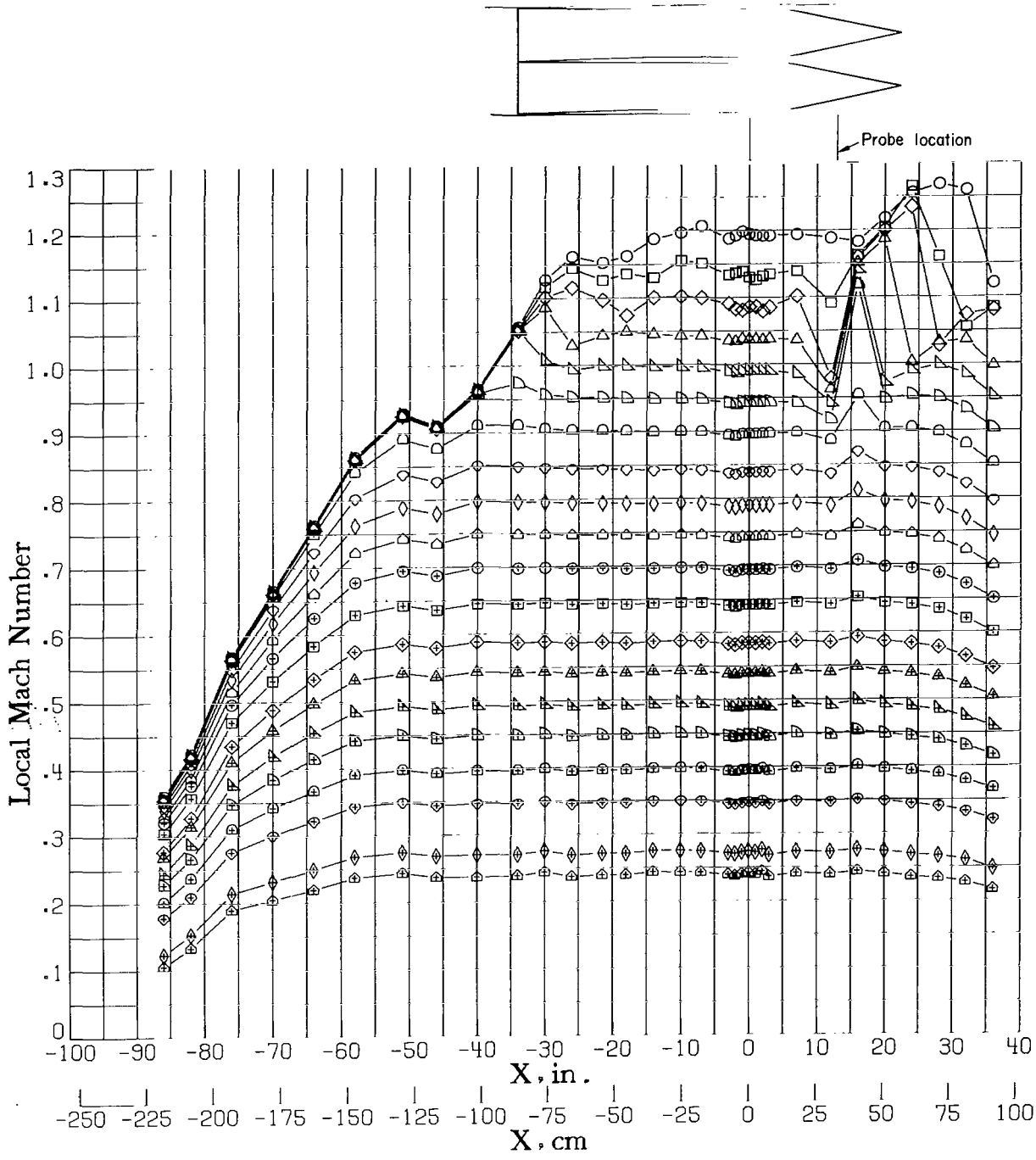

(a) Orifice row at z = 7.6 cm (3.0 in.).

Figure 18.- Longitudinal sidewall Mach number distribution with traversing survey probe at z = 7.6 cm (3.0 in.). $p_{t,\infty}$ = 207 kN/m^2 (30 lb/in^2).

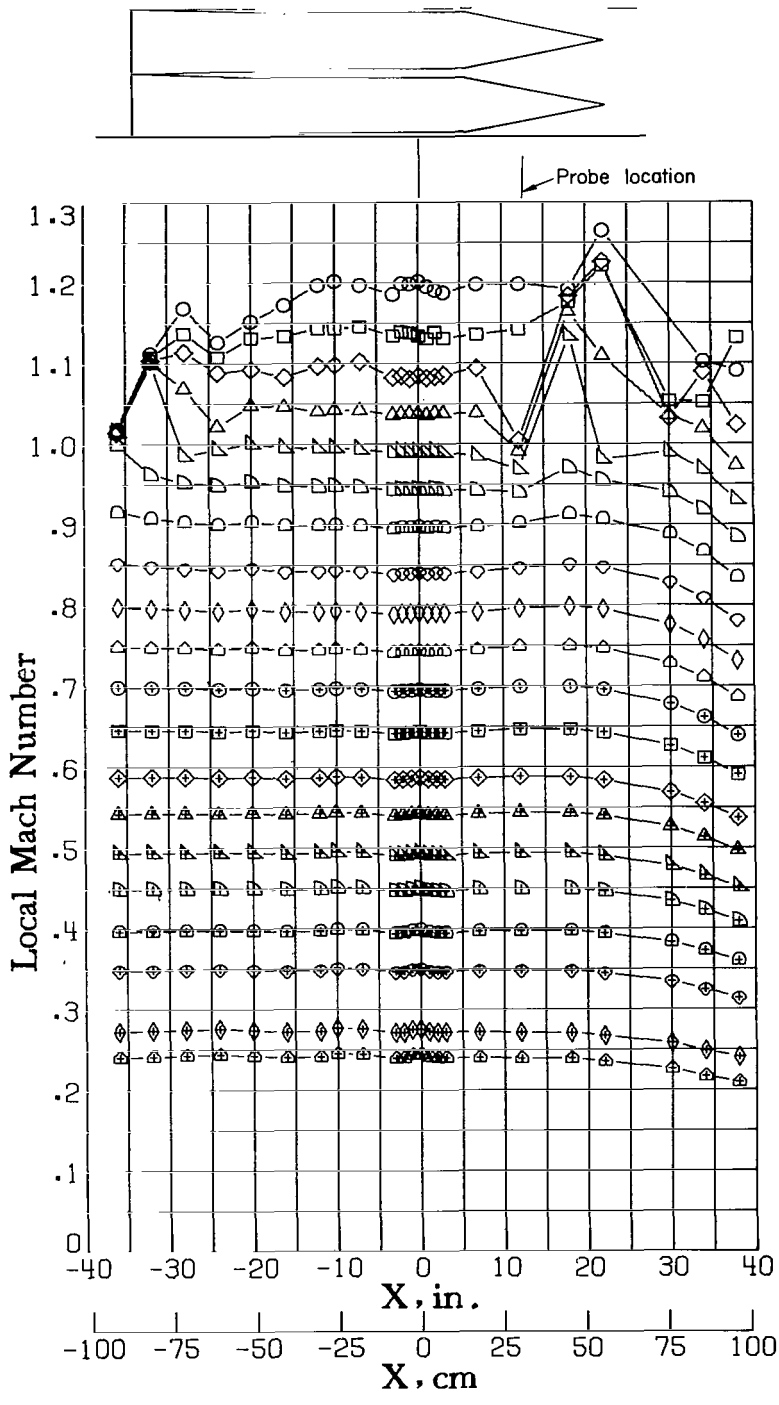

(b) Orifice row at z = -7.6 cm (-3.0 in.).

Figure 18.- Concluded.

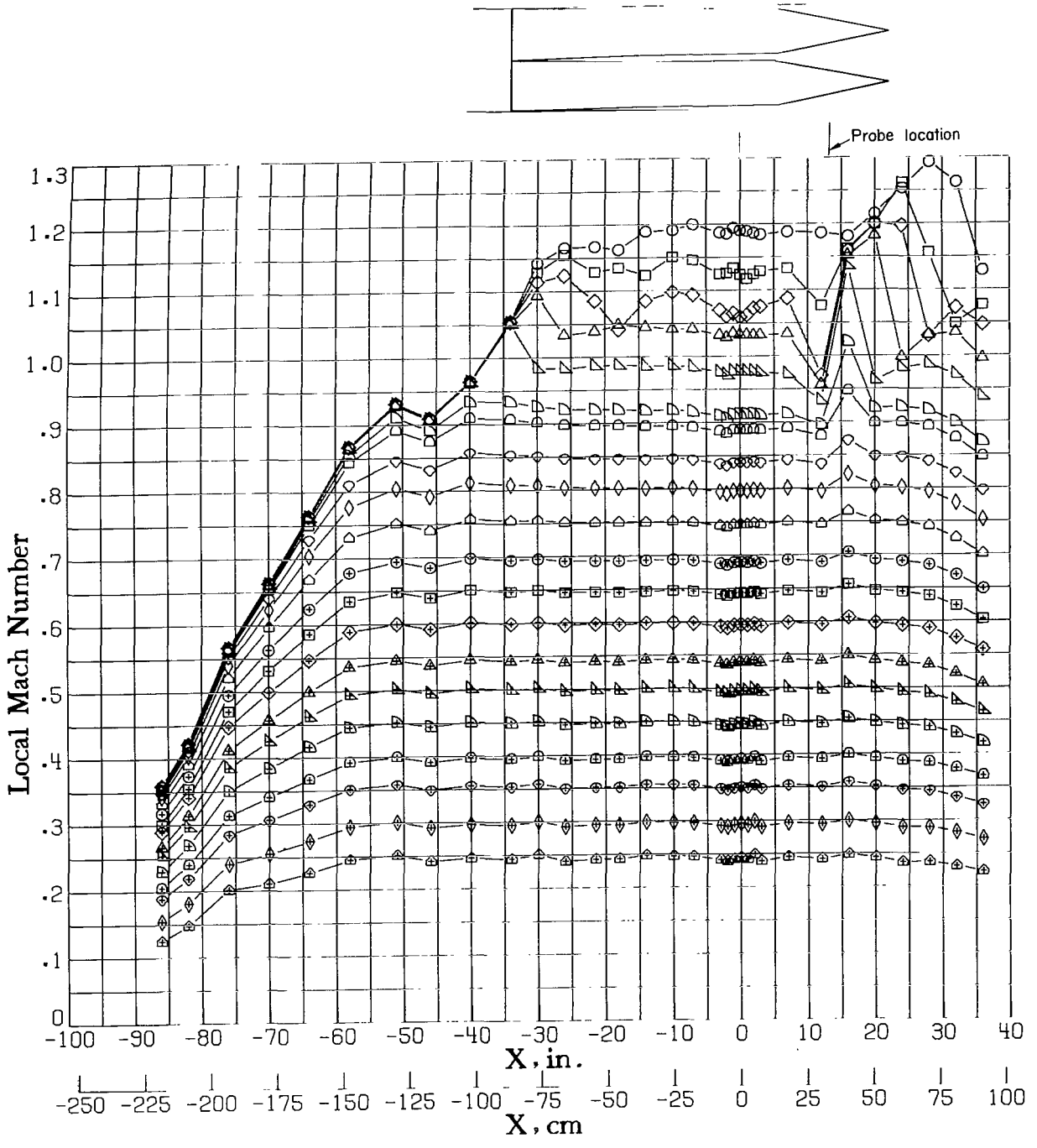

(a) Orifice row at z = 7.6 cm (3.0 in.).

Figure 19.- Longitudinal sidewall Mach number distribution with traversing survey probe at z = 7.6 cm (3.0 in.). $p_{t,\infty}$ = 414 kN/m^2 (60 lb/in^2).

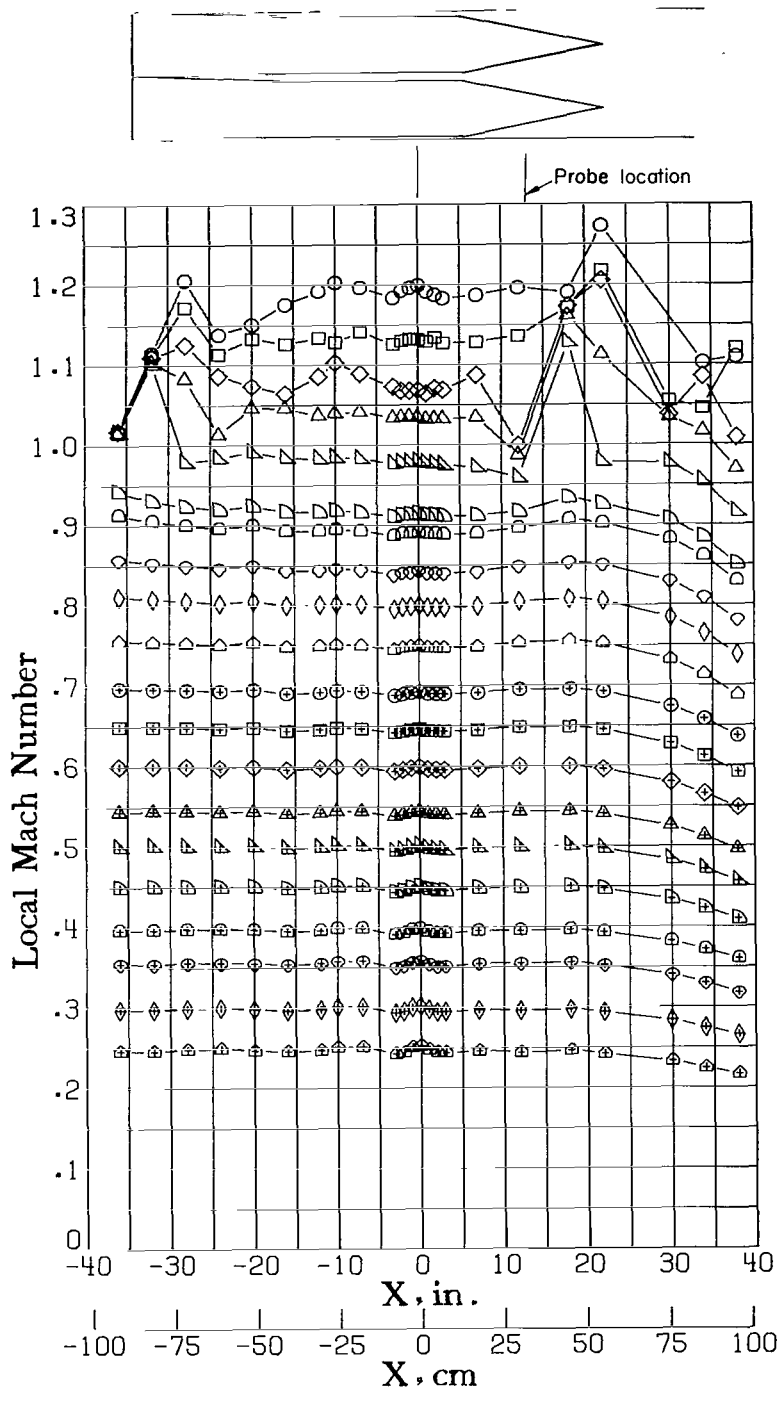

(b) Orifice row at z = -7.6 cm (-3.0 in.).

Figure 19.- Concluded.

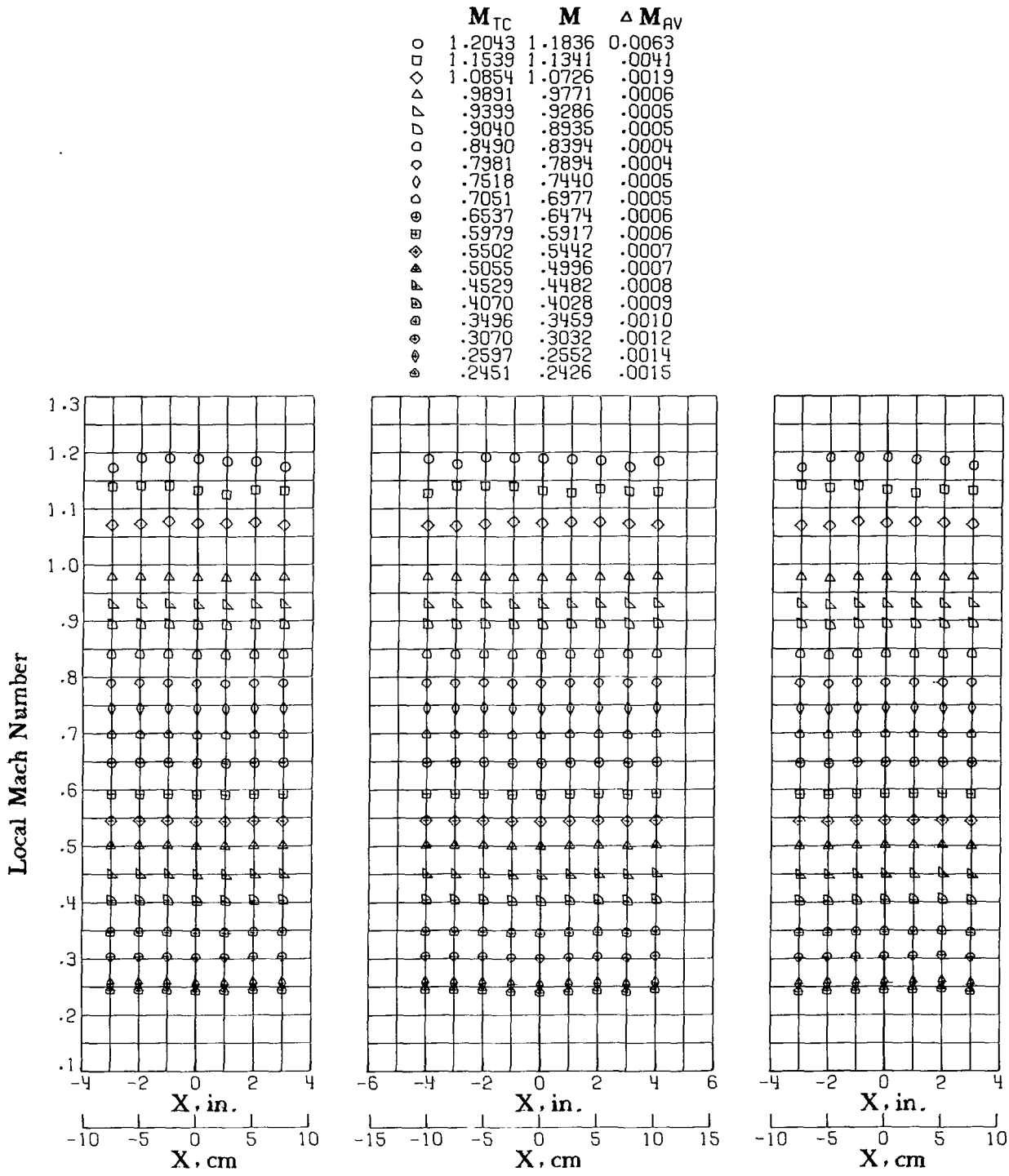

(a) Longitudinal distribution at z = -7.6 cm (-3.0 in.).

(b) Longitudinal distribution at z = 0.0 cm (0.0 in.).

(c) Longitudinal distribution at z = 7.6 cm (3.0 in.).

Figure 20.- Sidewall Mach number distribution in region occupied by model with traversing survey probe at z = -29.2 cm (-11.5 in.). $p_{t,\infty}$ = 207 kN/m^2 (30 lb/in^2).

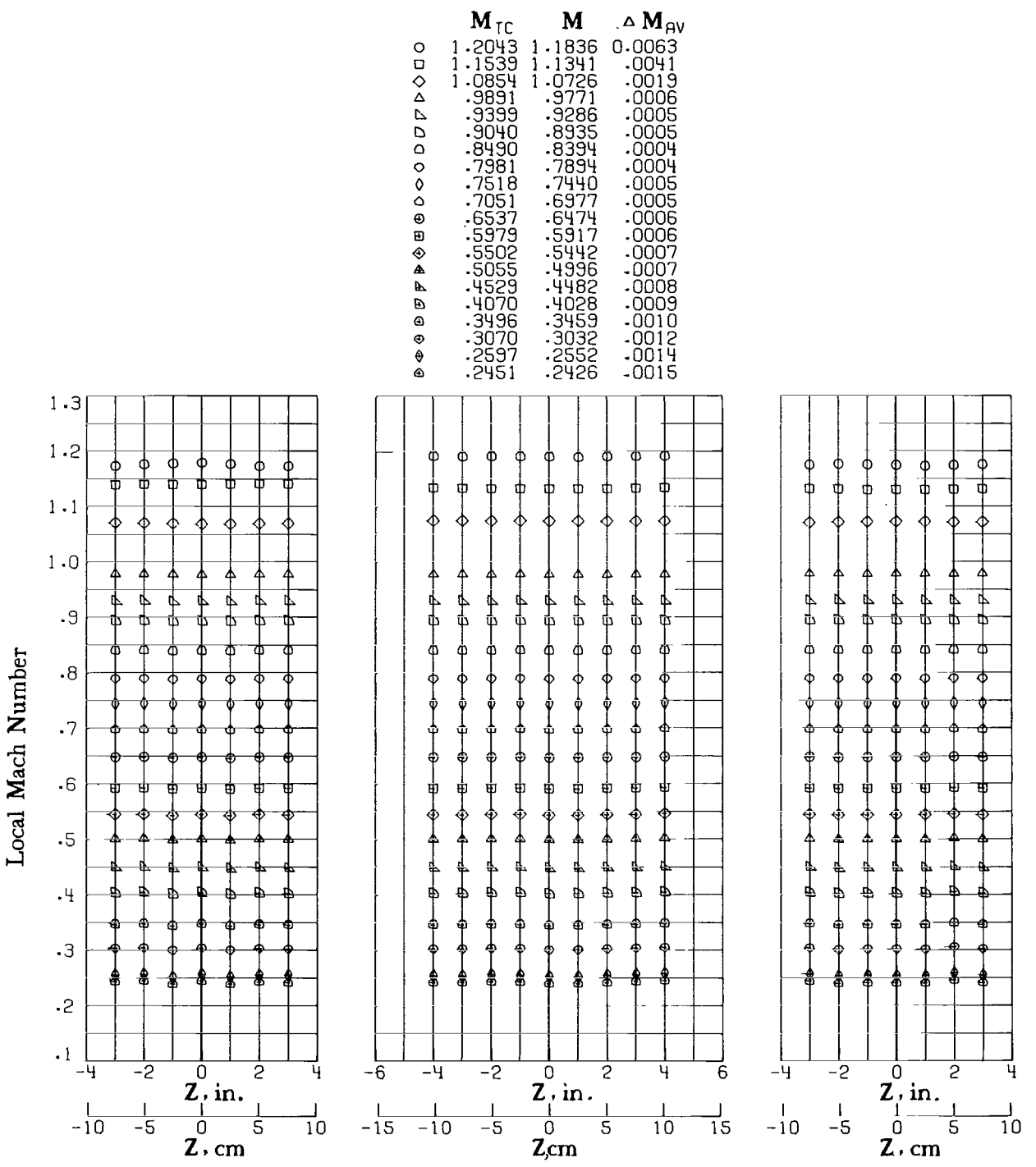

(d) Vertical distribution at x = -7.6 cm (-3.0 in.).

(e) Vertical distribution at x = 0.0 cm (0.0 in.).

(f) Vertical distribution at x = 7.6 cm (3.0 in.).

Figure 20.- Concluded.

	M_{TC}	M	ΔM_{AV}
○	1.2365	1.2190	0.0018
□	1.1272	1.1065	.0029
◇	1.0917	1.0744	.0014
△	1.0332	1.0176	.0012
▽	.9511	.9390	.0007
▷	.9389	.9270	.0007
◁	.8837	.8732	.0007
⬡	.7594	.7513	.0007
◇	.6935	.6852	.0008
△	.6514	.6441	.0008
⊕	.6033	.5968	.0009
⊞	.5510	.5449	.0010
◈	.5038	.4976	.0011
▲	.4476	.4421	.0012
◣	.3939	.3887	.0013
⊞	.3063	.3027	.0017
⊕	.2416	.2384	.0021
⊕	.2043	.2023	.0025

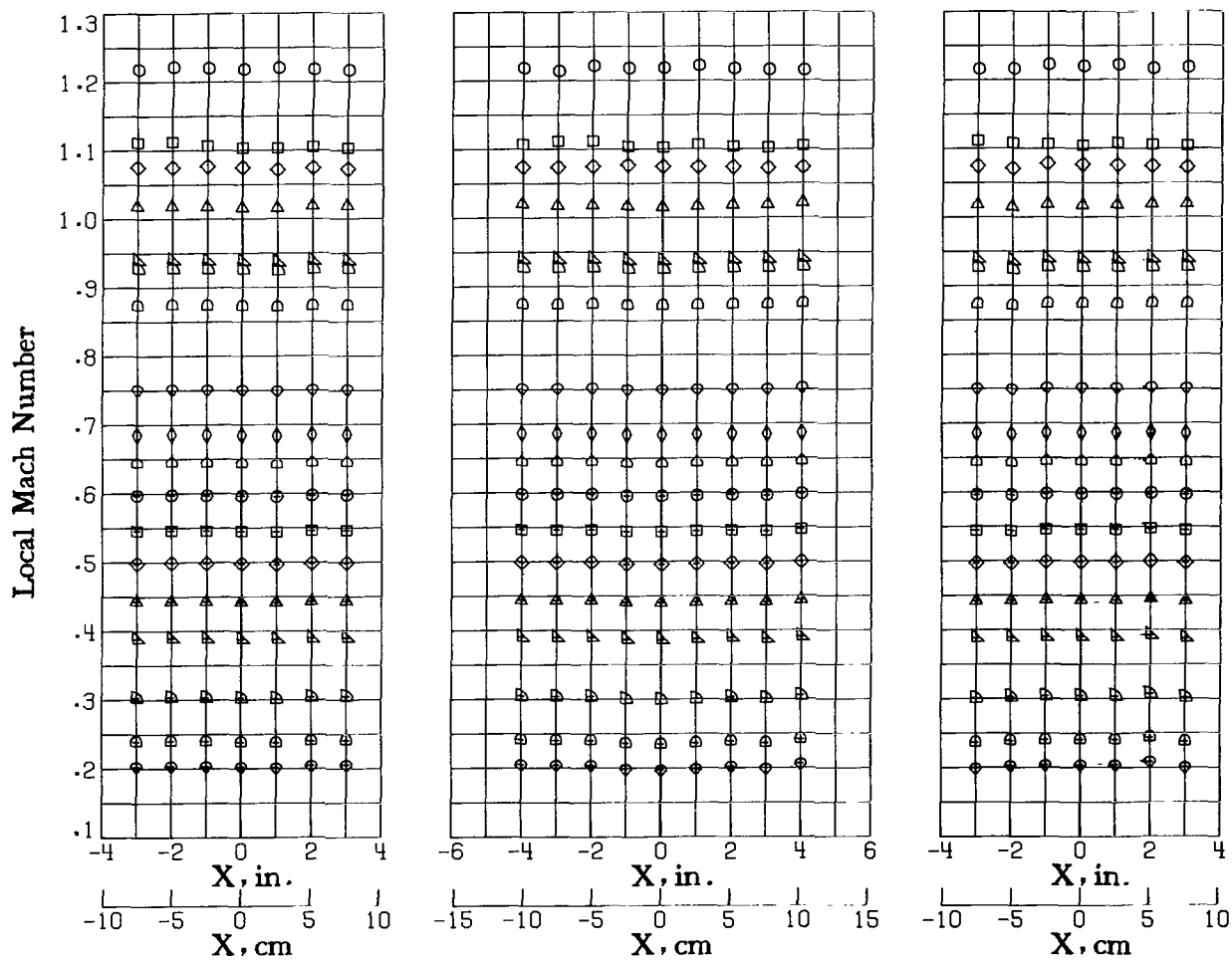

(a) Longitudinal distribution at z = -7.6 cm (-3.0 in.).

(b) Longitudinal distribution at z = 0.0 cm (0.0 in.).

(c) Longitudinal distribution at z = 7.6 cm (3.0 in.).

Figure 21.- Sidewall Mach number distribution in region occupied by model with traversing survey probe at z = -29.2 cm (-11.5 in.). $p_{t,\infty}$ = 310 kN/m^2 (45 lb/in^2).

	M_{TC}	M	ΔM_{AV}
○	1.2365	1.2190	0.0018
□	1.1272	1.1065	.0029
◇	1.0917	1.0744	.0014
△	1.0332	1.0176	.0012
◁	.9511	.9390	.0007
▷	.9389	.9270	.0007
⌂	.8837	.8732	.0007
◇	.7594	.7513	.0007
◊	.6935	.6852	.0008
△	.6514	.6441	.0008
⊕	.6033	.5968	.0009
⊞	.5510	.5449	.0010
◈	.5038	.4976	.0011
▲	.4476	.4421	.0012
◣	.3939	.3887	.0013
⊠	.3063	.3027	.0017
⊕	.2416	.2384	.0021
◈	.2043	.2023	.0025

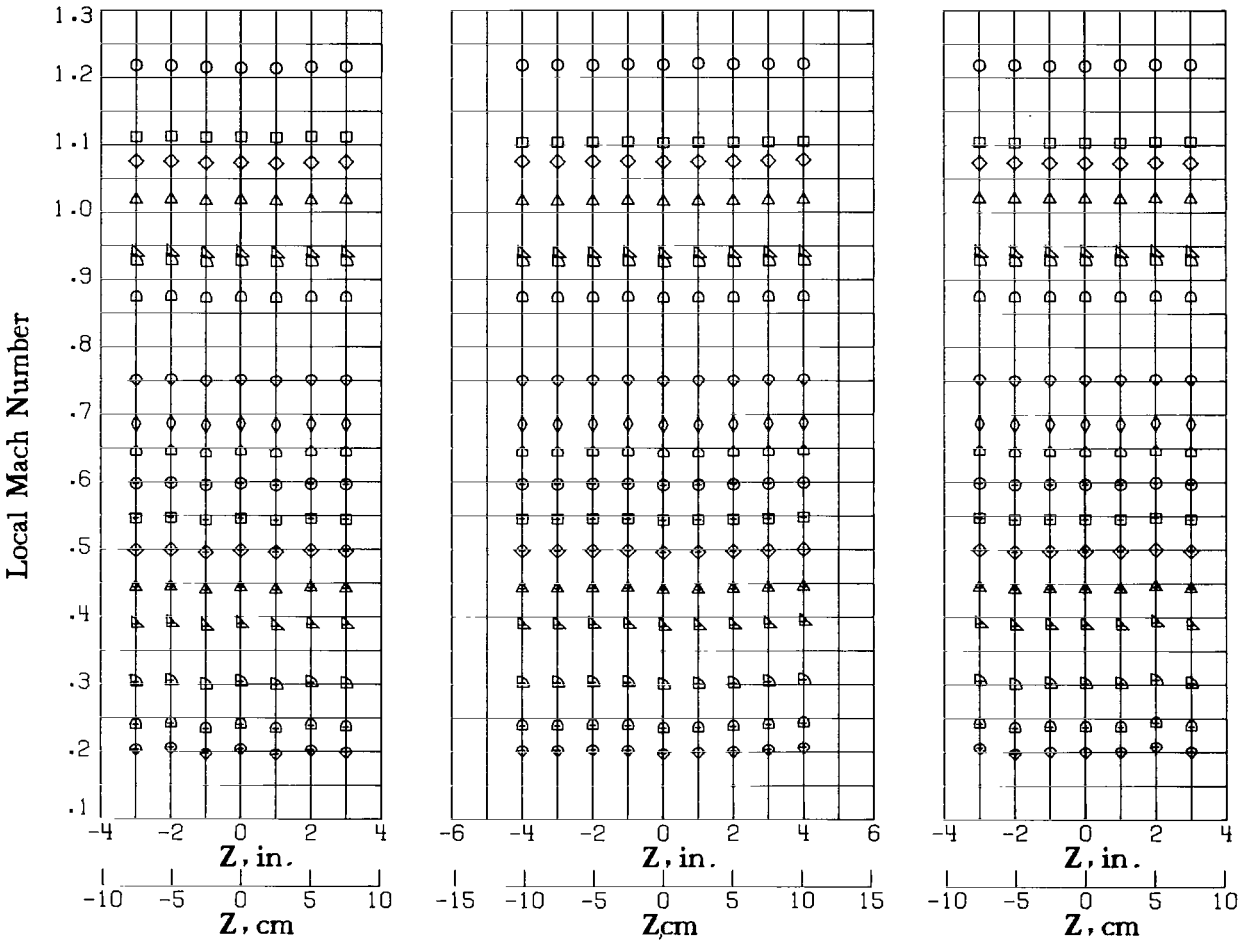

(d) Vertical distribution at x = -7.6 cm (-3.0 in.).

(e) Vertical distribution at x = 0.0 cm (0.0 in.).

(f) Vertical distribution at x = 7.6 cm (3.0 in.).

Figure 21.- Concluded.

	M_{TC}	M	ΔM_{AV}
○	1.1835	1.1650	0.0040
□	1.1540	1.1340	.0039
◇	1.0921	1.0769	.0019
△	1.0160	1.0006	.0012
▷	.8647	.8535	.0009
▱	.7727	.7635	.0009
▱	.6960	.6884	.0010
◇	.5911	.5847	.0011
◇	.5581	.5526	.0012
△	.4840	.4778	.0013
⊕	.4276	.4226	.0014
⊞	.3841	.3794	.0016
◈	.3373	.3339	.0017
⧋	.2887	.2858	.0020

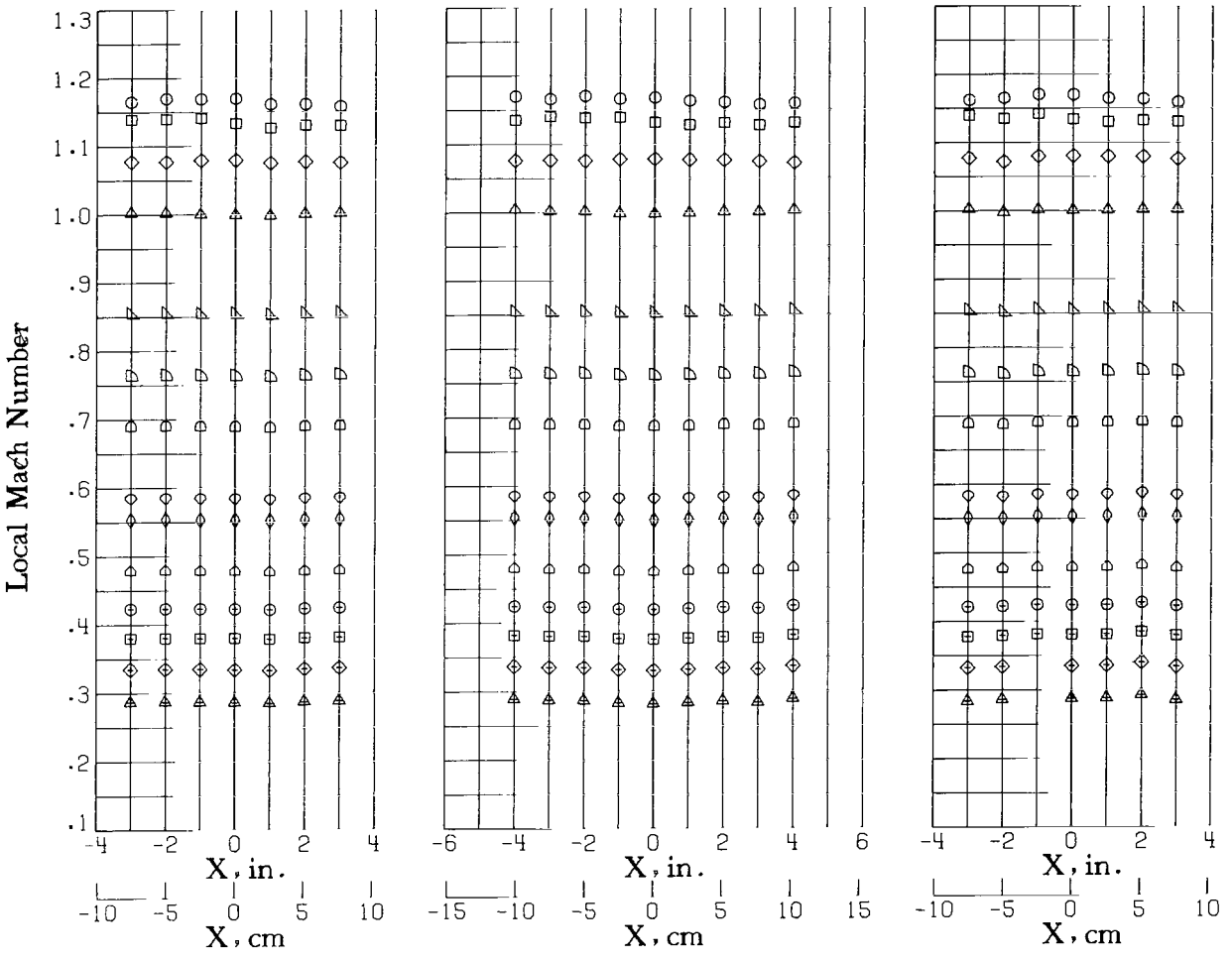

(a) Longitudinal distribution at z = -7.6 cm (-3.0 in.).

(b) Longitudinal distribution at z = 0.0 cm (0.0 in.).

(c) Longitudinal distribution at z = 7.6 cm (3.0 in.).

Figure 22.- Sidewall Mach number distribution in region occupied by model with traversing survey probe at z = -29.2 cm (-11.5 in.). $p_{t,\infty}$ = 414 kN/m^2 (60 lb/in^2).

	M_{TC}	M	ΔM_{AV}
○	1.1835	1.1650	0.0040
□	1.1540	1.1340	.0039
◇	1.0921	1.0769	.0019
△	1.0160	1.0006	.0012
◸	.8647	.8535	.0009
◗	.7727	.7635	.0009
▱	.6960	.6884	.0010
◇	.5911	.5847	.0011
◇	.5581	.5526	.0012
△	.4840	.4778	.0013
⊛	.4276	.4226	.0014
⊡	.3841	.3794	.0016
◈	.3373	.3339	.0017
◬	.2887	.2858	.0020

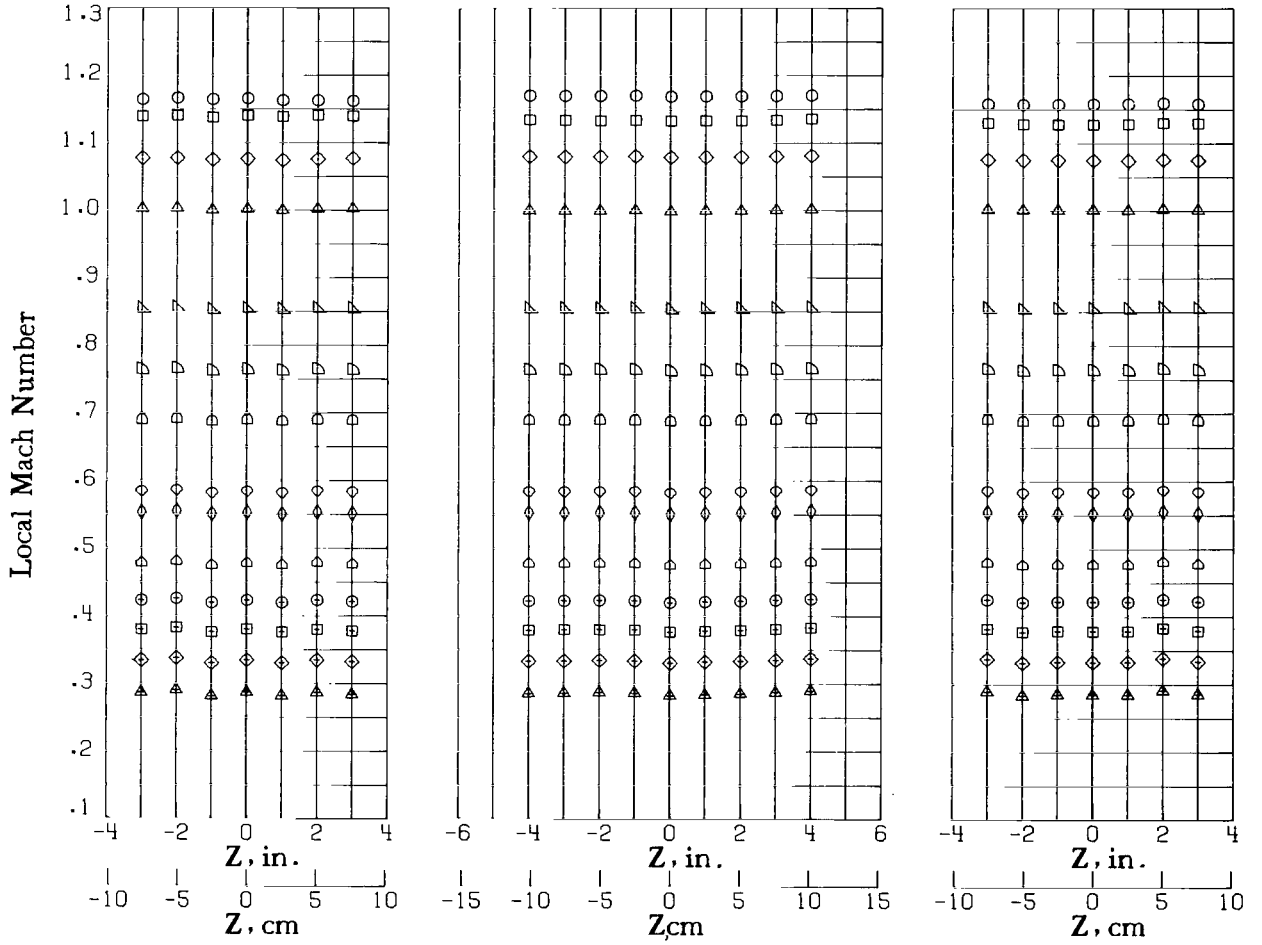

(d) Vertical distribution at x = -7.6 cm (-3.0 in.).

(e) Vertical distribution at x = 0.0 cm (0.0 in.).

(f) Vertical distribution at x = 7.6 cm (3.0 in.).

Figure 22.- Concluded.

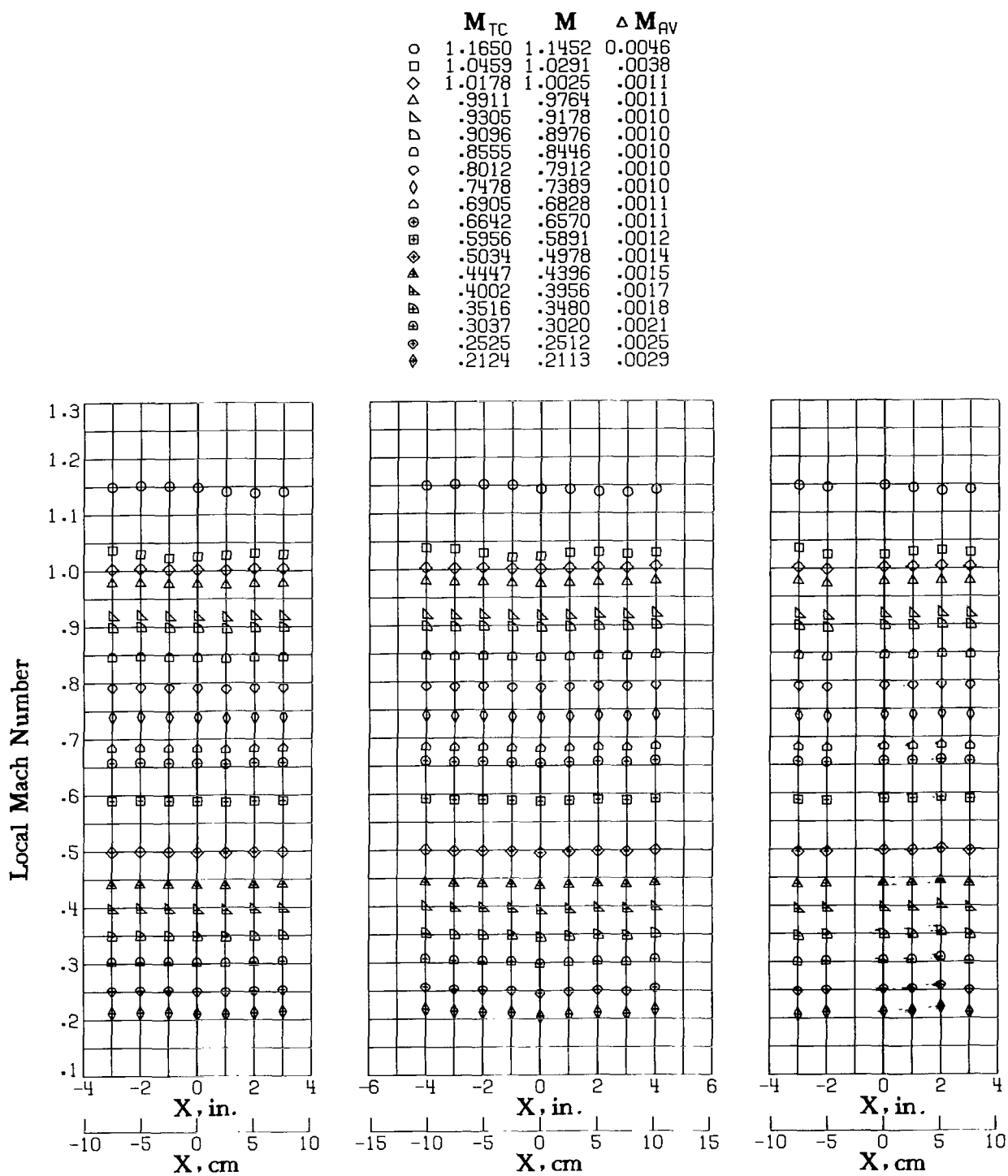

(a) Longitudinal distribution at z = -7.6 cm (-3.0 in.).

(b) Longitudinal distribution at z = 0.0 cm (0.0 in.).

(c) Longitudinal distribution at z = 7.6 cm (3.0 in.).

Figure 23.- Sidewall Mach number distribution in region occupied by model with traversing survey probe at z = -29.2 cm (-11.5 in.). $p_{t,\infty}$ = 517 kN/m^2 (75 lb/in^2).

	M_{TC}	M	ΔM_{AV}
○	1.1650	1.1452	0.0046
□	1.0459	1.0291	.0038
◇	1.0178	1.0025	.0011
△	.9911	.9764	.0011
▷	.9305	.9178	.0010
▷	.9096	.8976	.0010
▫	.8555	.8446	.0010
◇	.8012	.7912	.0010
◇	.7478	.7389	.0010
△	.6905	.6828	.0011
⊕	.6642	.6570	.0011
⊞	.5956	.5891	.0012
◈	.5034	.4978	.0014
▲	.4447	.4396	.0015
▶	.4002	.3956	.0017
⊞	.3516	.3480	.0018
⊕	.3037	.3020	.0021
⊕	.2525	.2512	.0025
◆	.2124	.2113	.0029

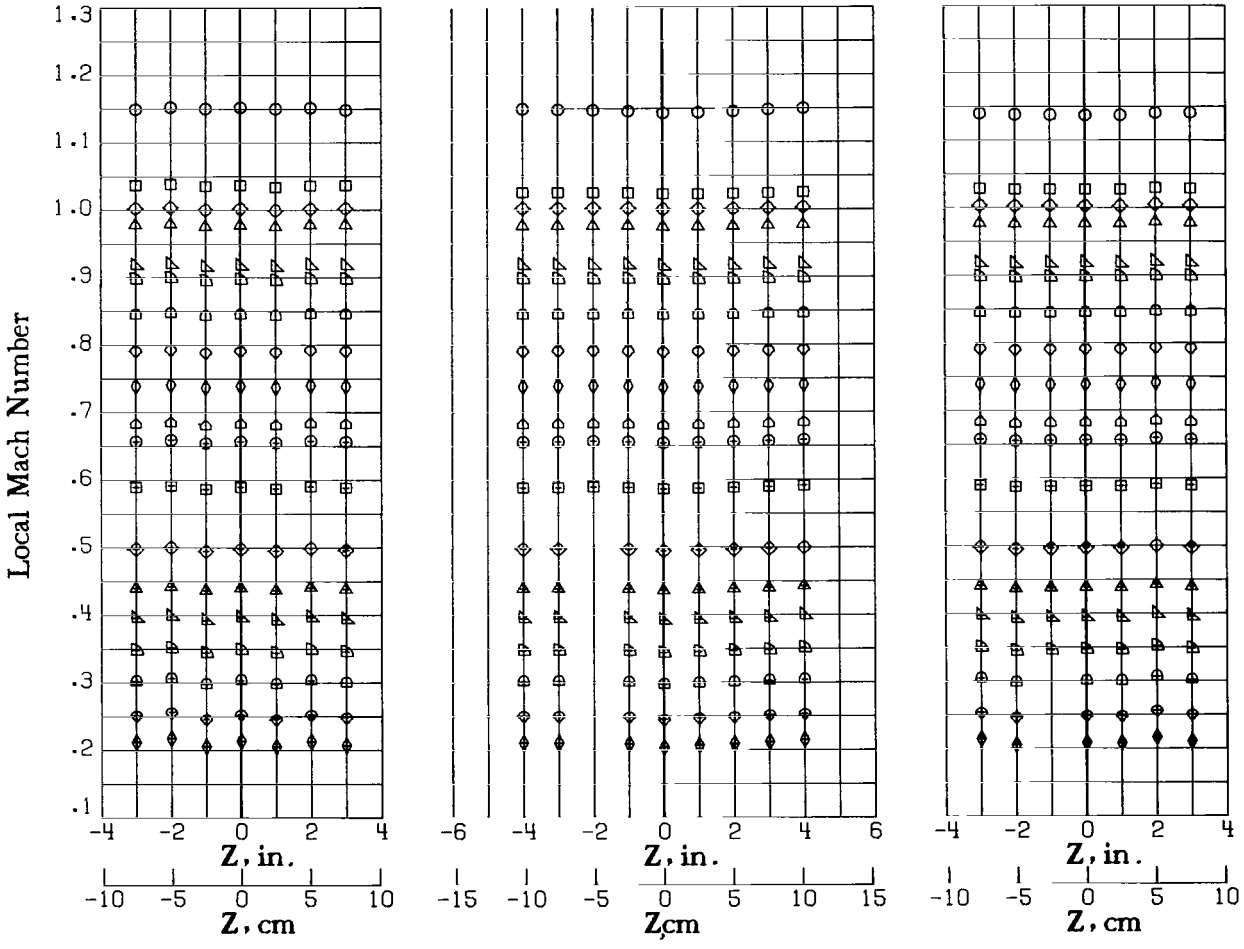

(d) Vertical distribution at x = -7.6 cm (-3.0 in.).

(e) Vertical distribution at x = 0.0 cm (0.0 in.).

(f) Vertical distribution at x = 7.6 cm (3.0 in.).

Figure 23.- Concluded.

	M_{TC}	M	ΔM_{AV}
○	1.2082	1.1816	0.0060
□	1.1514	1.1255	.0048
◇	1.0900	1.0622	.0023
△	1.0343	1.0141	.0017
▷	.9301	.9138	.0013
▯	.8881	.8730	.0012
▱	.8488	.8265	.0029
◇	.8237	.8102	.0011
◇	.7532	.7420	.0014
△	.6830	.6731	.0014
⊛	.6068	.5987	.0013
⊞	.5487	.5421	.0016
◈	.5048	.4982	.0017
▲	.4482	.4423	.0018
▶	.4114	.4060	.0018
▣	.3495	.3467	.0021
⊕	.2975	.2955	.0023

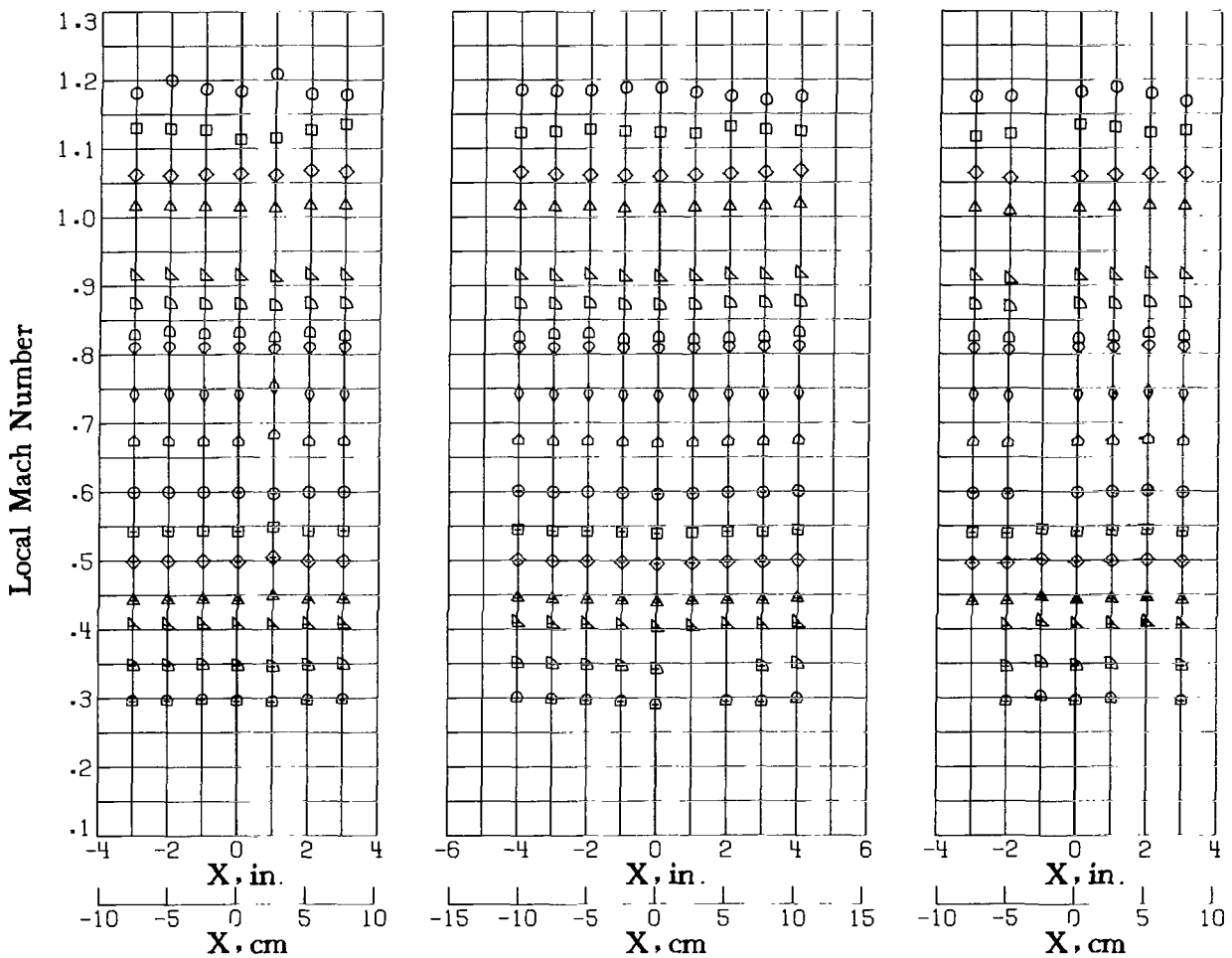

(a) Longitudinal distribution at z = -7.6 cm (-3.0 in.).

(b) Longitudinal distribution at z = 0.0 cm (0.0 in.).

(c) Longitudinal distribution at z = 7.6 cm (3.0 in.).

Figure 24.- Sidewall Mach number distribution in region occupied by model with traversing survey probe at z = -29.2 cm (-11.5 in.). $p_{t,\infty}$ = 620 kN/m^2 (90 lb/in^2).

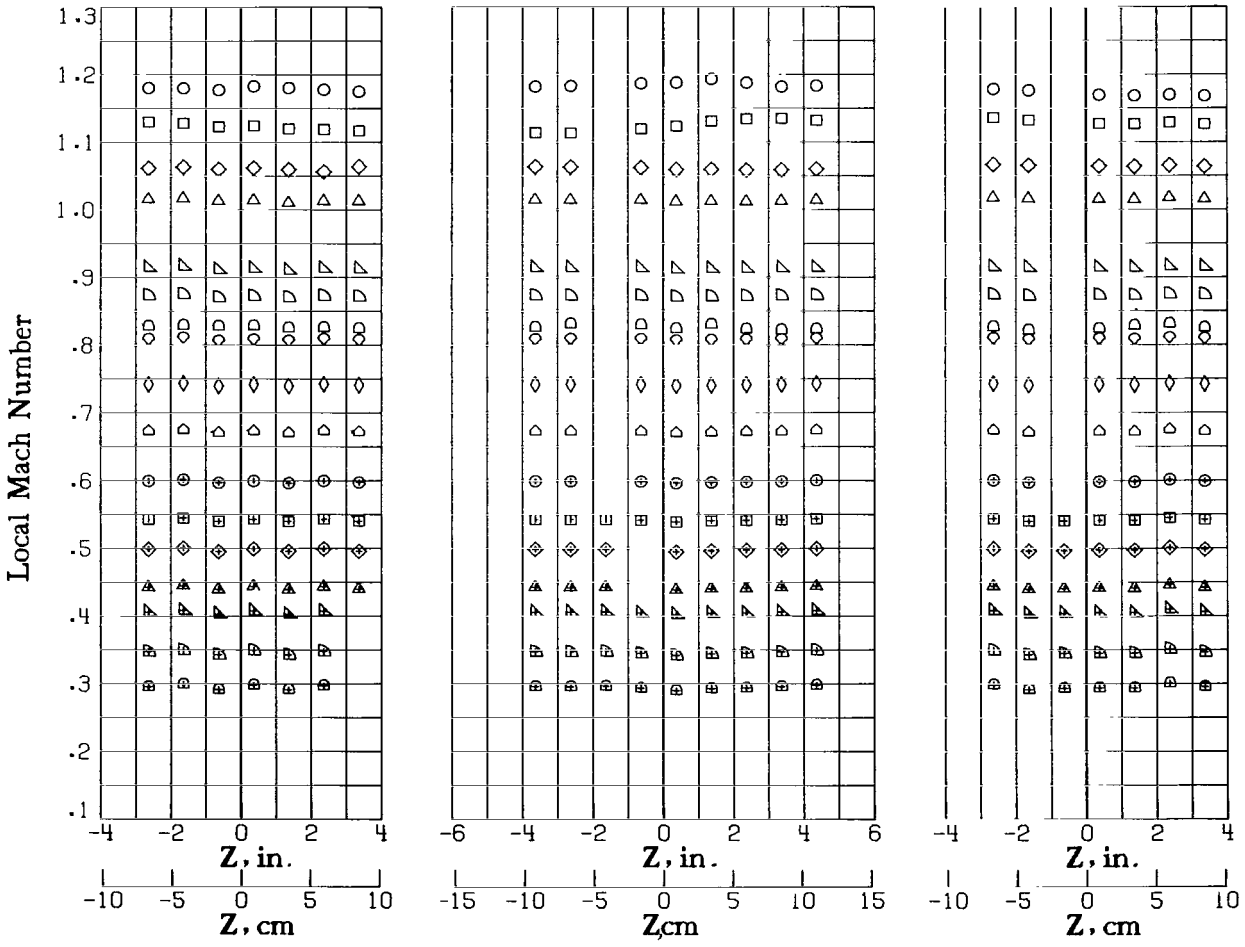

(d) Vertical distribution at x = -7.6 cm (-3.0 in.).

(e) Vertical distribution at x = 0.0 cm (0.0 in.).

(f) Vertical distribution at x = 7.6 cm (3.0 in.).

Figure 24.- Concluded.

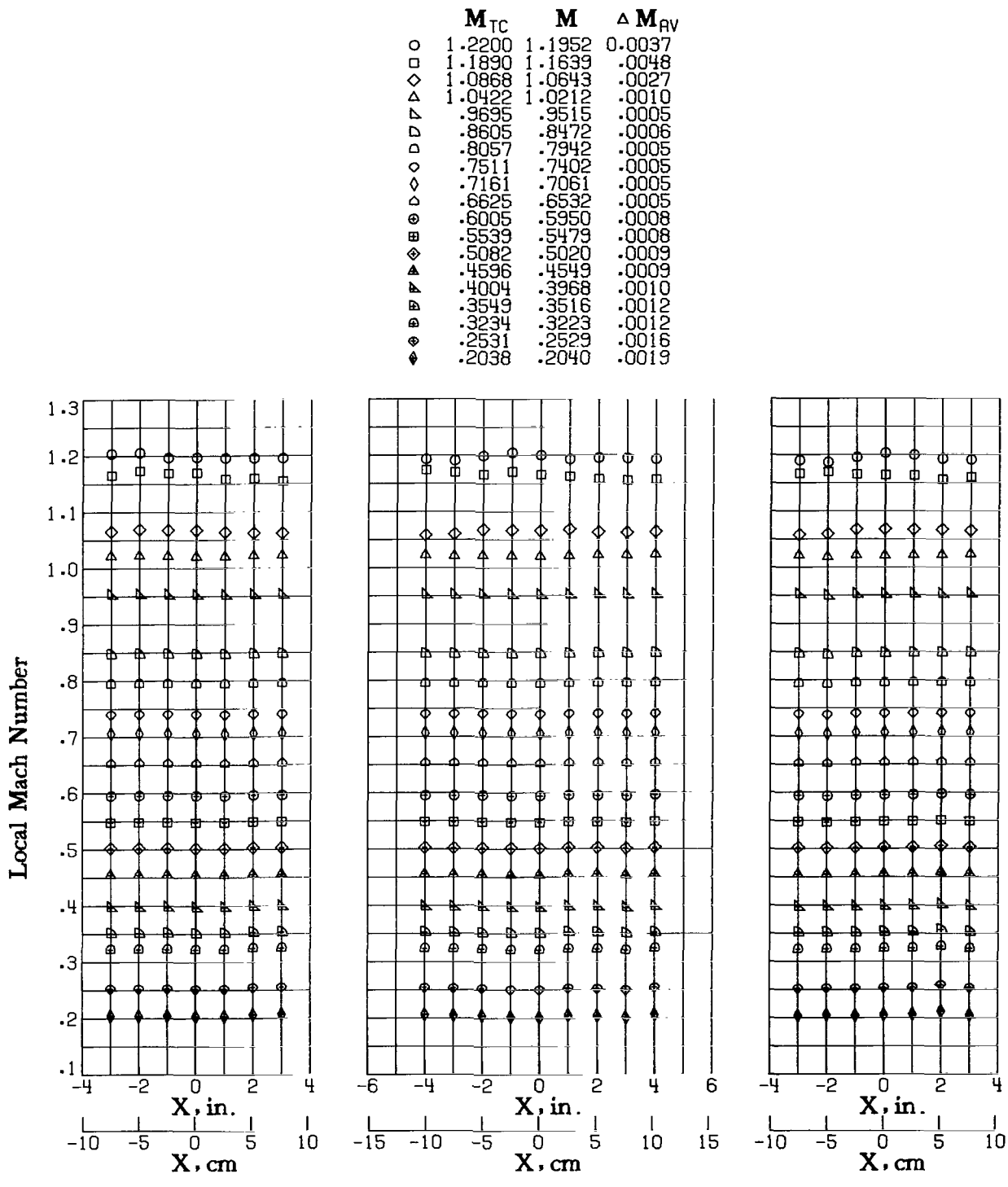

(a) Longitudinal distribution at z = -7.6 cm (-3.0 in.).

(b) Longitudinal distribution at z = 0.0 cm (0.0 in.).

(c) Longitudinal distribution at z = 7.6 cm (3.0 in.).

Figure 25.- Sidewall Mach number distribution in region occupied by model with traversing survey probe at z = 7.6 cm (3.0 in.). $p_{t,\infty}$ = 207 kN/m^2 (30 lb/in^2).

	M_{TC}	M	ΔM_{RV}
○	1.2200	1.1952	0.0037
□	1.1890	1.1639	.0048
◇	1.0868	1.0643	.0027
△	1.0422	1.0212	.0010
▷	.9695	.9515	.0005
▷	.8605	.8472	.0006
□	.8057	.7942	.0005
○	.7511	.7402	.0005
◇	.7161	.7061	.0005
△	.6625	.6532	.0005
⊕	.6005	.5950	.0008
⊞	.5539	.5479	.0008
◈	.5082	.5020	.0009
▲	.4596	.4549	.0009
◢	.4004	.3968	.0010
⊞	.3549	.3516	.0012
⊕	.3234	.3223	.0012
⊕	.2531	.2529	.0016
♦	.2038	.2040	.0019

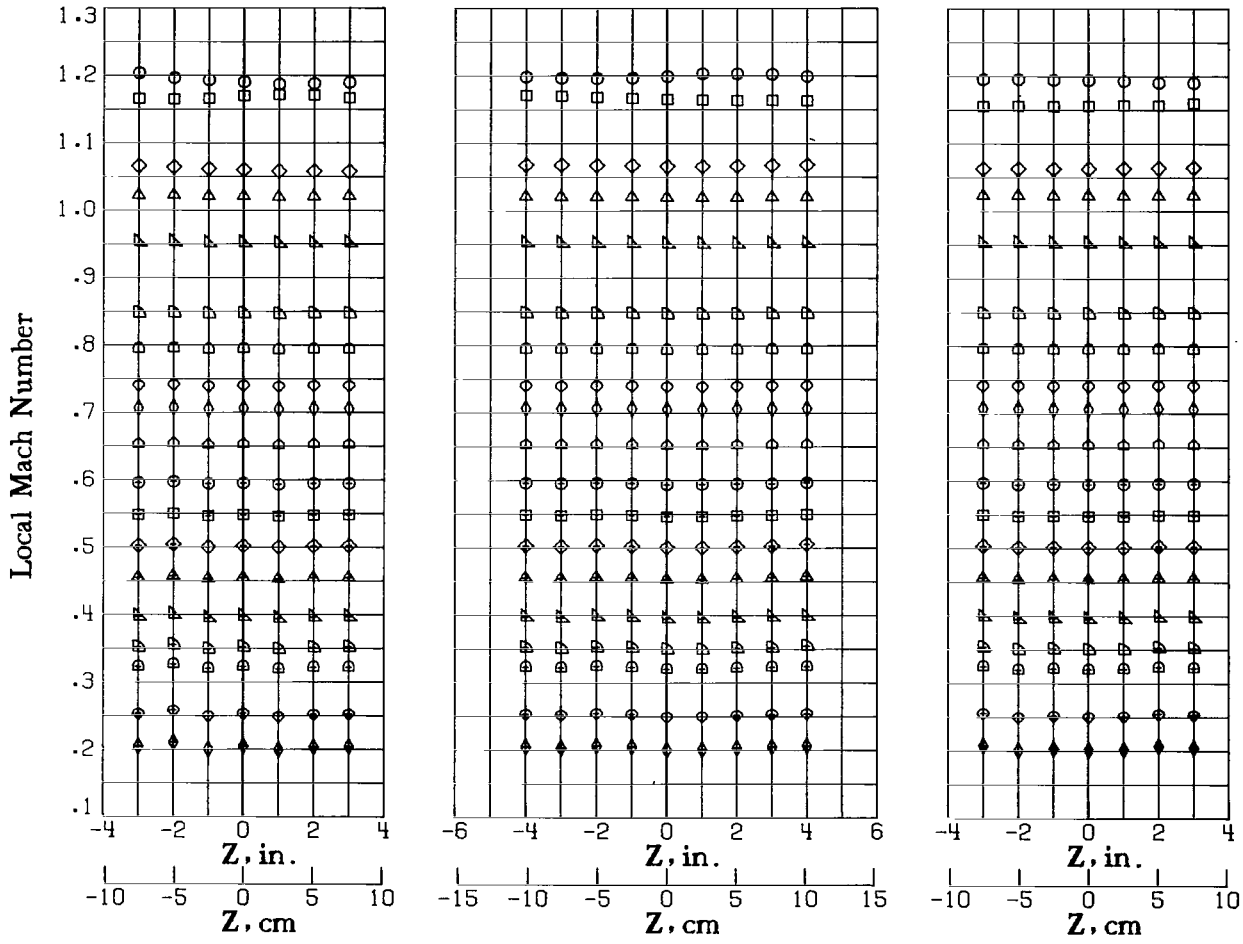

(d) Vertical distribution at x = -7.6 cm (-3.0 in.).

(e) Vertical distribution at x = 0.0 cm (0.0 in.).

(f) Vertical distribution at x = 7.6 cm (3.0 in.).

Figure 25.- Concluded.

	M_{TC}	M	ΔM_{AV}
○	1.2092	1.1848	0.0049
□	1.1596	1.1350	.0038
◇	1.1102	1.0856	.0042
△	1.0708	1.0494	.0017
◁	1.0151	.9954	.0007
▷	.9536	.9369	.0007
▱	.9089	.8944	.0008
◇	.8624	.8487	.0007
◇	.7941	.7825	.0007
△	.7199	.7094	.0007
⊕	.6811	.6726	.0008
⊞	.6352	.6267	.0009
◈	.5880	.5806	.0009
◭	.5365	.5292	.0011
◭	.4920	.4845	.0011
◭	.4367	.4299	.0012
⊕	.3990	.3931	.0013
◈	.3433	.3384	.0015

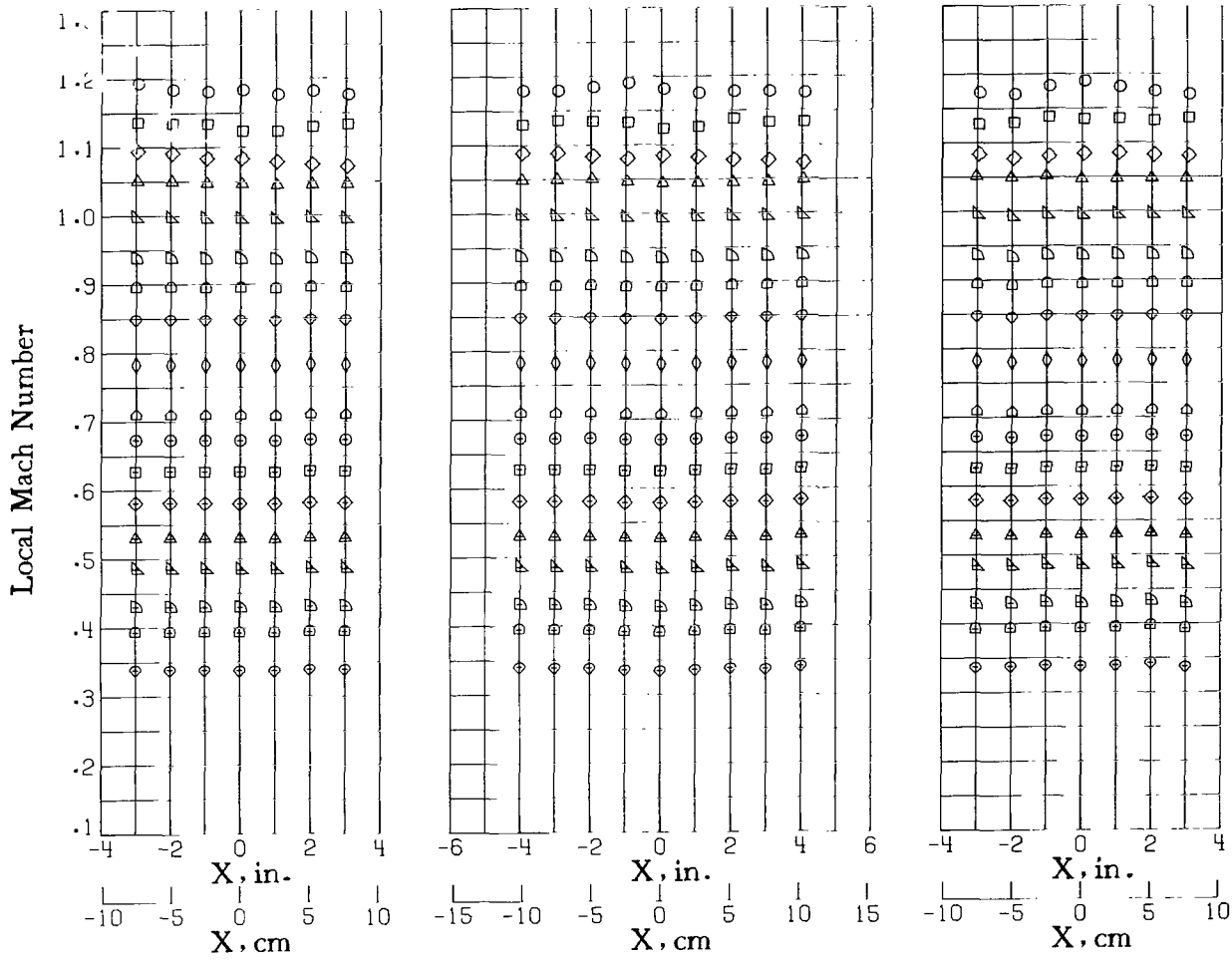

(a) Longitudinal distribution at z = -7.6 cm (-3.0 in.).

(b) Longitudinal distribution at z = 0.0 cm (0.0 in.).

(c) Longitudinal distribution at z = 7.6 cm (3.0 in.).

Figure 26.- Sidewall Mach number distribution in region occupied by model with traversing survey probe at z = 7.6 cm (3.0 in.). $p_{t,\infty}$ = 310 kN/m^2 (45 lb/in^2).

	M_{TC}	M	ΔM_{AV}
○	1.2092	1.1848	0.0049
□	1.1596	1.1350	.0038
◇	1.1102	1.0856	.0042
△	1.0708	1.0494	.0017
◿	1.0151	.9954	.0007
◻	.9536	.9369	.0007
○	.9089	.8944	.0008
◇	.8624	.8487	.0007
◇	.7941	.7825	.0007
△	.7199	.7094	.0007
⊕	.6811	.6726	.0008
⊞	.6352	.6267	.0009
◈	.5880	.5806	.0009
▲	.5365	.5292	.0011
◿	.4920	.4845	.0011
⊞	.4367	.4299	.0012
⊕	.3990	.3931	.0013
◈	.3433	.3384	.0015

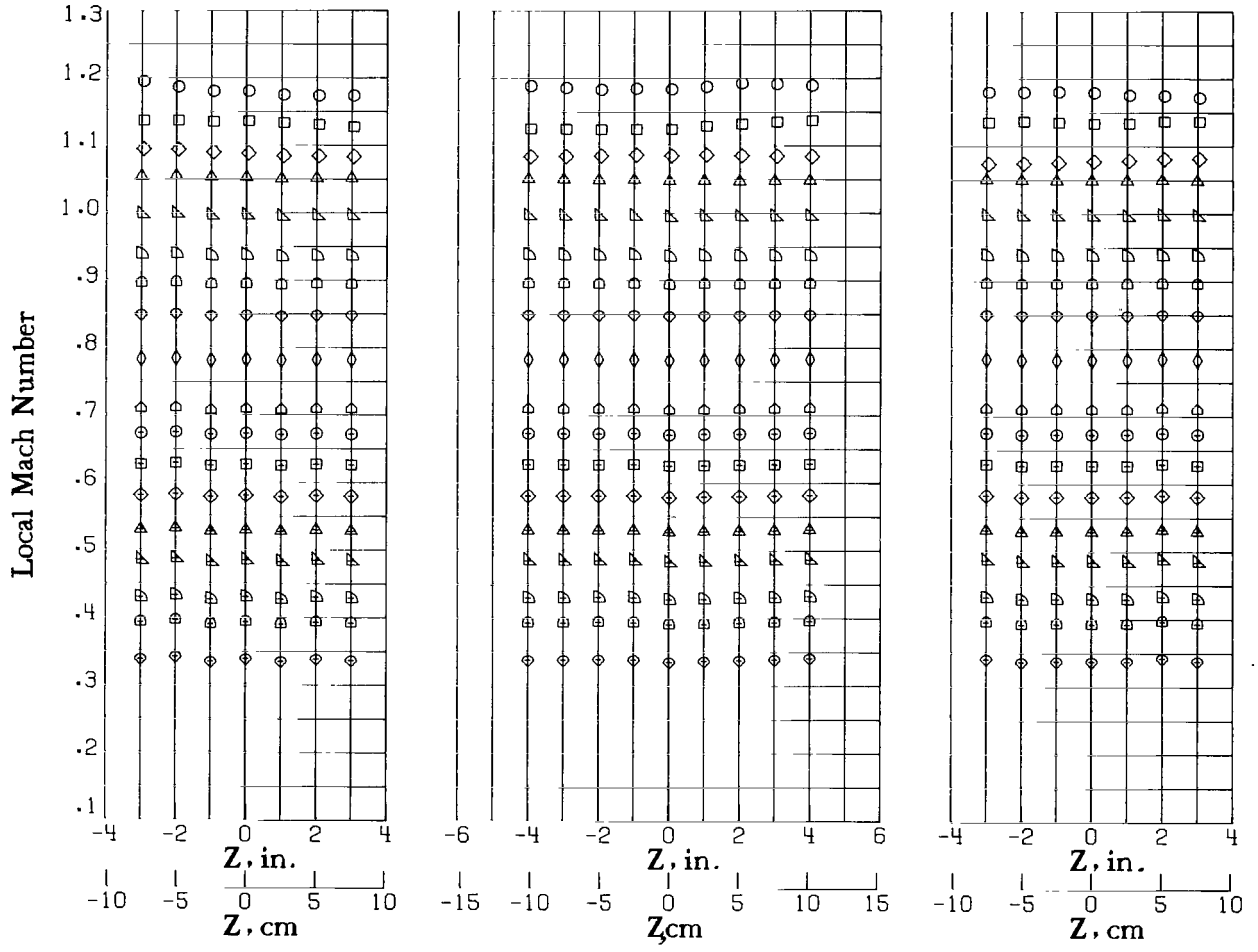

(d) Vertical distribution at x = -7.6 cm (-3.0 in.).

(e) Vertical distribution at x = 0.0 cm (0.0 in.).

(f) Vertical distribution at x = 7.6 cm (3.0 in.).

Figure 26.- Concluded.

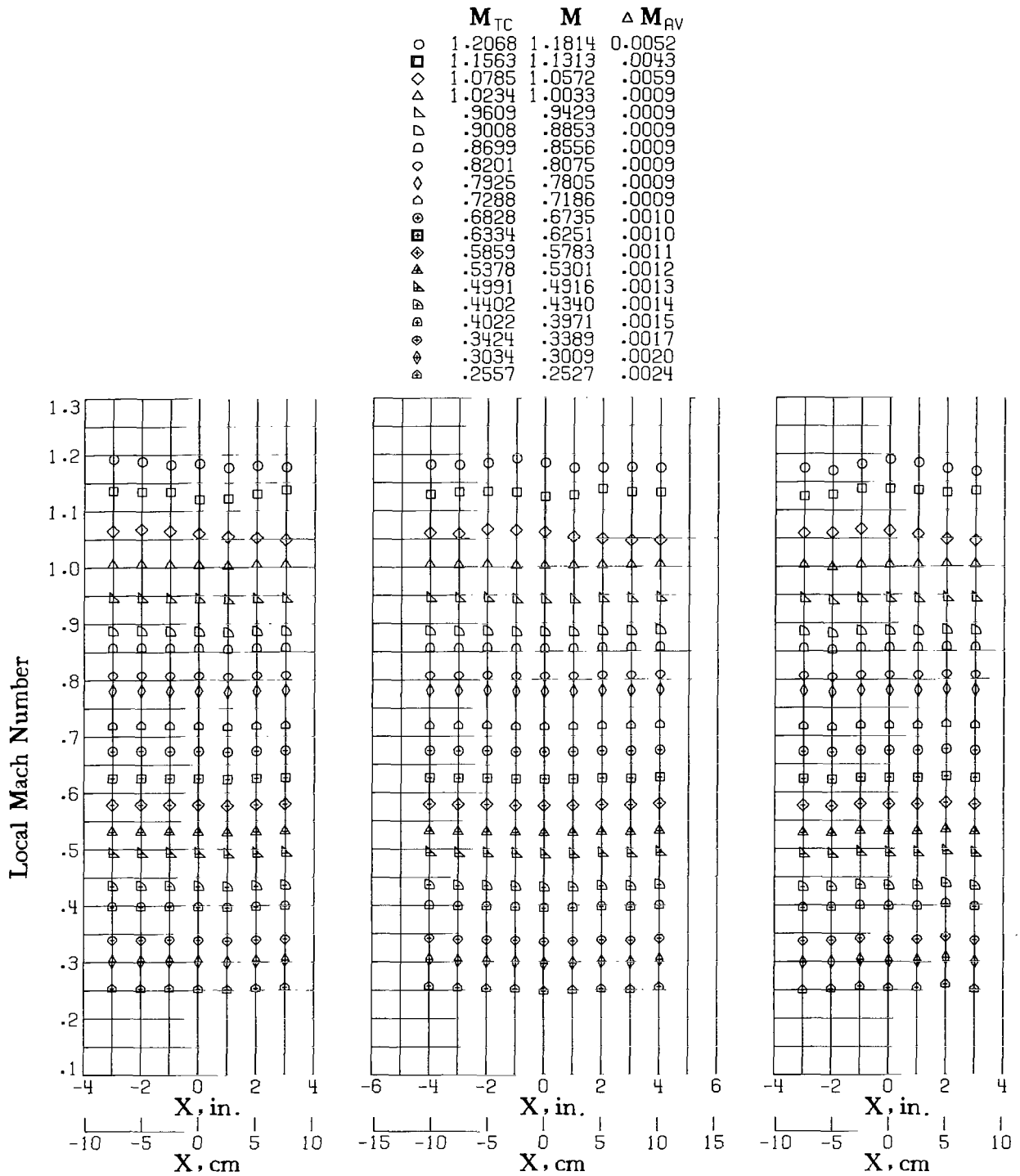

(a) Longitudinal distribution at z = -7.6 cm (-3.0 in.).

(b) Longitudinal distribution at z = 0.0 cm (0.0 in.).

(c) Longitudinal distribution at z = 7.6 cm (3.0 in.).

Figure 27.- Sidewall Mach number distribution in region occupied by model with traversing survey probe at z = 7.6 cm (3.0 in.). $p_{t,\infty}$ = 414 kN/m^2 (60 lb/in^2).

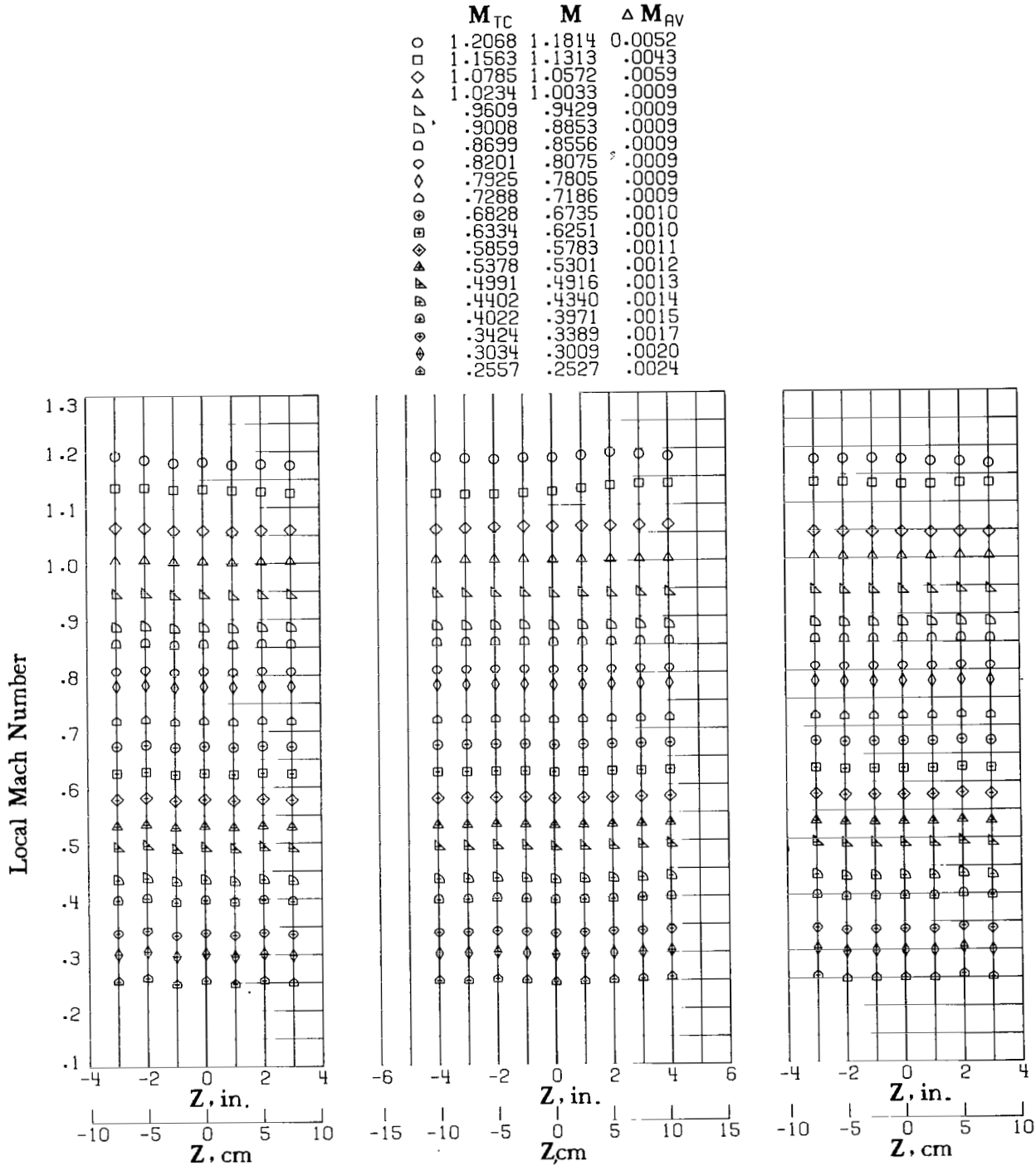

(d) Vertical distribution at x = -7.6 cm (-3.0 in.).

(e) Vertical distribution at x = 0.0 cm (0.0 in.).

(f) Vertical distribution at x = 7.6 cm (3.0 in.).

Figure 27.- Concluded.

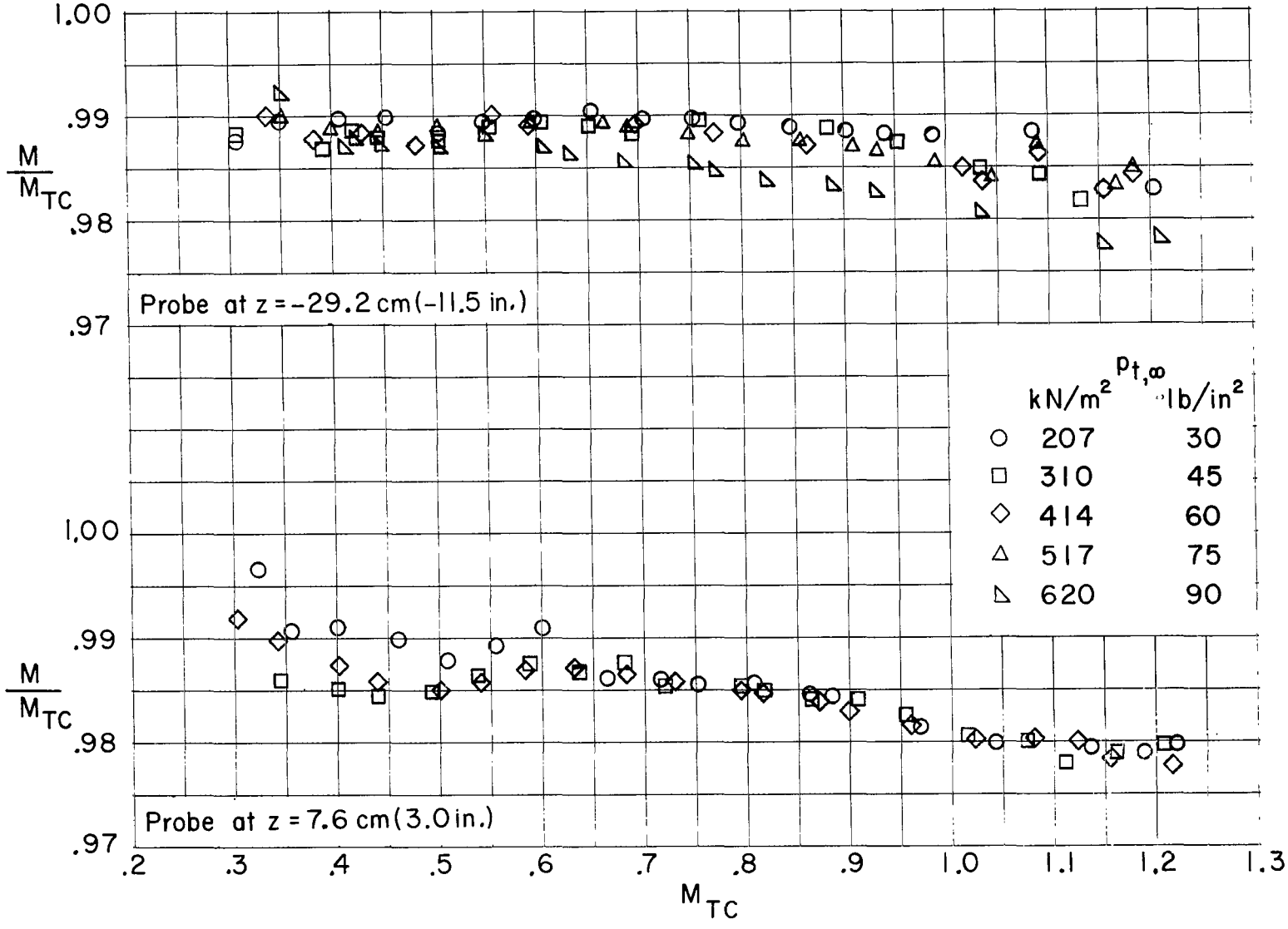

Figure 28.- Effect of stagnation pressure and traversing-probe position on ratio of stream Mach number to test-chamber Mach number.

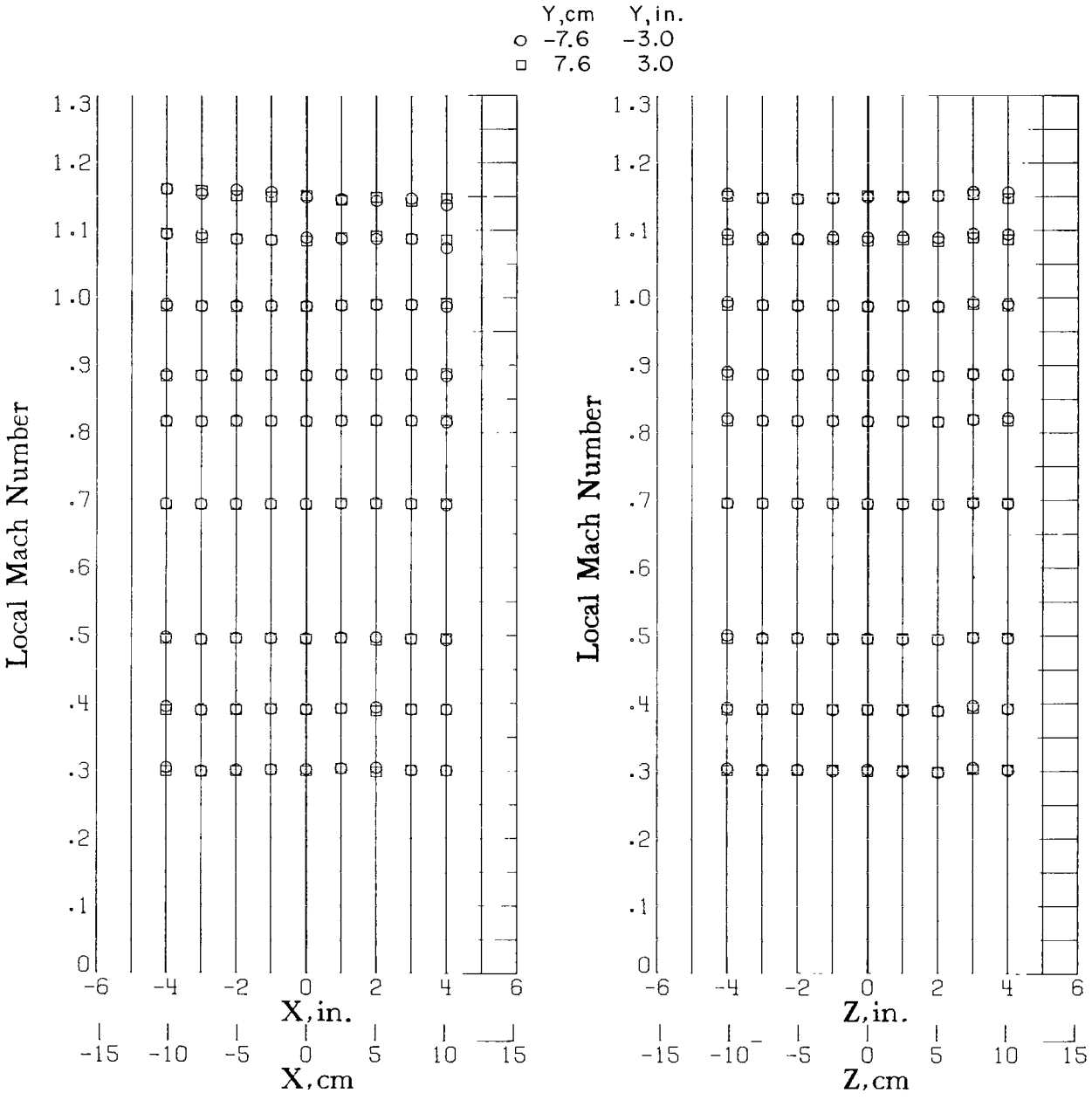

Figure 29.- Comparison of left and right sidewall Mach number distributions in region occupied by model with traversing survey probe at z = -29.2 cm (-11.5 in.). $p_{t,\infty}$ = 207 kN/m^2 (30 lb/in^2).

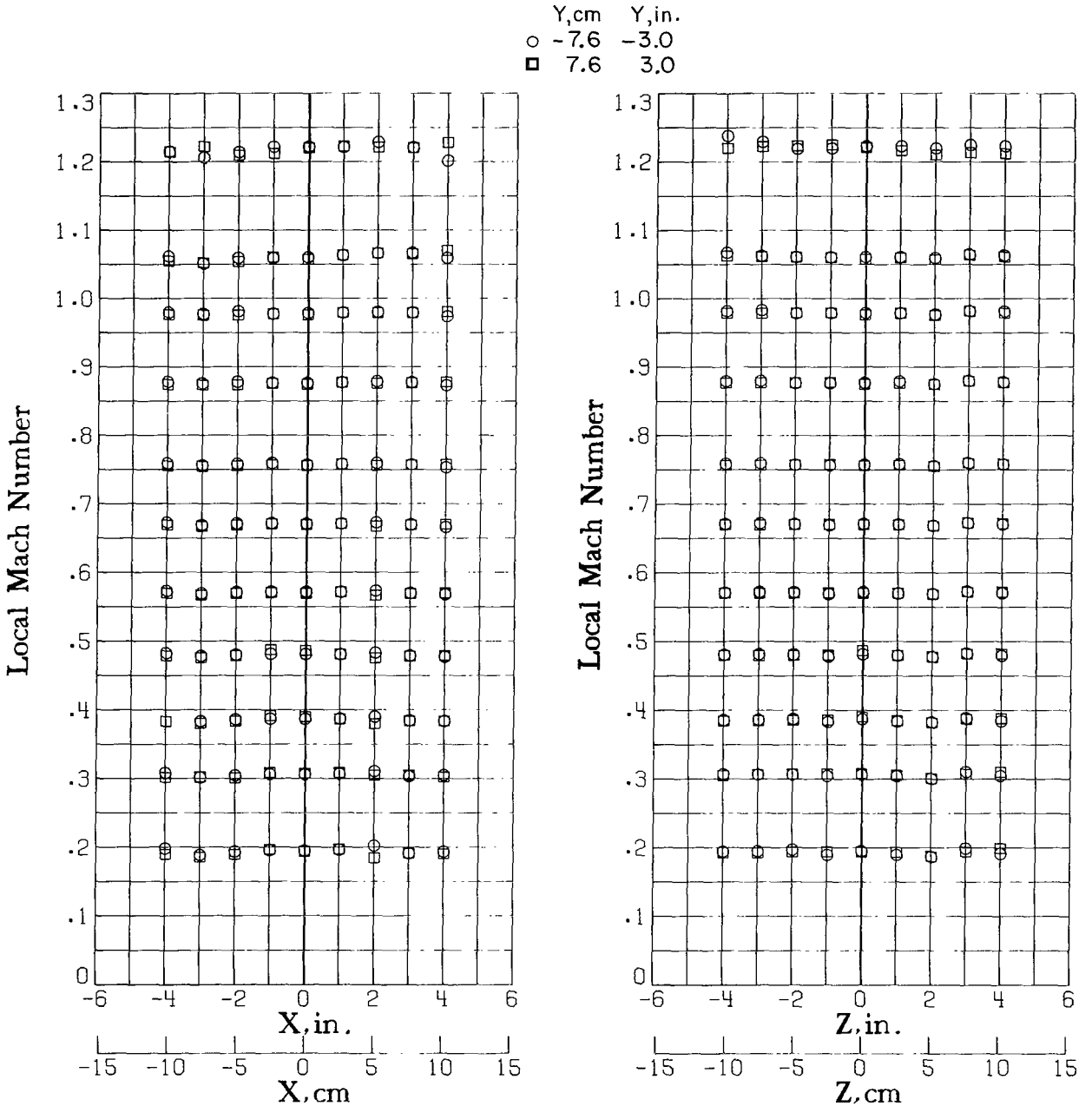

Figure 30.- Comparison of left and right sidewall Mach number distributions in region occupied by model with traversing survey probe at z = -29.2 cm (-11.5 in.). $p_{t,\infty}$ = 414 kN/m^2 (60 lb/in^2).

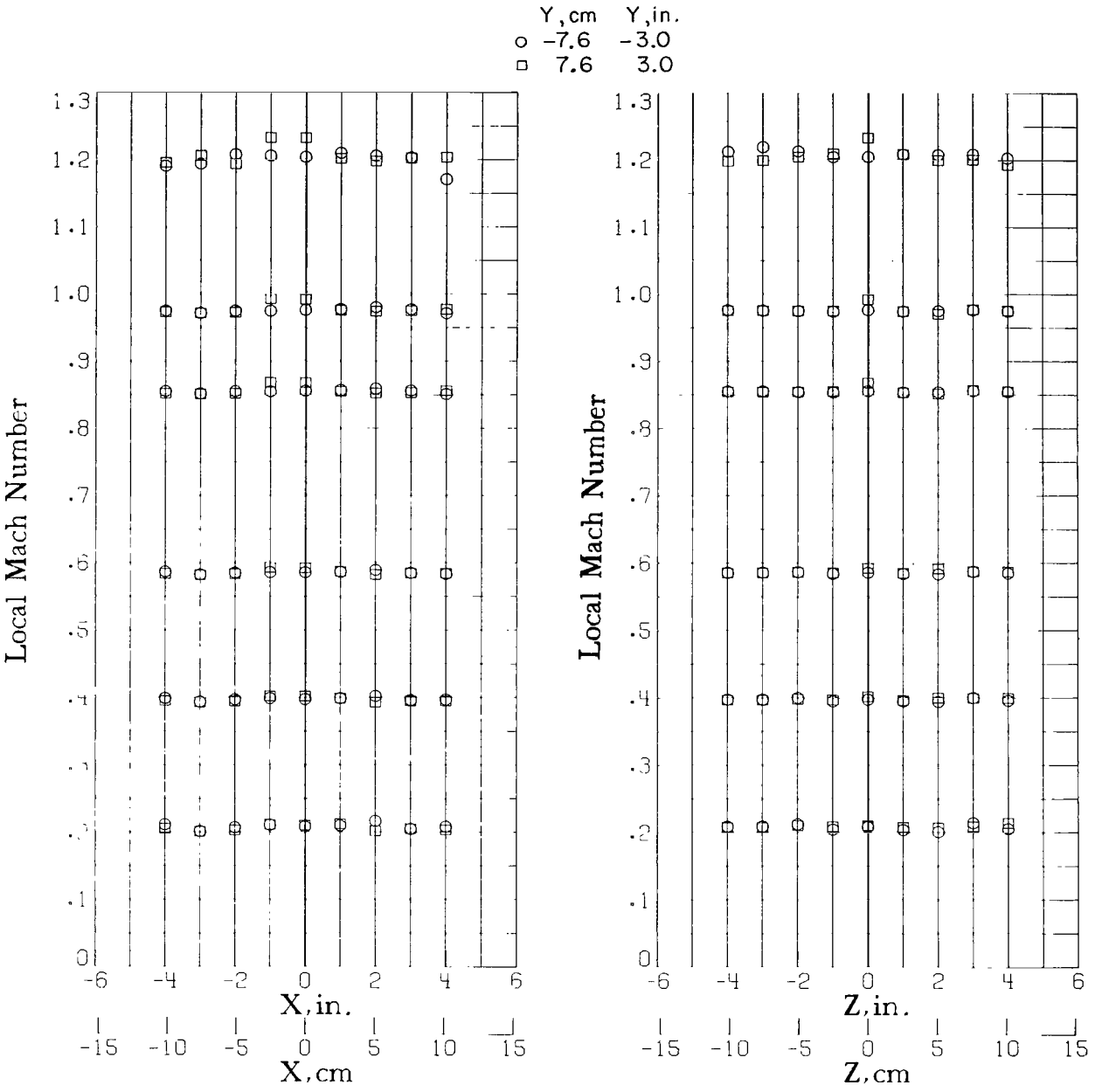

Figure 31.- Comparison of left and right sidewall Mach number distributions in region occupied by model with traversing survey probe at z = -29.2 cm (-11.5 in.). $p_{t,\infty}$ = 620 kN/m^2 (90 lb/in^2).

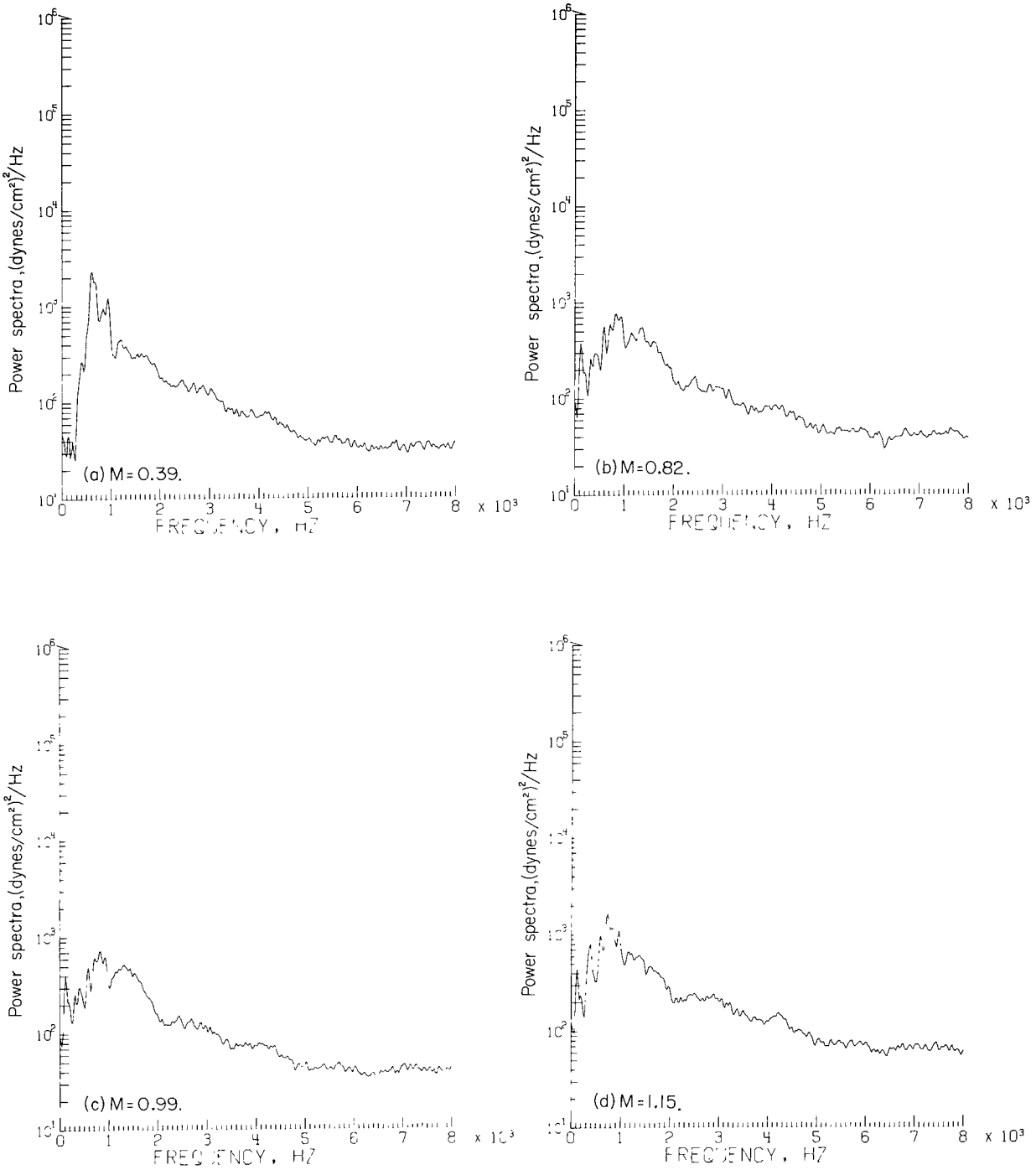

Figure 32.- Power-spectra distribution of noise in settling chamber. $p_{t,\infty}$ = 207 kN/m^2 (30 lb/in^2).

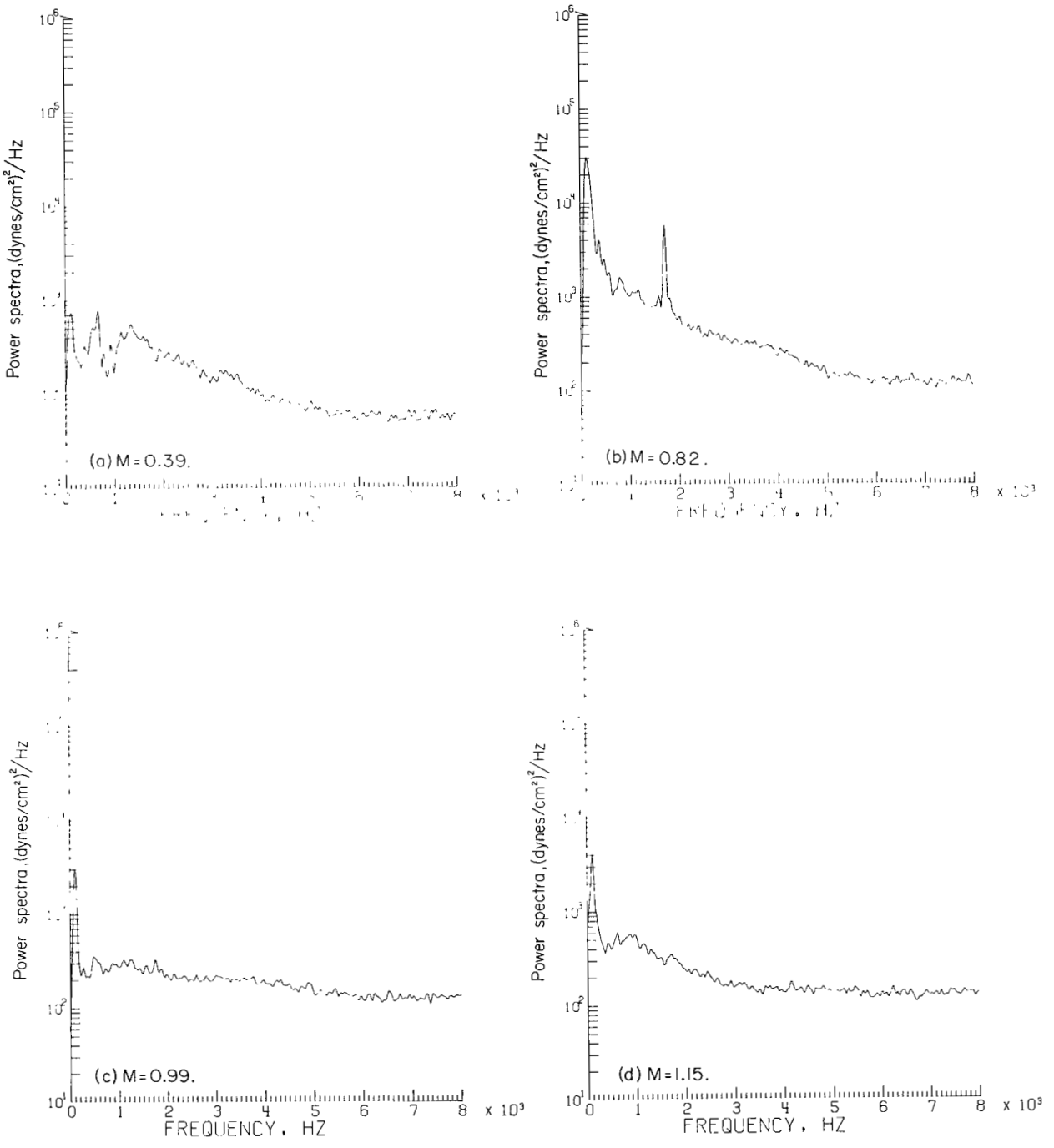

Figure 33.- Power-spectra distribution of noise on test-section sidewall at x = 3.8 cm (1.5 in.). $p_{t,\infty}$ = 207 kN/m^2 (30 lb/in^2).

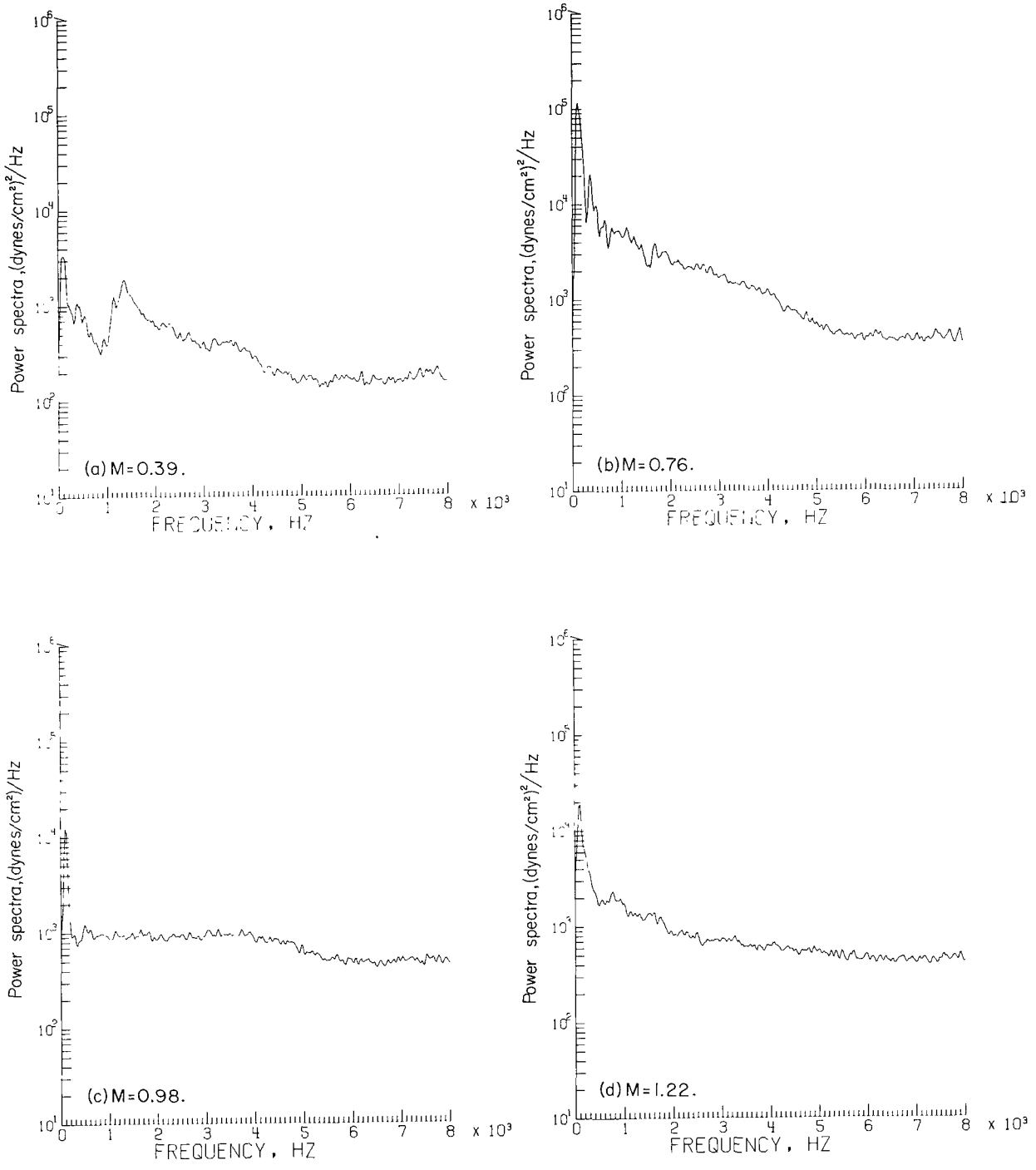

Figure 34.- Power-spectra distribution of noise on test-section sidewall at x = 3.8 cm (1.5 in.). $p_{t,\infty}$ = 414 kN/m^2 (60 lb/in^2).

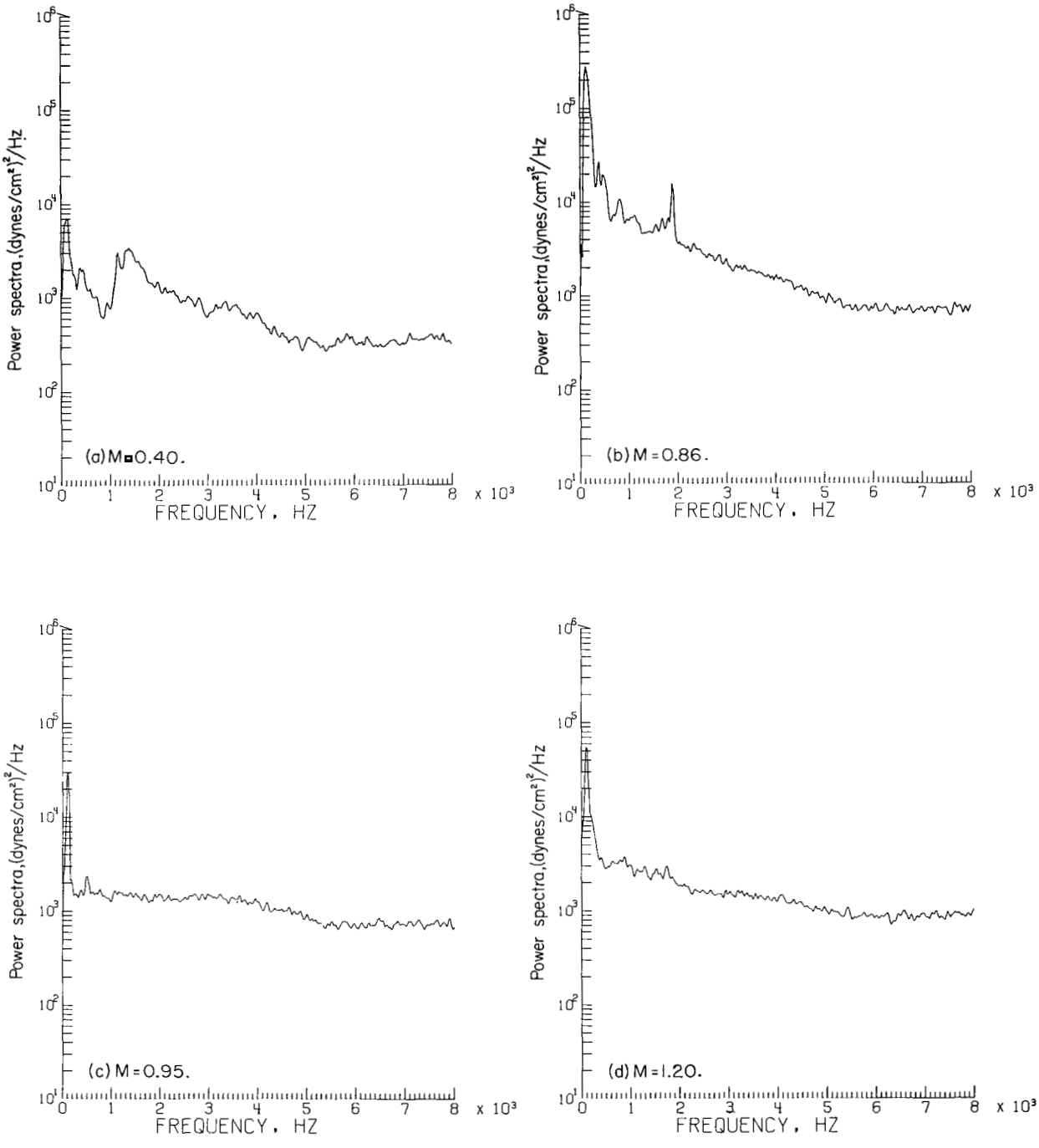

Figure 35.- Power-spectra distribution of noise on test-section sidewall at x = 3.8 cm (1.5 in.). $p_{t,\infty}$ = 620 kN/m^2 (90 lb/in^2).

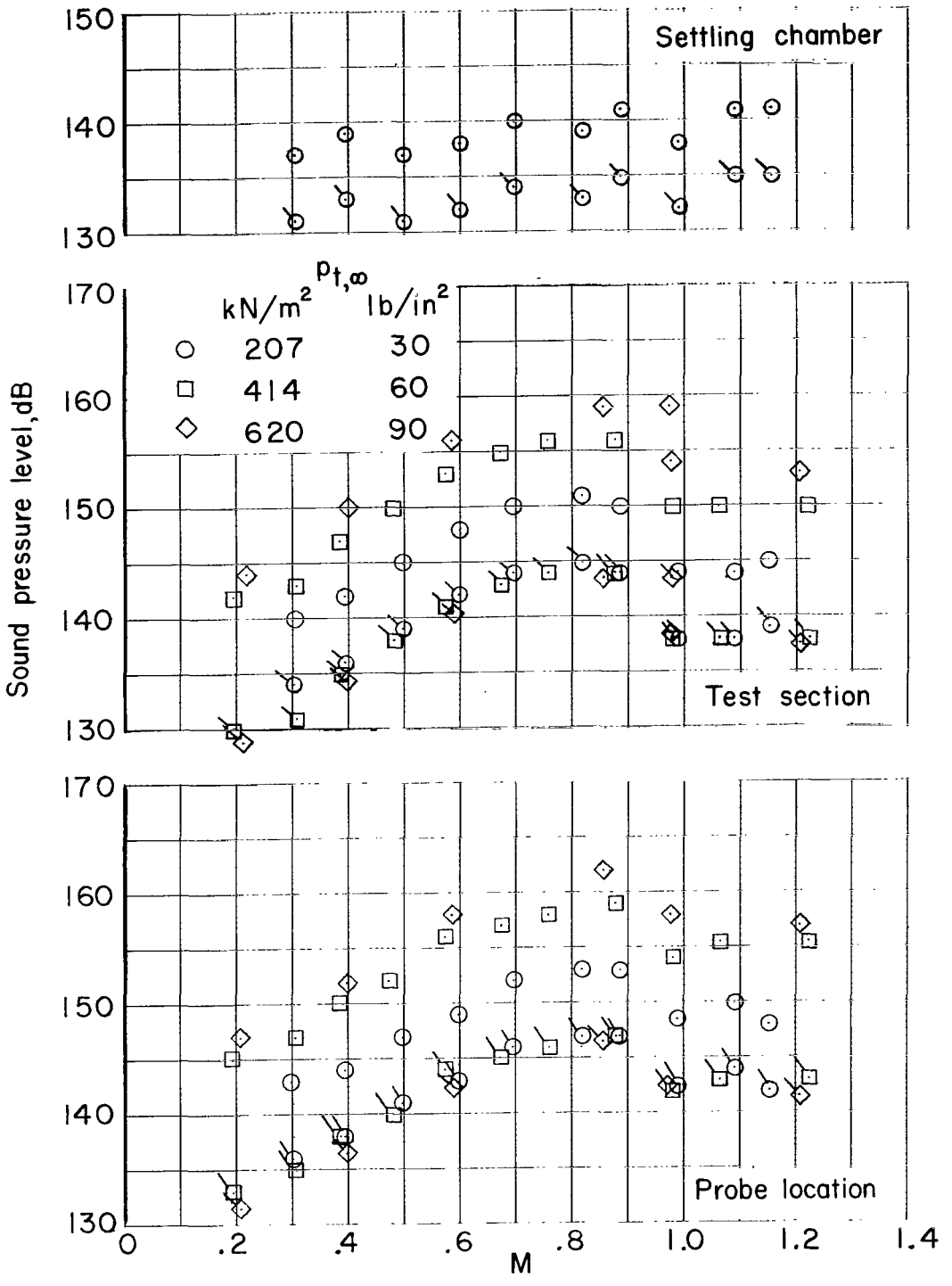

Figure 36.- Effects of Mach number and stagnation pressure on sound pressure level. Flagged symbols denote data scaled to 1 atmosphere.

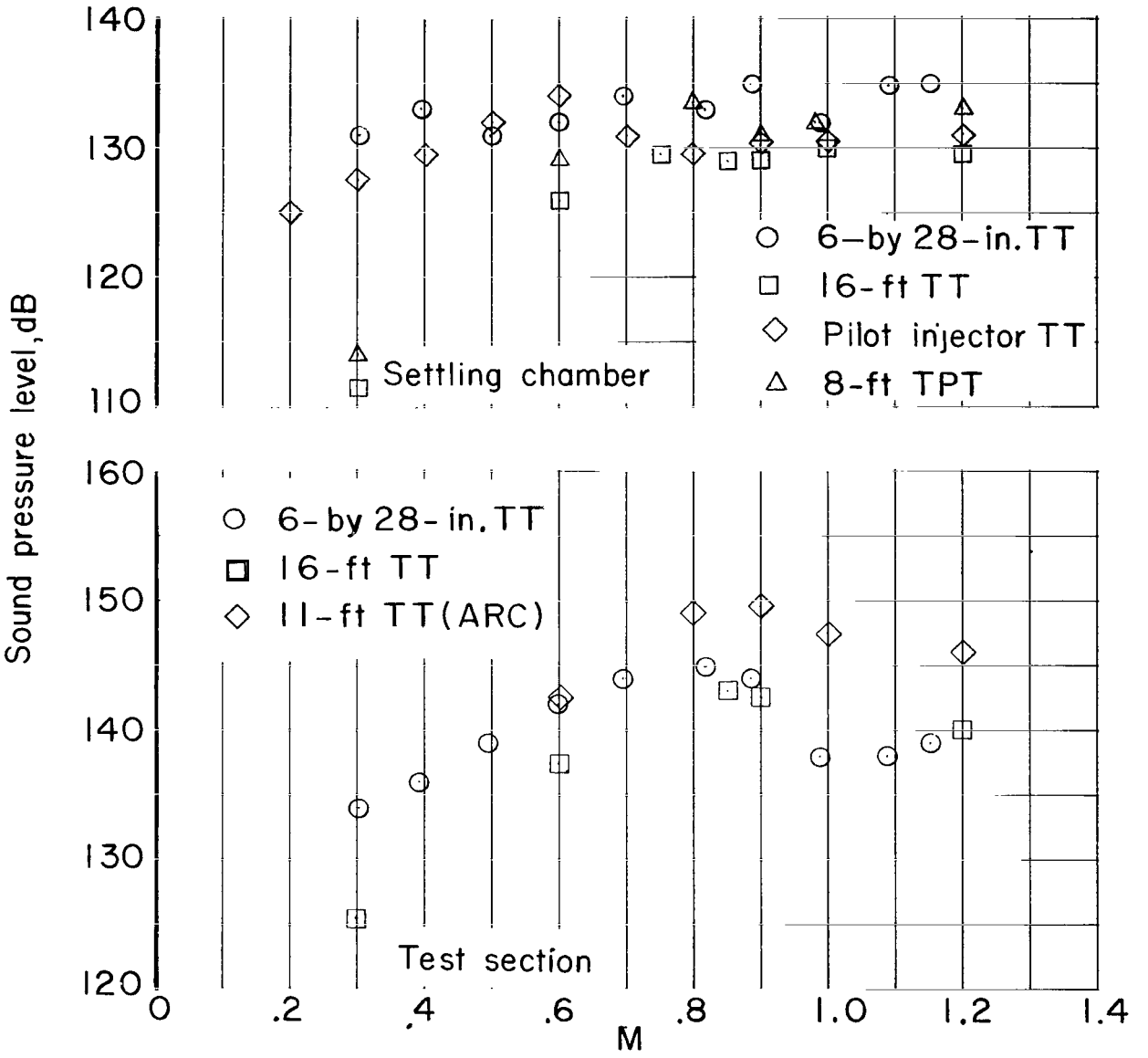

Figure 37.- Comparison of sound pressure levels in several facilities. $p_{t,\infty}$ = 103 kN/m^2 (15 lb/in^2).

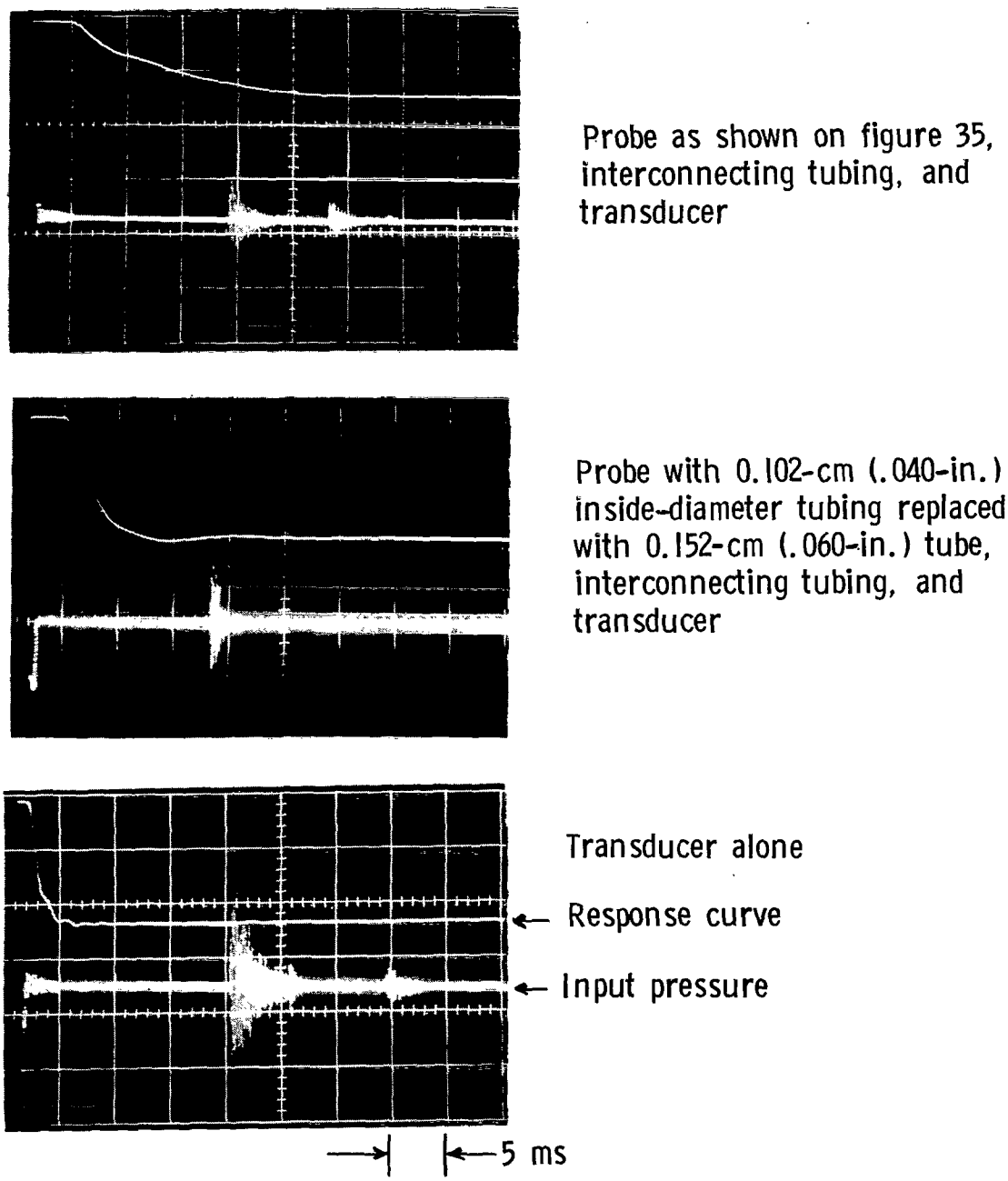

L-75-235

Figure 38.- Response time of pitot tube and transducer system to a step pressure input.

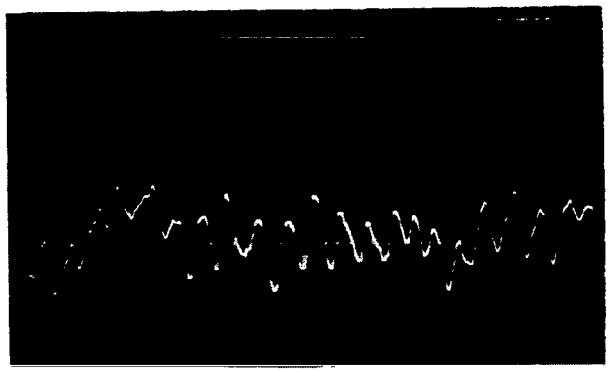

$\frac{\Delta p_t}{q} = 0.0075$

$f_c = 200$ kHz

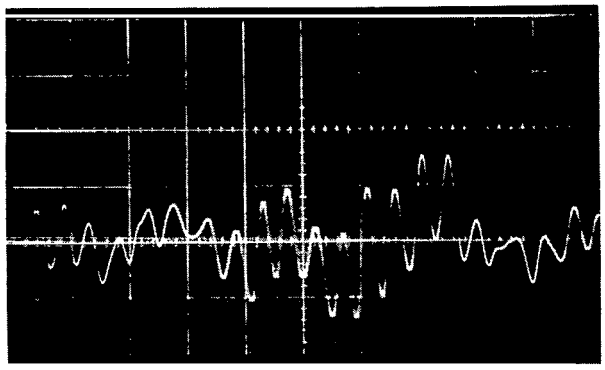

$f_c = 200$ Hz

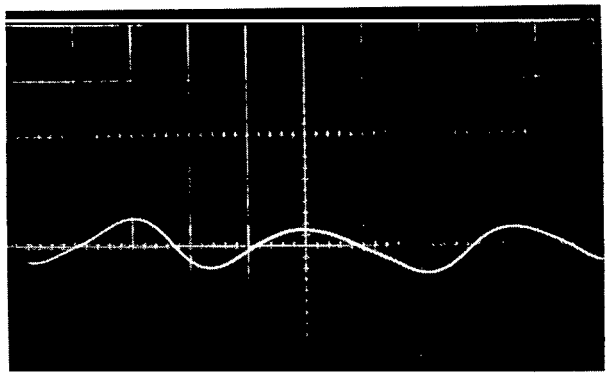

$f_c = 20$ Hz

20 ms

L-75-236

Figure 39.- Effect of electrical filters on measured total-pressure oscillations on tunnel center line at z = 33.0 cm (13.0 in.). M = 0.7; $p_{t,\infty}$ = 207 kN/m^2 (30 lb/in^2).

"The aeronautical and space activities of the United States shall be conducted so as to contribute . . . to the expansion of human knowledge of phenomena in the atmosphere and space. The Administration shall provide for the widest practicable and appropriate dissemination of information concerning its activities and the results thereof."

—NATIONAL AERONAUTICS AND SPACE ACT OF 1958

NASA SCIENTIFIC AND TECHNICAL PUBLICATIONS

TECHNICAL REPORTS: Scientific and technical information considered important, complete, and a lasting contribution to existing knowledge.

TECHNICAL NOTES: Information less broad in scope but nevertheless of importance as a contribution to existing knowledge.

TECHNICAL MEMORANDUMS: Information receiving limited distribution because of preliminary data, security classification, or other reasons. Also includes conference proceedings with either limited or unlimited distribution.

CONTRACTOR REPORTS: Scientific and technical information generated under a NASA contract or grant and considered an important contribution to existing knowledge.

TECHNICAL TRANSLATIONS: Information published in a foreign language considered to merit NASA distribution in English.

SPECIAL PUBLICATIONS: Information derived from or of value to NASA activities. Publications include final reports of major projects, monographs, data compilations, handbooks, sourcebooks, and special bibliographies.

TECHNOLOGY UTILIZATION PUBLICATIONS: Information on technology used by NASA that may be of particular interest in commercial and other non-aerospace applications. Publications include Tech Briefs, Technology Utilization Reports and Technology Surveys.

Details on the availability of these publications may be obtained from:

SCIENTIFIC AND TECHNICAL INFORMATION OFFICE

NATIONAL AERONAUTICS AND SPACE ADMINISTRATION

Washington, D.C. 20546